AD-A069 223 PURDUE UNIV LAFAYETTE IND SCHOOL OF AERONAUTICS AND --ETC F/G 20/4
FLUTTER ANALYSIS OF TWO-DIMENSIONAL AND TWO-DEGREE-OF-FREEDOM A--ETC(U)
DEC 78 T Y YANG, A G STRIZ, P GURUSWAMY AFOSR-78-3523
UNCLASSIFIED AFFDL-TR-78-202 NL

1 OF 2
AD
A069223

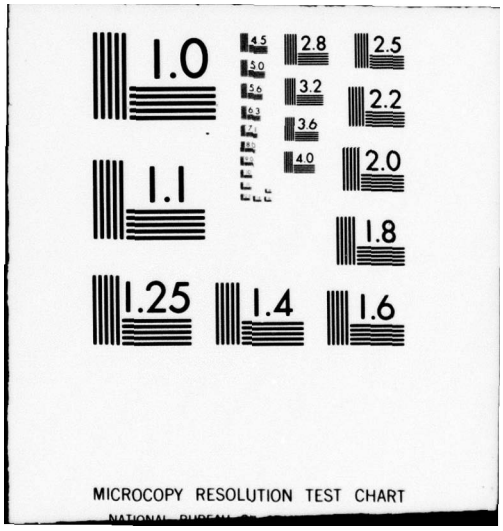
1.0
1.1
1.25
1.4
1.6
1.8
2.0
2.2
2.5
2.8
3.2
3.6
4.0
4.5
5.0
5.6
6.3
MICROCOPY RESOLUTION TEST CHART

AFFDL-TR-78-202

LEVEL II

FLUTTER ANALYSIS OF TWO-DIMENSIONAL AND TWO-DEGREE-OF-FREEDOM AIRFOILS IN SMALL-DISTURBANCE UNSTEADY TRANSONIC FLOW

T. Y. Yang, A. G. Striz, and P. Guruswamy

Purdue University
West Lafayette, IN 47907

December 1978

TECHNICAL REPORT AFFDL-TR-78-202
FINAL REPORT FOR PERIOD NOVEMBER 1977 - OCTOBER 1978

Approved for public release; distribution unlimited.

Air Force Flight Dynamics Laboratory
Air Force Wright Aeronautical Laboratories
Air Force Systems Command
Wright Patterson Air Force Base, Ohio 45433

NOTICE

When Government drawings, specifications, or other data are used for any purpose other than in connection with a definitely related Government procurement operation, the United States Government thereby incurs no responsibility nor any obligation whatsoever; and the fact that the government may have formulated, furnished, or in any way supplied the said drawings, specifications, or other data, is not to be regarded by implication or otherwise as in any manner licensing the holder or any other person or corporation, or conveying any rights or permission to manufacture, use, or sell any patented invention that may in any way be related thereto.

This report has been reviewed by the Information Office, (ASD/OIP) and is releasable to the National Technical Information Service (NTIS). At NTIS, it will be available to the general public, including foreign nations.

This technical report has been reviewed and is approved for publication.

Lawrence J. Huttsell

LAWRENCE J. HUTTSELL
Project Engineer
Aeroelastic Group
Analysis & Optimization Branch

Charles A. Bair

CHARLES A. BAIR, Jr, Major, USAF
Chief, Analysis & Optimization Branch
Structural Mechanics Division

FOR THE COMMANDER

Ralph L. Kuster, Jr.

RALPH L. KUSTER, JR., Colonel, USAF
Chief, Structural Mechanics Division

Copies of this report should not be returned unless return is required by security considerations, contractual obligations, or notice on a specific document.

AIR FORCE/56780/30 April 1979 — 140

Unclassified

SECURITY CLASSIFICATION OF THIS PAGE (When Data Entered)

(19) REPORT DOCUMENTATION PAGE	READ INSTRUCTIONS BEFORE COMPLETING FORM
(18) 1. REPORT NUMBER: AFFDL-TR-78-202	2. GOVT ACCESSION NO. / 3. RECIPIENT'S CATALOG NUMBER (9)
(6) 4. TITLE (and Subtitle): Flutter Analysis of Two-Dimensional and Two-Degree-of-Freedom Airfoils in Small-Disturbance, Unsteady Transonic Flow.	5. TYPE OF REPORT & PERIOD COVERED: FINAL REPORT. Nov 77-Oct 78 / 6. PERFORMING ORG. REPORT NUMBER
(10) 7. AUTHOR(s): T. Y. Yang, Alfred G. Striz, P. Guruswamy	8. CONTRACT OR GRANT NUMBER(s): (15) AFOSR-78-3523
9. PERFORMING ORGANIZATION NAME AND ADDRESS: School of Aeronautics and Astronautics, Purdue University, Lafayette, IND 47907	10. PROGRAM ELEMENT, PROJECT, TASK AREA & WORK UNIT NUMBERS: PE 61102F / (16) 2307/N5/11 (17) N5
11. CONTROLLING OFFICE NAME AND ADDRESS: Air Force Flight Dynamics Laboratory (FBRC) (11) Wright-Patterson AFB, Ohio 45433	12. REPORT DATE: Dec 78 / 13. NUMBER OF PAGES: (12) 116 p.
14. MONITORING AGENCY NAME & ADDRESS (if different from Controlling Office)	15. SECURITY CLASS. (of this report): UNCLASSIFIED / 15a. DECLASSIFICATION/DOWNGRADING SCHEDULE

16. DISTRIBUTION STATEMENT (of this Report)

Approved for public release; distribution unlimited.

17. DISTRIBUTION STATEMENT (of the abstract entered in Block 20, if different from Report)

18. SUPPLEMENTARY NOTES

19. KEY WORDS (Continue on reverse side if necessary and identify by block number)

Airfoils
Flutter
Transonic
Unsteady Aerodynamics

20. ABSTRACT (Continue on reverse side if necessary and identify by block number)

Flutter analyses are performed for an NACA 64A006 and an NACA 64A010 airfoil by simultaneously using two transonic aerodynamic computational codes: (1) STRANS2 and UTRANS2 based on the relaxation method and (2) LTRAN2 based on the indicial and time-integration methods. → over

Aerodynamic coefficients are obtained for the NACA 64A006 airfoils at M_∞ = 0.7, 0.8, and 0.85 and the NACA 64A010 airfoil at M_∞ = 0.72, 0.76 and 0.8 and at various values of low reduced frequencies. The NACA 64A006 airfoil is assumed

DD FORM 1 JAN 73 1473 EDITION OF 1 NOV 65 IS OBSOLETE

Unclassified

SECURITY CLASSIFICATION OF THIS PAGE (When Data Entered)

291 850

to pitch both at the leading edge and at the ¼-chord axis and the NACA 64A010 airfoil is assumed to pitch at the ¼-chord axis. Plots of the distributions of steady pressure coefficients are also given. The results obtained by the two different computer codes are compared and discussed.

Flutter results are obtained as plots of flutter speeds and the corresponding reduced frequencies versus one of the four parameters; airfoil-air mass ratio; position of the mass center; position of the elastic axis; and free stream Mach number. On each figure, several sets of curves for different values of plunge-to-pitch frequency ratios are shown simultaneously.

The flutter results obtained by using relaxation and the indicial methods are, in general, in good agreement. The present flutter results for a special case of a thin parabolic airfoil at a low transonic Mach number of 0.7 compare favorably with that obtained by using linear flat plate theory. The trend of each flutter curve and the effect of each parameter are discussed in detail.

FOREWORD

This report was prepared by Professor T.Y. Yang of the School of Aeronautics and Astronautics of Purdue University under AFOSR Grant 78-3523, "Application of Time-Accurate Transonic Aerodynamics to Aeroelastic Problems." The research was administered by Dr. James J. Olsen and Lawrence J. Huttsell of the Structural Mechanics Division, Air Force Flight Dynamics Laboratory, Wright-Patterson Air Force Base, Ohio.

The report covers work conducted from November 1977 to October 1978. T.Y. Yang was the principal investigator. Alfred G. Striz and P. Guruswamy were the graduate research assistants. Dr. Samuel R. Bland of NASA Langley Research Center and Dr. William F. Ballhaus of NASA Ames Research Center served as technical consultants.

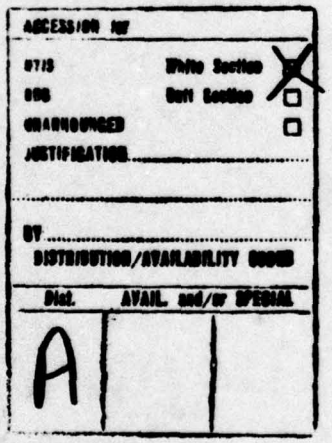

TABLE OF CONTENTS

SECTION		PAGE
I	INTRODUCTION	1
II	DEVELOPMENTS IN TRANSONIC FLOW COMPUTATION	6
	(a) The Harmonic or Relaxation Approach	6
	(b) The Time-Integration Approach	8
	(c) Indicial Method	10
	(d) Other Methods	11
III	AEROELASTIC EQUATIONS OF MOTION FOR TWO-DIMENSIONAL AIRFOIL WITH PITCH AND PLUNGE DEGREES OF FREEDOM	12
IV	TRANSFORMATION OF AERODYNAMIC COEFFICIENTS	19
V	FLUTTER SOLUTION PROCEDURE	25
VI	FLUTTER RESULTS FOR NACA 64A006 AIRFOIL	28
	(a) NACA 64A006 Airfoil Configuration	28
	(b) Aerodynamic Coefficients	30
	(c) Flutter Results	45
	1. Flutter Speeds for Flat Plate Pitching about ¼-Chord Axis at $M_\infty = 0.7$	51
	2. Flutter Speeds for NACA 64A006 Airfoil Pitching about ¼-Chord Axis with Varying μ at $M_\infty = 0.7$, 0.8, and 0.85	51
	3. Flutter Speeds for NACA 64A006 Airfoil Pitching about ¼-Chord Axis with Varying x_α at $M_\infty = 0.7$, 0.8, and 0.85	57
	4. Flutter Speeds for NACA 64A006 Airfoil Pitching about ¼-Chord Axis with Varying a_h at $M_\infty = 0.7$, 0.8, and 0.85	57
	5. Effect of Transformation of Aerodynamic Coefficients on the Flutter Results of NACA 64A006 Airfoil at $M_\infty = 0.8$ and 0.85	61
	6. Effect of Mach Number on Flutter Speed for NACA 64A006 Airfoil	65
VII	FLUTTER RESULTS FOR NACA 64A010 Airfoil	72
	(a) NACA 64A010 Airfoil Configuration	72
	(b) Aerodynamic Coefficients	72
	(c) Flutter Results	78
	1. Flutter Speeds for NACA 64A010 Airfoil Pitching about ¼-Chord Axis with Varying μ at $M_\infty = 0.72$, 0.76, and 0.8	78
	2. Flutter Speeds for NACA 64A010 Airfoil Pitching about ¼-Chord Axis with Varying x_α at $M_\infty = 0.72$, 0.76, and 0.8	84
	3. Flutter Speeds for NACA 64A010 Airfoil Pitching about ¼-Chord Axis with Varying a_h at $M_\infty = 0.72$, 0.76, and 0.8	90

TABLE OF CONTENTS (continued)

4. Effect of Mach Number on Flutter Speed for NACA 64A010 Airfoil 94

VIII CONCLUDING REMARKS 97

REFERENCES 101

LIST OF ILLUSTRATIONS

FIGURE		PAGE
1.	Definition of Parameters for Two Degrees of Freedom Aeroelastic Analysis	13
2.	Transformation of Aeroelastic Coefficients From Point O_1 to Point O_2	20
3.	NACA 64A006 Airfoil Configuration	29
4.	Distribution of Steady Pressure Coefficients for Thin Parabolic Airfoil (τ = 0.01) at M = 0.7	32
5.	Distribution of Unsteady Pressure Coefficients (Real Part) for Plates Pitching About 1/4 Chord with k_b = 0.05 and M = 0.7	34
6.	Distribution of Unsteady Pressure Coefficients (Imaginary Part) for Plates Pitching About 1/4 Chord with k_b = 0.05 and M = 0.7	35
7.	Distribution of Steady Pressure Coefficients for NACA 64A006 Airfoil at M = 0.7	41
8.	Distribution of Steady Pressure Coefficients for NACA 64A006 Airfoil at M = 0.8	42
9.	Distribution of Steady Pressure Coefficients for NACA 64A006 Airfoil at M = 0.85	43
10.	Distribution of Steady Pressure Coefficients for NACA 64A006 Airfoil at M = 0.9	44
11.	A Typical U-g Plot for NACA 64A006 Airfoil	50
12.	Comparison of Flutter Results Between Linear Flat Plate Theory and Present Parabolic Arc (τ = 0.01) Approximations By LTRAN2 and UTRANS2 at M = 0.7	52
13.	Effect of Mass Ratio on Flutter Speed for NACA 64A006 Airfoil for Various Frequency Ratios at M = 0.7	54
14.	Effect of Mass Ratio on Flutter Speed for NACA 64A006 Airfoil for Various Frequency Ratios at M = 0.8	55
15.	Effect of Mass Ratio on Flutter Speed for NACA 64A006 Airfoil for Various Frequency Ratios at M = 0.85	56
16.	Effect of Position of Mass Center on Flutter Speed for NACA 64A006 Airfoil for Various Frequency Ratios at M = 0.7	58

LIST OF ILLUSTRATIONS (continued)

FIGURE PAGE

17. Effect of Position of Mass Center on Flutter Speed for NACA 64A006 Airfoil for Various Frequency Ratios at M = 0.8 59

18. Effect of Position of Mass Center on Flutter Speed for NACA 64A006 Airfoil for Various Frequency Ratios at M = 0.85. 60

19. Effect of Position of Elastic Axis on Flutter Speed for NACA 64A006 Airfoil for Various Frequency Ratios at M = 0.7 62

20. Effect of Position of Elastic Axis on Flutter Speed for NACA 64A006 Airfoil for Various Frequency Ratios at M = 0.8. 63

21. Effect of Position of Elastic Axis on Flutter Speed for NACA 64A006 Aifoil for Various Frequency Ratios at M = 0.85 64

22. Effect of Transformation of Aerodynamic Coefficients (By Relaxation Method) on Flutter Speed for NACA 64A006 Airfoil at M = 0.8. 66

23. Effect of Transformation of Aerodynamic Coefficients (By Relaxation Method) on Flutter Speed for NACA 64A006 Airfoil at M = 0.85. 67

24. Effect of Transformation of Aerodynamic Coefficients (By Indicial Method) on Flutter Speed for NACA 64A006 Airfoil at M = 0.8. 68

25. Effect of Transformation of Aerodynamic Coefficients (By Indicial Method) on Flutter Speed for NACA 64A006 Airfoil at M = 0.85 69

26. Effect of Mach number on Flutter Speed of NACA 64A006 Airfoil for Various Frequency Ratios 71

27. NACA 64A010 Airfoil Configuration. 73

28. Distribution of Steady Pressure Coefficients for NACA 64A010 Airfoil at M = 0.72. 79

29. Distribution of Steady Pressure Coefficients for NACA 64A010 Airfoil at M = 0.76. 80

30. Distribution of Steady Pressure Coefficients for NACA 64A010 Airfoil at M = 0.8 81

31. Distribution of Steady Pressure Coefficients for NACA 64A010 Airfoil at M = 0.84. 82

32. Effect of Mass Ratio on Flutter Speed for NACA 64A010 Airfoil for Various Frequency Ratios at M = 0.72 83

33. Effect of Mass Ratio on Flutter Speed for NACA 64A010 Airfoil for Various Frequency Ratios at M = 0.76 85

LIST OF ILLUSTRATIONS (continued)

FIGURE		PAGE
34.	Effect of Mass Ratio on Flutter Speed for NACA 64A010 Airfoil for Various Frequency Ratios at M = 0.8.	86
35.	Effect of Position of Mass Center on Flutter Speed for NACA 64A010 Airfoil for Various Frequency Ratios at M = 0.72	87
36.	Effect of Position of Mass Center on Flutter Speed for NACA 64A010 Airfoil for Various Frequency Ratios at M = 0.76	88
37.	Effect of Position of Mass Center on Flutter Speed for NACA 64A010 Airfoil for Various Frequency Ratios at M = 0.8.	89
38.	Effect of Position of Elastic Axis on Flutter Speed for NACA 64A010 Airfoil for Various Frequency Ratios at M = 0.72	91
39.	Effect of Position of Elastic Axis on Flutter Speed for NACA 64A010 Airfoil for Various Frequency Ratios at M = 0.76	92
40.	Effect of Position of Elastic Axis on Flutter Speed for NACA 64A010 Airfoil for Various Frequency Ratios at M = 0.8.	93
41.	Effect of Mach Number on Flutter Speed of NACA 64A010 Airfoil for Various Frequency Ratios	96

LIST OF TABLES

TABLE		PAGE
1.	Aerodynamic coefficients for flat plates pitching at the quarter chord at M = 0.70	33
2.	Aerodynamic coefficients for NACA 64A006 pitching at the quarter chord at M = 0.70	37
3.	Aerodynamic coefficients for NACA 64A006 pitching at the quarter chord at M = 0.80	38
4.	Aerodynamic coefficients for NACA 64A006 pitching at the quarter chord at M = 0.85	39
5.	Aerodynamic coefficients for NACA 64A006 pitching at the quarter chord at M = 0.90	40
6.	Aerodynamic coefficients for NACA 64A006 pitching at the leading edge at M = 0.80	46
7.	Aerodynamic coefficients for NACA 64A006 pitching at the leading edge at M = 0.85	47
8.	Aerodynamic coefficients for NACA 64A006 pitching at the leading edge at M = 0.90	48
9.	Aerodynamic coefficients for NACA 64A006 pitching at the leading edge at M = 0.95	49
10.	Aerodynamic coefficients for NACA 64A010 pitching at the quarter chord at M = 0.72	74
11.	Aerodynamic coefficients for NACA 64A010 pitching at the quarter chord at M = 0.76	75
12.	Aerodynamic coefficients for NACA 64A010 pitching at the quarter chord at M = 0.80	76
13.	Aerodynamic coefficients for NACA 64A010 pitching at the quarter chord at M = 0.84	77

LIST OF SYMBOLS

SYMBOL	DEFINITION
a_h	distance between midchord and elastic axis measured in semi-chords, positive towards the trailing edge
[A]	aerodynamic matrix
b	semi-chord of the airfoil
c	full chord of the airfoil
$c_{\ell\delta}$	lift coefficient of the airfoil due to plunging
$c_{\ell\alpha}$	lift coefficient of the airfoil due to pitching
$c_{m\delta}$	moment coefficient of the airfoil due to plunging
$c_{m\alpha}$	moment coefficient of the airfoil due to pitching
g	structural damping coefficient
h	plunging degree of freedom, positive when measured downwards
I_α	polar moment of inertia about elastic axis
k_b	$\omega b/U$, reduced frequency with respect to semichord length b
k_c	$\omega c/U$, reduced frequency with respect to full chord length c
K_h	bending stiffness coefficient corresponding to plunging displacement
K_α	torsional stiffness coefficient corresponding to pitching rotation
[K]	matrix of stiffness coefficients
m	mass of the airfoil per unit span
M or M_∞	free stream Mach number
[M]	mass matrix
q	$\rho U^2/2$, dynamic pressure
Q_h	total aerodynamic lifting force
Q_α	total aerodynamic moment
r	distance measured along airfoil from elastic axis, positive towards trailing edge
r_α	$(I_\alpha/mb^2)^{1/2}$, radius of gyration about elastic axis

LIST OF SYMBOLS (continued)

SYMBOL	DEFINITION
S	airfoil static moment about elastic axis
t	time in seconds
U	free stream velocity
U^*	$U/b\omega_\alpha$, nondimensional flutter speed
x_p	distance between midchord and pitching axis measured in semi-chord, positive toward the trailing edge
x_α	distance between elastic axis and center of mass measured in semi-chord, positive toward trailing edge, (S/mb)
α	pitching degree of freedom
γ	ratio of specific heats
δ	h/c
λ	flutter eigenvalue
μ	$m/\pi\rho b^2$, airfoil-air mass ratio
ξ	h/b
ρ	free stream air density
τ	ratio between thickness of airfoil and chord length
ϕ	disturbance velocity potential
ω	flutter frequency of harmonic oscillation
ω_h	$\sqrt{K_h/m}$, uncoupled plunging frequency of airfoil
ω_α	$\sqrt{k_\alpha/I_\alpha}$, uncoupled torsional frequency of airfoil
ω_r	reference frequency used in flutter analysis
ω^*	ω/ω_α, nondimensional flutter frequency

SECTION I
INTRODUCTION

The numerical methods for the computation of aerodynamic forces of small-disturbance transonic flows about oscillating airfoils and planar wings have been rapidly developed in recent years. Such developments (References 1-32) are briefly discussed in the next section. The numerical methods for the computation of free vibration frequencies and normal modes and the time-history dynamic responses of wing structures have been well-developed. It is the time to integrate the developments in transonic aerodynamics and structural dynamics for aeroelastic applications.

Such aeroelastic applications have recently begun. In References 5, Traci, et al. performed a flutter analysis for the NACA 64A006 and NACA 64A410 airfoils based on the aerodynamic coefficients computed by using relaxation programs STRANS and UTRANS (References 4 and 6). The aerodynamic coefficients were obtained for the case that the airfoil pitches about the leading edge. The moment coefficients were then transformed from the leading edge to the elastic axis for flutter analysis. The flutter velocities and frequencies were obtained by using the U-g method (Reference 33). Primary results were obtained for the NACA 64A006 airfoil with two degrees of freedom, plunge and pitch. The results demonstrated the crucial importance of the transonic range by way of the drop in the flutter velocity parameter at $M = 0.85$ and the corresponding large variation in flutter frequency in this range. The restricted Mach number range of the aerodynamic data did not permit an in-depth examination of NACA 64A410 airfoil.

The effect of mean angle of attack and wind tunnel wall interference on the flutter parameters for the NACA 64A006 airfoil was also examined for the limited case for which the aerodynamic coefficients had been calculated.

Flutter calculations were also attempted for the NACA 64A006 airfoil with an additional degree of freedom of aileron oscillation. Due to the rather restricted reduced frequency range of their aerodynamic data, the true flutter velocity was not obtainable because an aileron dominated mode was fluttering at a frequency out of the data range. It was determined, however, that the aileron oscillation significantly damped the plunge mode which dominated the flutter boundary in the two degree of freedom case. The curious coupling of the aileron oscillation and plunge modes and the high frequency aileron buzz phenomena appear to be peculiar. A thorough examination of the three degree of freedom case, however, requires the generation of unsteady aerodynamic coefficients over a wider range of reduced frequencies than those calculated in Reference 5.

As an alternative but more complete solution, Ballhaus and Goorjian (Reference 28) proposed to use the time-integration and the indicial approaches for the aeroelastic response problems. They performed an aeroelastic response analysis for an NACA 64A006 airfoil with a single pitching degree of freedom. The time-history responses were computed using the computer program LTRAN2 for unsteady transonic flow coupled with an integration procedure for the simple differential equation of motion for the airfoil. The motion of the airfoil in a flow at $M_\infty = 0.88$ was forced for the first few cycles with an amplitude of 0.5 degrees until the pitching moment became periodic, after which the airfoil motion and the aerodynamic response were left free to drive each other. As the structural damping coefficient was varied parametrically, the responses were obtained for the highly damped, neutral, slightly divergent, and highly divergent cases. Another case with an initial amplitude of 1.5° and $M_\infty = 0.87$ was also calculated. This example illustrated the non-sinusoidal pitching-moment behavior that could result from the large shock-

wave excursions encountered at larger airfoil motion amplitudes.

From the development in Reference 28, it appears promising that the simultaneous integration of the flow and structure may lead to the solution of the transonic aeroelastic response problems for the multiple degree of freedom system.

As a visiting scientist at the Air Force Flight Dynamics Laboratory, Rizzetta published three reports (References 34-36) on his investigation of the transonic aeroelastic problems of two-dimensional airfoils.

In Reference 34, Rizzetta performed a flutter analysis of an NACA 64A010 airfoil with two degrees of freedom, plunge and pitch. The steady and unsteady transonic flows were computed by using the relaxation computer programs STRANS and UTRANS, respectively (Reference 4). The flutter velocities and frequencies were computed using the standard U-g method. Flutter data were obtained for two Mach numbers (0.72 and 0.80) and two angles of attack (0^{o} and 1^{o}).

It was reported that for both angles of attack and both Mach numbers the flutter velocity parameter decreased monotonically with increasing altitude and with increasing first mass moment. The flutter velocity parameter increased with increasing frequency ratio, defined as the square of the ratio of the plunge frequency to the pitch frequency. The increase in Mach number noticeably decreased the flutter speed parameter, especially in the presence of a shock. The study of the first mass moment was for its effect on the flutter suppression.

In Reference 35, Rizzetta performed a comparative study of the relaxation programs STRANS2 and UTRANS2 and the time-integration program LTRAN2 for calculating steady and unsteady aerodynamic pressures for an NACA 64A010 airfoil.

A finite difference mesh of 43x70 was used in the relaxation method and a mesh of 79x99 was used in the time integration method. Mach numbers considered were 0.72 and 0.82. The airfoil was pitching at an amplitude of $\alpha=1^{o}$ with reduced frequency k_c of 0.05 and 0.2, respectively. A mean angle of attack of 1 degree was also considered for M = 0.72, $\alpha = 0.5^{o}$ and $k_c = 0.05$. The agreement between the two solutions was good except for the unsteady results at M = 0.82 with the presence of shock. In that case, the peak lift value obtained from the time-integration method was approximately 50% higher than that from the harmonic analysis.

In Reference 36, Rizzetta performed an aeroelastic response study of an NACA 64A010 airfoil by simultaneously integrating the LTRAN2 aerodynamics program and the structural equations of motion. The study included a single degree of freedom case with airfoil pitching at quarter chord and a three degree of freedom case with airfoil pitching, plunging, and aileron pitching. The study, however, included neither the single degree of freedom case of airfoil plunging nor the two degree of freedom case with airfoil pitching and plunging.

Mach numbers considered were 0.72 and 0.82. Results were obtained as plots of nondimensional pitching displacement (and moment), plunging displacement (and lift), and aileron displacement (and moment) versus time for various values of the airfoil-air mass ratio μ. All these displacements and force quantities in the figures were divided by $\alpha'(o)$, the nondimensional initial pitching velocity defined in Reference 36. The values used for $\alpha'(o)$ ranges from 1 to a very high value of 7.5. By varying the values of μ, convergent, divergent, and neutral stable response curves were obtained.

In this report, flutter analyses were performed for an NACA 64A006 and an NACA 64A010 airfoil with pitching and plunging degrees of freedom. Two parallel sets of aerodynamic coefficients were obtained by using both the

relaxation method (STRANS2 and UTRANS2) and the indicial method (LTRAN2). The two sets of aerodynamic coefficients and the two corresponding sets of flutter results are compared and discussed.

To evaluate the linear solution obtained by using LTRAN2 and UTRANS2, a flat plate pitching about the quarter chord axis and plunging in the flow with M = 0.7 was considered. The solutions obtained for the unsteady pressure distributions by both methods were found to be in close agreement with the linear theory solution based on Kernel function method (The computer program was provided by Dr. Samuel R. Bland of NASA-Langley through private communication). Flutter results corresponding to these three sets of aerodynamic coefficients were obtained and compared.

For the NACA 64A006 airfoil, the Mach numbers considered were 0.7, 0.8, and 0.85, respectively. For the NACA 64A010 airfoil, the Mach numbers considered were 0.72, 0.76, and 0.80, respectively. For each airfoil and each Mach number, flutter velocities and the corresponding reduced frequencies were obtained by varying the airfoil-air mass ratio μ, plunge-pitch frequency ratio ω_h/ω_α, location of the mass center x_α, and location of the elastic axis a_h.

The two sets of flutter velocity curves, one based on the aerodynamic coefficients computed by using LTRAN2 and the other computed by using UTRANS2 are compared and discussed.

SECTION II

DEVELOPMENTS IN TRANSONIC FLOW COMPUTATION

Due to the fast development in digital computers, advances in the numerical computations of transonic flow fields around oscillating two-dimensional airfoils have been extensive.

The simplified basic aerodynamic equations, following the assumptions that the flow is two-dimensional, inviscid, transonic ($M_\infty \approx 1$), and that the velocity disturbances are small compared to the free stream velocity U, can be deduced from the general equation of continuity of gas dynamics as (Reference 1),

$$k_c^2 M_\infty^2 \phi_{tt} + 2k_c M_\infty^2 \phi_{xt} = V_c \phi_{xx} + \phi_{yy} \qquad (1)$$

where $k_c = \omega c/U$ is the reduced frequency; M is the free stream Mach number; ϕ is the disturbance velocity potential; $V_c = 1 - M^2 - (\gamma + 1) M^m \phi_x$; m is a function of M; and γ is the ratio of specific heats.

In deriving the above equation, the coordinate system is fixed with respect to the airfoil, and x is aligned with the free stream direction. The flow is defined as locally subsonic or supersonic, relative to the fixed coordinate system, for $V_c > 0$ or $V_c < 0$, respectively. A measure of the degree of unsteadiness is given by the reduced frequency k_c when the airfoil is oscillating periodically with a frequency ω.

Several numerical approaches have been developed for the solution of transonic flow fields governed by Equation 1.

(a) The Harmonic or Relaxation Approach

This appraoch was first developed for steady flows by Murman and Cole (Reference 2). It was improved and extended by many computational aerodynamicists to treat the small - disturbance steady and unsteady transonic flows about

oscillating airfoils and planar wings (see, for example, References 2 to 32). To solve for Equation 1, it requires the solution of the following perturbation equation for the potential functions

$$\phi(x,y,z,t) = \phi_0(x,y,z) + \varepsilon\phi_1(x,y,z)e^{i\omega t} \qquad (2)$$

where ϕ is the small-disturbance velocity potential; $\varepsilon << 1$ is related to the small amplitude of the body motion; ϕ_0 is the mean steady-state solution and ϕ_1 is dependent upon ϕ_0. The small-disturbance potential equation for the steady flow is nonlinear. The equation for the first order unsteady flow is linear when ϕ^2 is dropped, and for the case of harmonic boundary disturbances, its reduced wave equation form is of mixed elliptical/hyperbolic type depending upon the nature of the steady solution. Both steady and unsteady equations can be solved by the mixed differencing line relaxation procedure first proposed for steady flows by Murman and Cole (Reference 2).

Based on this approach, Traci et al. developed four computer programs: STRANS; UTRANS; TDSTRN; and TDUTRN. Programs STRANS and UTRANS are for two-dimensional small-disturbance steady and unsteady transonic flows about oscillating airfoils, respectively (References 3 and 4). Programs TDSTRN and TDUTRN are the three-dimensional versions of STRANS and UTRANS, respectively, for flows about oscillating rectangular planar wings (References 5 and 6). A user's guide for the improved version of the computer programs STRANS2 and UTRANS2 was prepared by Holman (Reference 8).

Within the basic framework of the relaxation method, Ehlers (Reference 9) and Weatherill, Sebastian, and Ehlers (Reference 10) developed numerical methods comparable to those done in References 3 to 8 but less extensive. They computed the flow fields around a flat plate, an NACA 64A006 airfoil, and a rectangular planform wing with an aspect ratio of 5. Ballhaus and Bailey

(Reference 11) dealt with a constant chord, 23.75° sweptback planform model with an aspect ratio of 4 and with a Lockheed C141 airfoil section. Ballhaus, Bailey, and Frick later included two additional terms in the governing flow equations and computed the surface pressures for the HiMAT wing and the ONERA M-6 wing (Reference 12). Krupp and Cole (Reference 13) analyzed an NACA 0012 airfoil performing plunging oscillations at high subsonic speeds. The results showed the existence of a moving shock in the locally supersonic zone.

In a recent study (Reference 14), Ballhaus, Jameson, and Albert compared the implicit approximate-factorization (AF) algorithms with the successive line over-relaxation (SLOR) method for the solution of nonlinear, two-dimensional, steady transonic small disturbance equation for flows about several airfoils. They concluded that the AF method required substantially less computer time than the SLOR method.

(b) The Time-Integration Approach

As a further simplification of Equation 1, the frequency of the transonic flow can be assumed as low so that $k_c \approx 1 - M_\infty^2 \approx \tau^{2/3} << 1$. Equation 1 may then be reduced to

$$2 k_c M_\infty^2 \phi_{xt} = V_c \phi_{xx} + \phi_{yy} \qquad (3)$$

where τ is the thickness-chord ratio of the airfoil.

Equation 3 is suitable for the time-integration approach. This approach is based on the finite-difference scheme that integrates Equation 3 in time for harmonic aerodynamic motions until the transient states in the solution disappear and the forces become periodic.

This method can handle mixed flows and shocks within the accuracy of the finite-difference mesh (Reference 15). Computations of flows about two-dimensional airfoils oscillating at supercritical Mach numbers were performed by Magnus and Yoshihara (Reference 16) and Beam and Warming (Reference 17). Such time dependent calculations involve no inherent limiting assumption so they are quite expensive in computing time.

A semi-implicit scheme was used by Ballhaus and Lomax (Reference 18) to obtain the time-accurate solution to the low-frequency unsteady small-disturbance transonic flow potential equation. Fully implicit schemes were developed by Beam and Warming (Reference 19) and Ballhaus and Steger (Reference 20) which permit time-step selection based on accuracy rather than stability considerations. More recently, a computer code, LTRAN2, was developed by Ballhaus and Goorjian (Reference 21) which solves the two-dimensional, nonlinear, low-frequency, small-disturbance transonic flow equation by an alternating-direction implicit algorithm. The program showed considerable improvement in computing efficiency.

A time-marching semi-implicit finite-difference technique was used by Isogai (Reference 22) to solve the full potential equation for unsteady transonic flow fields around oscillating airfoils. The shock-wave motions were properly captured using the quasi-conservative scheme proposed by Jameson (Reference 23) and Bauer and Korn (Reference 24) for the steady flow problem. Numerical examples showed that for weak shock waves, the method could give a reliable result for a thick, blunt-nosed airfoil, such as a modern supercritical airfoil

In a recent study (Reference 25), Yu, Seebass, and Ballhaus improved the LTRAN2 program by including an implicit shock-fitting algorithm and an analytically stretched coordinate system. Shock waves were treated as discontinuities normal to the free stream. Results were given for an NACA

64A006 airfoil with oscillating quarter-chord flap. In Reference 26 Fung, Yu, and Seebass provided a method that accounted for shock wave motions due to arbitrary but unsteady changes in the boundary conditions. Thus both harmonic and indicial responses may be determined. Similar work was also carried out by Nixon (Reference 27).

(c) Indicial Method

In solving for the flutter eigenvalue equations, it is required to evaluate the aerodynamic coefficients for a wide range of reduced frequencies and different modes of motion such as plunging, pitching, and aileron pitching, etc. For each given Mach number, reduced frequency, and mode of motion, both the aforementioned relaxation and time-integration methods require the solution of complete flow fields in order to provide the aerodynamic coefficients. Both methods are thus highly time-consuming for the purpose of flutter analysis.

For the purpose of generating aerodynamic coefficients, a computationally more efficient approach, the indicial method, was used by Ballhaus and Goorjian (Reference 28). This method was commonly used in the case of subsonic flow (see, for example, Reference 29). In the transonic application, the method has a major advantage that the aerodynamic coefficients can be computed for a given Mach number, mode of motion and a wide range of reduced frequencies by performing only a single flow field computation, the indicial response.

The indicial response is the flow-field response to a step change in the given mode of motion, and it is computed using a time-accurate finite-difference scheme. From the indicial response, the solution for all oscillation frequencies can be obtained by computing the simple integrals in the form of Duhamel's integral at a small fraction of the cost of the complete flow-field solution

needed by the relaxation approach. For the indicial approach, the unsteady solution must be treated as a small linear perturbation about some nonlinear steady-state solution.

The indicial approach was described in Reference 28 by Ballhaus and Goorjian and applied for an aeroelastic response analysis of an NACA 64A006 airfoil pitching in the small-disturbance unsteady transonic flow.

(d) Other Methods

Another promising approach for both the steady and unsteady transonic aerodynamics, which is in a separate category, is the finite element approach. The development of this approach is still in the early stage. An account of such developments can be found in a special section in Reference 30 and Reference 31.

In a recent report, Tijdeman (Reference 32) presented wind tunnel results of a conventional airfoil with an oscillating flap and a supercritical airfoil oscillating in pitch in high subsonic and transonic flow. The current status of unsteady transonic flow theory was reviewed and his test data were used to evaluate some of the recently developed computational methods.

SECTION III

AEROELASTIC EQUATIONS OF MOTION FOR TWO-DIMENSIONAL AIRFOIL WITH PITCH AND PLUNGE DEGREES OF FREEDOM

In the present flutter analysis of two-dimensional airfoils in the transonic flow, it is assumed that the airfoils oscillate with two degrees of freedom, plunge and pitch. The aeroelastic equations of motion will be derived in this section.

Figure 1 shows an airfoil plunging with a positive displacement h (down) and pitching with a positive angle α (with the nose up) about the elastic axis. The elastic axis is located at a distance $a_h b$ from the midchord while the mass center is located at a distance $x_\alpha b$ from the elastic axis. Both distances are defined as positive when measured toward the trailing edge. For example, if the elastic axis is at 1/4 chord from the leading edge, $a_h = -0.5$.

The aeroelastic equations of motion are derived by setting up the equilibrium equations for three physical quantities: the inertia forces, the elastic forces, and the aerodynamic forces.

The total vertical inertia force per unit span is equal to

$$- \int (\ddot{h} + r\ddot{\alpha})dm = - (m\ddot{h} + S\ddot{\alpha}) \qquad (4)$$

where

m = total mass of the airfoil with unit span;

r = distance from elastic axis, positive when measured toward trailing edge

dm = a differential element of mass; and

$S = \int r dm$ = static moment of the airfoil about the elastic axis.

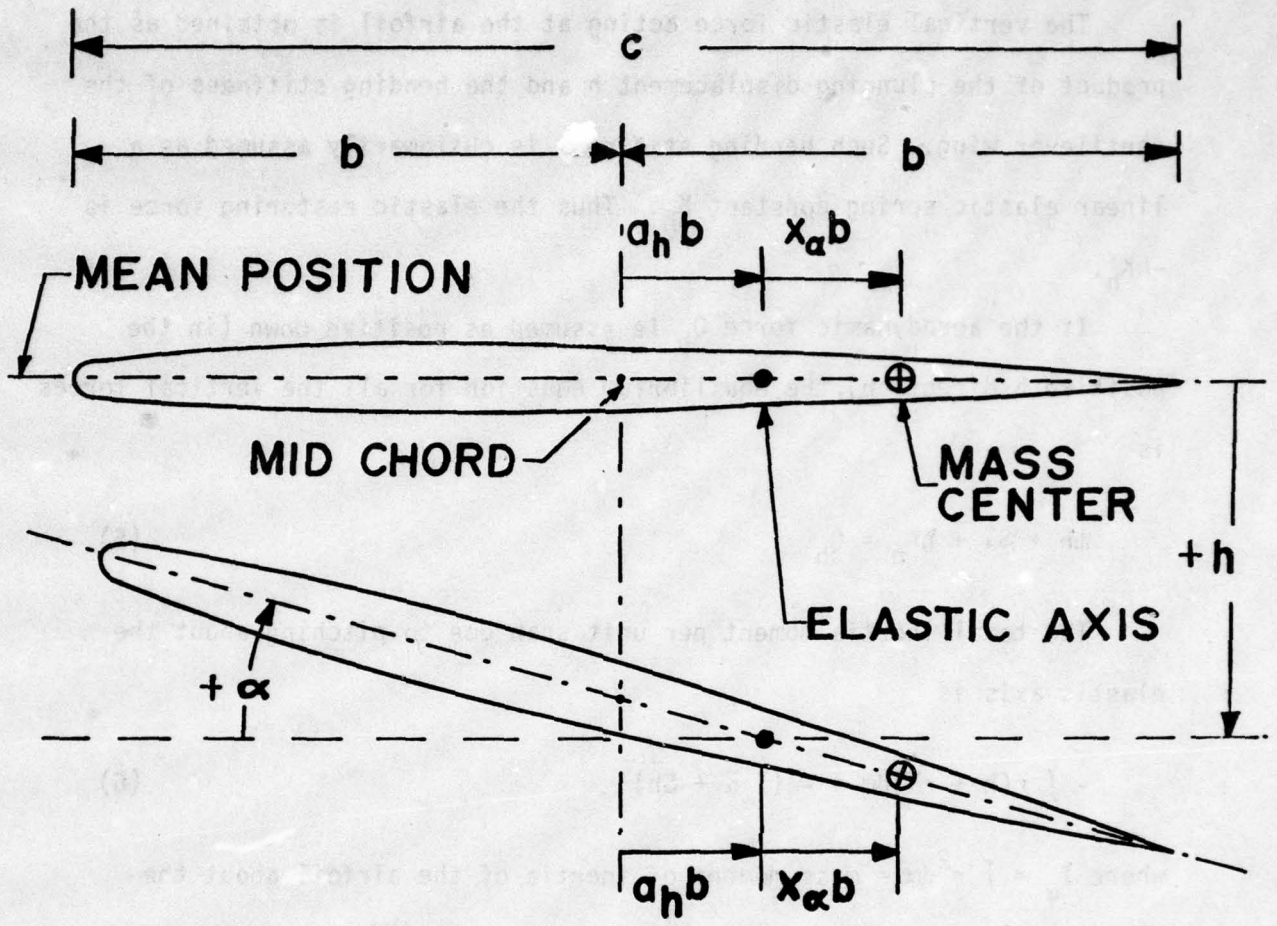

Figure 1. Definition of Parameters for Two Degrees of Freedom Aeroelastic Analysis

The vertical elastic force acting at the airfoil is obtained as the product of the plunging displacement h and the bending stiffness of the cantilever wing. Such bending stiffness is customarily assumed as a linear elastic spring constant K_h. Thus the elastic restoring force is $-hK_h$.

If the aerodynamic force Q_h is assumed as positive down (in the positive h direction), the equilibrium equation for all the vertical forces is

$$m\ddot{h} + S\ddot{\alpha} + hK_h = Q_h \tag{5}$$

The total inertia moment per unit span due to pitching about the elastic axis is

$$-\int r(\ddot{h} + r\ddot{\alpha})dm = -(I_\alpha \ddot{\alpha} + S\ddot{h}) \tag{6}$$

where $I_\alpha = \int r^2 dm$ = mass moment of inertia of the airfoil about the elastic axis.

The elastic torsional moment acting at the airfoil is obtained as the product of the angle of pitch and the torsional stiffness of the cantilever wing. Such torsional stiffness is assumed as a linear elastic spring constant K_α. Thus the elastic restoring moment is $-\alpha K_\alpha$.

If the aerodynamic moment Q_α acting at the elastic axis is assumed as positive in the positive α direction, the equilibrium equation for all the moments is

$$S\ddot{h} + I_\alpha \ddot{\alpha} + \alpha K_\alpha = Q_\alpha \tag{7}$$

Equation 5 can be written in a nondimensional form by dividing by mb,

$$\ddot{\xi} + x_\alpha \ddot{\alpha} + \xi \omega_h^2 = Q_h/mb \tag{8}$$

where $\xi = h/b$ is the nondimensional plunging displacement; $\omega_h = (K_h/m)^{1/2}$ is the uncoupled plunging frequency; and $x_\alpha = S/mb$ is a coefficient to be multiplied by the semichord length to locate the mass center from elastic axis.

Assuming harmonic oscillation, ξ and α may be written as

$$\begin{cases} \xi = \xi_o e^{i\omega t} \\ \alpha = \alpha_o e^{i\omega t} \end{cases} \tag{9}$$

where ω is the circular frequency of oscillation and ξ_o and α_o are the amplitudes in plunge and pitch, respectively. Following the definitions of Equation 9, Equation 8 becomes

$$-\xi_o - x_\alpha \alpha_o + \xi_o (\omega_h/\omega)^2 = Q_h e^{-i\omega t}/mb\omega^2 \tag{10}$$

For more general application, the right hand side of Equation 10 is rewritten to include the customary aeroelastic constant μ, q, and k_b,

$$-\xi_o - x_\alpha \alpha_o + \xi_o (\omega_h/\omega)^2 = Q_h e^{-i\omega t}/2\pi bq\mu k_b^2 \tag{11}$$

where $\mu = m/\pi b^2 \rho$ is the airfoil - air mass ratio; $q = \rho U^2/2$ is the dynamic pressure; and $k_b = \omega b/U$ is the reduced frequency.

The aerodynamic lifting force Q_h is attributed to both plunging and pitching motions. It can be obtained by superposing the effects of the two motions through the use of aerodynamic coefficients $c_{\ell\delta}$ and $c_{\ell\alpha}$. Such superposition is valid when the aerodynamic equations considered are linear. When the aerodynamic equations considered are nonlinear, such superposition may, however, still be valid under the assumption of

linearization of the unsteady part of the flow. The linearization is valid when the displacements are assumed to be small. Such assumption is in agreement with the small perturbation aerodynamic theory used to solve the present nonlinear transonic flow equations.

The lifting force Q_h can then be written as

$$Q_h = - (c_{\ell\delta}\delta + c_{\ell\alpha}\alpha)qc \tag{12}$$

where $c_{\ell\delta}$ is the lifting coefficient of the airfoil due to plunging; $c_{\ell\alpha}$ is the lifting coefficient of the airfoil due to pitching about the elastic axis; and $\delta = h/c = \xi/2$. It should be noted that the lifting force is defined as positive upward in the aerodynamic equations and this sign convention is used in the presentation of the subsequent tables of aerodynamic coefficients. On the other hand, the lifting force is defined as positive downward in the present flutter equations. Thus there is a negative sign in Equation 12.

Assuming that the airfoil oscillates harmonically with circular frequency ω yields

$$Q_h = - e^{i\omega t} (c_{\ell\delta}\xi_o/2 + c_{\ell\alpha}\alpha_o)qc \tag{13}$$

Substituting Equation 13 into Equation 11 and rearranging the terms gives

$$\mu k_b^2(\xi_o + x_\alpha\alpha_o) - \frac{1}{\pi} (c_{\ell\delta}\xi_o/2 + c_{\ell\alpha}\alpha_o)$$

$$= \xi_o\mu k_b^2(\omega_h/\omega)^2 \tag{14}$$

A similar procedure can be used to treat the second equation of motion. Dividing Equation 7 by mb^2 yields

$$x_\alpha\ddot{\xi} + r_\alpha^2\ddot{\alpha} + r_\alpha^2\omega_\alpha^2\alpha = Q_\alpha/mb^2 \tag{15}$$

where $r_\alpha = (I_\alpha/mb^2)^{1/2}$ is the coefficient to be multiplied by the semi-chord to give the radius of gyration about the elastic axis; and $\omega_\alpha = (K_\alpha/I_\alpha)^{1/2}$ is the uncoupled pitching frequency.

Assuming harmonic oscillation gives

$$- x_\alpha \xi_o - r_\alpha^2 \alpha_o + r_\alpha^2 (\omega_\alpha/\omega)^2 \alpha_o = Q_\alpha e^{-i\omega t}/mb^2\omega^2.$$

$$= 2\, Q_\alpha e^{-i\omega t}/\pi\mu k_b^2 qc^2 \tag{16}$$

Based on the aforementioned assumption of linear superposition, the aerodynamic moment can be obtained as

$$Q_\alpha = qc^2 c_{m\delta}\delta + qc^2 c_{m\alpha}\alpha \tag{17}$$

where $c_{m\delta}$ and $c_{m\alpha}$ are the moment coefficients of the airfoil about the elastic axis due to plunging and pitching (about the elastic axis), respectively.

For harmonic oscillation

$$Q_\alpha = e^{i\omega t}(c_{m\delta}\xi_o/2 + c_{m\alpha}\alpha_o)qc^2 \tag{18}$$

Substituting Equation 18 into Equation 16 and rearranging the terms gives

$$\mu k_b^2 (x_\alpha \xi_o + r_\alpha^2 \alpha_o) + \frac{2}{\pi}(c_{m\delta}\xi_o/2 + c_{m\alpha}\alpha_o)$$

$$= r_\alpha^2 (\omega_\alpha/\omega)^2 \alpha_o \mu k_b^2 \tag{19}$$

Grouping the terms in Equations 14 and 19, the final eigenvalue equations for flutter analysis of an airfoil with plunging and pitching degrees of freedom are obtained,

$$\left[\mu k_b^2 [M] - [A]\right]\begin{Bmatrix}\xi_o \\ \alpha_o\end{Bmatrix} = \lambda [K]\begin{Bmatrix}\xi_o \\ \alpha_o\end{Bmatrix} \tag{20}$$

where [M], [A], and [K] are termed here as mass, aerodynamic, and stiffness matrices, respectively, and they are defined as

$$[M] = \left[\begin{array}{c|c} 1 & x_\alpha \\ \hline x_\alpha & r_\alpha^2 \end{array}\right]$$

$$[A] = \frac{1}{\pi}\left[\begin{array}{c|c} c_{\ell\delta}/2 & c_{\ell\alpha} \\ \hline -c_{m\delta} & -2c_{m\alpha} \end{array}\right] \tag{21}$$

$$[K] = \left[\begin{array}{c|c} (\omega_h/\omega_r)^2 & 0 \\ \hline 0 & r_\alpha^2(\omega_\alpha/\omega_r)^2 \end{array}\right]$$

where ω_r is a reference frequency.

The eigenvalue λ is a complex number defined as

$$\lambda = \mu(1 + ig)\omega_r^2 b^2/U^2 \tag{22}$$

where g is the so-called structural damping coefficient which is assumed to be small (as defined in Reference 33) and it is assumed to be the same for both plunging and pitching modes.

SECTION IV

TRANSFORMATION OF AERODYNAMIC COEFFICIENTS

In obtaining the aerodynamic coefficients, it is a common practice to pitch the airfoil about the elastic axis so that such coefficients can be directly used to compute the aerodynamic matrix [A] for aeroelastic analysis. It is, however, not uncommon that the pitching axis for obtaining the aerodynamic coefficients is different from the elastic axis. In that case, the aerodynamic coefficients with reference to the pitching axis must be transformed to those with reference to the elastic axis for aeroelastic analysis. It is the purpose of this section to derive a set of transformation equations.

The following derivations of the transformation equations for aerodynamic coefficients between two points of pitching are valid only for linear aerodynamic theory. In the transonic region where aerodynamic equations are nonlinear, the present transformation equations are valid only under the assumption of small linear disturbances about a nonlinear steady flow. Also it may be noted that the effect of local angle of attack which depends on the location of the point of pitching of the airfoil for a nonlinear case is not accounted for in the present derivation of transformation equations.

Figure 2 shows an airfoil pitching about point O_1 which is at a distance bx_p aft midchord point C. It is assumed that the aerodynamic coefficients have been computed for this pitching axis with the lift acting positive downward. The aerodynamic lifting force and moment at point O_1 are designated as Q_{h1} and $Q_{\alpha 1}$, respectively. The lifting and moment aerodynamic coefficients at O_1 due to plunging and pitching at O_1 are designated as $c_{\ell\delta 1}$, $c_{\ell\alpha 1}$, $c_{m\delta 1}$, and $c_{m\alpha 1}$, respectively. It is desired to transform these aerodynamic coefficients to those at point O_2, which is the pitching point assumed in

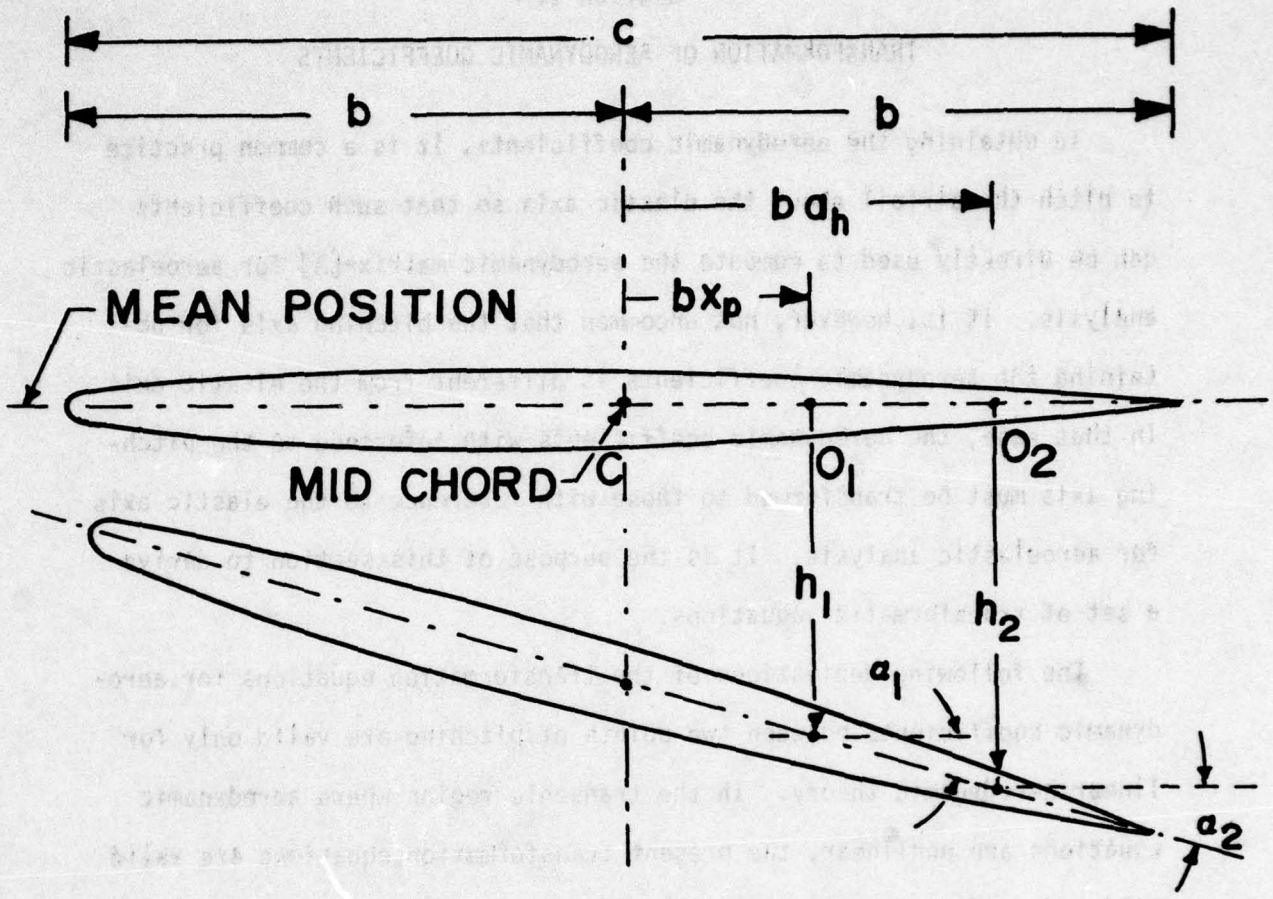

Figure 2. Transformation of Aeroelastic Coefficients from Point O_1 to Point O_2

the aeroelastic analysis and it is located at a distance ba_h aft the mid-chord point C.

After the transformation, the aerodynamic lifting force, moment, and the four aerodynamic coefficients at point O_2 are designated as Q_{h_2}, Q_{α_2}, $c_{\ell\delta_2}$, $c_{\ell\alpha_2}$, $c_{m\delta_2}$, and $c_{m\alpha_2}$, respectively.

Considering the equilibrium of the aerodynamic lifting forces and moments at point O_2 gives

$$\begin{cases} Q_{h_2} = Q_{h_1} \\ Q_{\alpha_2} = (a_h - x_p)(c/2)Q_{h_1} + Q_{\alpha_1} \end{cases} \tag{23}$$

Defining that

$$s = (a_h - x_p)/2 \tag{24}$$

gives

$$\begin{Bmatrix} Q_{h_2} \\ \hline Q_{\alpha_2} \end{Bmatrix} = \left[\begin{array}{c|c} 1 & 0 \\ \hline sc & 1 \end{array}\right] \begin{Bmatrix} Q_{h_1} \\ \hline Q_{\alpha_1} \end{Bmatrix} \tag{25}$$

For small angle of pitch and rigid airfoil

$$\begin{cases} h_2 = h_1 + sc\alpha_1 \\ \alpha_2 = \alpha_1 \end{cases} \tag{26}$$

With the definitions that

$$\begin{cases} \delta_1 = h_1/c \\ \delta_2 = h_2/c \end{cases} \tag{27}$$

Equations 26 can be written in a nondimensional matrix form

$$\left\{ \begin{matrix} \delta_2 \\ \alpha_2 \end{matrix} \right\} = \left[\begin{array}{c|c} 1 & s \\ \hline 0 & 1 \end{array} \right] \left\{ \begin{matrix} \delta_1 \\ \alpha_1 \end{matrix} \right\} \tag{28}$$

Based on the definitions of aerodynamic coefficients, the lifting force and moment at O_1 are given as

$$\begin{cases} Q_{h_1} = - qc(c_{\ell\delta_1}\delta_1 + c_{\ell\alpha_1}\alpha_1) \\ Q_{\alpha_1} = qc^2(c_{m\delta_1}\delta_1 + c_{m\alpha_1}\alpha_1) \end{cases} \tag{29}$$

Equation 29 can be written in a matrix form as

$$\left\{ \begin{matrix} Q_{h_1} \\ Q_{\alpha_1} \end{matrix} \right\} = [E] \left\{ \begin{matrix} \delta_1 \\ \alpha_1 \end{matrix} \right\} \tag{30}$$

where

$$[E] = qc \left[\begin{array}{c|c} -c_{\ell\delta_1} & -c_{\ell\alpha_1} \\ \hline cc_{m\delta_1} & cc_{m\alpha_1} \end{array} \right] \tag{31}$$

Similar relations can be obtained with reference to point O_2

$$\left\{ \begin{matrix} Q_{h_2} \\ Q_{\alpha_2} \end{matrix} \right\} = [F] \left\{ \begin{matrix} \delta_2 \\ \alpha_2 \end{matrix} \right\} \tag{32}$$

where

$$[F] = qc \left[\begin{array}{c|c} -c_{\ell\delta_2} & -c_{\ell\alpha_2} \\ \hline cc_{m\delta_2} & cc_{m\alpha_2} \end{array} \right] \tag{33}$$

Substituting Equations 30 and 32 into the equilibrium equation 25 yields

$$[F]\begin{Bmatrix}\delta_2\\ \alpha_2\end{Bmatrix} = \left[\begin{array}{c|c} 1 & 0 \\ \hline sc & 1 \end{array}\right] [E]\begin{Bmatrix}\delta_1\\ \alpha_1\end{Bmatrix} \tag{34}$$

Substituting Equation 28 for δ_2 and α_2 into Equation 34, cancelling out δ_1 and α_1, and then rearranging the equation gives

$$[F] = \left[\begin{array}{c|c} 1 & 0 \\ \hline sc & 1 \end{array}\right] [E] \left[\begin{array}{c|c} 1 & s \\ \hline 0 & 1 \end{array}\right]^{-1}$$

$$= \left[\begin{array}{c|c} f_{11} & f_{12} \\ \hline f_{21} & f_{22} \end{array}\right] \tag{35}$$

where

$$\begin{cases} f_{11} = -qcc_{\ell\delta_1} \\ f_{12} = qcsc_{\ell\delta_1} - qcc_{\ell\alpha_1} \\ f_{21} = -qc^2sc_{\ell\delta_1} + qc^2c_{m\delta_1} \\ f_{22} = qc^2s^2c_{\ell\delta_1} - qc^2sc_{\ell\alpha_1} - qc^2sc_{m\delta_1} \\ \qquad + qc^2c_{m\alpha_1} \end{cases} \tag{36}$$

Thus matrix [F] is defined in both Equations 33 and 36. Equating the corresponding entries in the two matrices gives

$$\begin{cases} c_{\ell\delta_2} = c_{\ell\delta_1} \\ c_{\ell\alpha_2} = c_{\ell\alpha_1} - sc_{\ell\delta_1} \\ c_{m\delta_2} = c_{m\delta_1} - sc_{\ell\delta_1} \\ c_{m\alpha_2} = c_{m\alpha_1} - s(c_{\ell\alpha_1} + c_{m\delta_1}) + s^2c_{\ell\delta_1} \end{cases} \tag{37}$$

The terms $sc_{\ell\delta_1}$, $sc_{m\delta_1}$, and $s^2c_{\ell\delta_1}$ are relatively small as compared with other terms. If these three terms are neglected, Equations 37 are reduced to precisely the same form as that presented in Reference 5 by Traci et al.

SECTION V

FLUTTER SOLUTION PROCEDURE

Methods for the solution of flutter eigenvalue equations are available in common texts of aeroelasticity (see, for example, Reference 33). In this study, the standard U-g method is used. The basic idea of the U-g method is to search for a set of aeroelastic parameters that result in a positive real eigenvalue λ or a zero structural damping coefficient g.

In the solution of the present flutter eigenvalue Equation 20, the mass matrix [M] and the stiffness matrix [K] can be obtained for a set of specified parameters: airfoil-air mass ratio μ; location of the mass center x_α; radius of gyration r_α; plunging frequency ω_h; pitching frequency ω_α; and a reference frequency ω_r (used for nondimensionalization). In this study, ω_r is always assumed as unity.

To obtain the aerodynamic matrix [A], aerodynamic coefficents $c_{\ell\delta}$, $c_{\ell\alpha}$, $c_{m\delta}$, and $c_{m\alpha}$ must be first computed based on the following given conditions: airfoil configuration; free stream Mach number M; location of the point of pitching x_p, and reduced frequency k_c. If the point of pitching does not coincide with the elastic axis, the four aerodynamic coefficients must be transformed to the elastic axis. Such transformation procedure has been given in detail in Section IV.

After the three matrices [M], [A], and [K] are found, Equation 20 can be solved directly and the two complex eigenvalues λ_1 and λ_2 can be obtained. The flutter phenomenon is obtained when either of the two eigenvalues is positive and real or when either of the two corresponding structural damping coefficients g is zero. The eigenvector corresponding

to λ_1 or λ_2, respectively, gives the ratio between plunging and pitching mode amplitudes which describes the flutter mode.

In order to search for the flutter solution, the reduced frequency k_c is varied in small increments, the corresponding aerodynamic coefficients are computed, and the corresponding eigenvalues λ's are obtained from Equation 20. The flutter solution is obtained when a positive real eigenvalue λ is found. The repetitive computations of such transonic aerodynamic coefficients are enormously laborious and expensive. It appears desirable to compute a table of aerodynamic coefficients based on selected values of k_c with appropriate intervals so that the aerodynamic coefficients for any k_c value within the acceptable range can be obtained by the method of interpolation or extrapolation. In this study, typical values chosen for k_c are 0.0, 0.05, 0.10, 0.15, 0.2, 0.25, and 0.3. The method of interpolation is based on the Lagrange interpolation formula as described in common texts on numerical methods (see, for example, Reference 37).

In this study, the eigenvalue is defined as

$$\lambda = \mu(1 + ig)\omega_r^2 b^2/U^2 \tag{38}$$

Thus the search for a positive real eigenvalue λ becomes the search for zero value of g, the so-called structural damping coefficient. As the reduced frequency k_c varies in small increment, the corresponding g value changes. The zero g value is obtained when it changes sign. Physically, the airfoil goes from a stable state to an unstable state when the g value changes from negative to positive, and vice versa.

At the flutter points, g = 0 and

$$\lambda = \mu\omega_r^2 b^2/U^2 \tag{39}$$

For general application, the results for the flutter speed and flutter frequency are nondimensionalized as

$$U^* = U/b\omega_\alpha \tag{40}$$

and

$$\omega^* = \omega/\omega_\alpha \tag{41}$$

respectively.

Incorporating Equation 39 into Equations 40 and 41 in an appropriate manner and using the definition that $k_b = \omega b/U$ gives

$$U^* = (\omega_r/\omega_\alpha)\sqrt{\mu/\lambda} \tag{42}$$

and

$$\omega^* = k_b(\omega_r/\omega_\alpha)\sqrt{\mu/\lambda} \tag{43}$$

SECTION VI

FLUTTER RESULTS FOR NACA 64A006 AIRFOIL

(a) NACA 64A006 Airfoil Configuration

In order to perform accurate aerodynamic computations, it is necessary to use accurate data for the airfoil configurations, especially in the region of the leading edge. The equations for accurate curve fitting and tabulated data for eight AGARD/SMP standard airfoil configurations were provided by Dr. J.J. Olsen of the Air Force Flight Dynamics Laboratory (Reference 38).

The equations for the eight airfoil configurations were given by Dr. Olsen as

$$\begin{cases} Z_u(x) = c(x) + 0.5\ t(x) \\ Z_\ell(x) = c(x) - 0.5\ t(x) \\ t(x) = a_0\sqrt{x} + a_1 + a_2x + a_3x^2 + a_4x^3 + a_5x^4 \\ c(x) = \quad b_1 + b_2x + b_3x^2 + b_4x^3 + b_5x^4 \end{cases} \tag{44}$$

where $Z_u(x)$ and $Z_\ell(x)$ are the equations for the upper and lower surfaces, respectively; x is the nondimensional axis with leading edge at x = 0 and trailing edge at x = 1; c(x) is the function of camber; t(x) is the function of thickness; and constants a's and b's for the eight airfoils are available in Reference 38.

In this study, an NACA 64A006 airfoil was first selected for flutter analysis. There is no camber for this airfoil. The constants for the thickness function are: $a_0 = 0.1369014$; $a_1 = 0$; $a_2 = -0.0496509$; $a_3 = 0.0609015$; $a_4 = -0.3455406$; $a_5 = 0.1976486$. The airfoil configuration was plotted in Figure 3. Part IV of Reference 38 contains revised coefficients, however the above values are suitable for purpose of illustration.

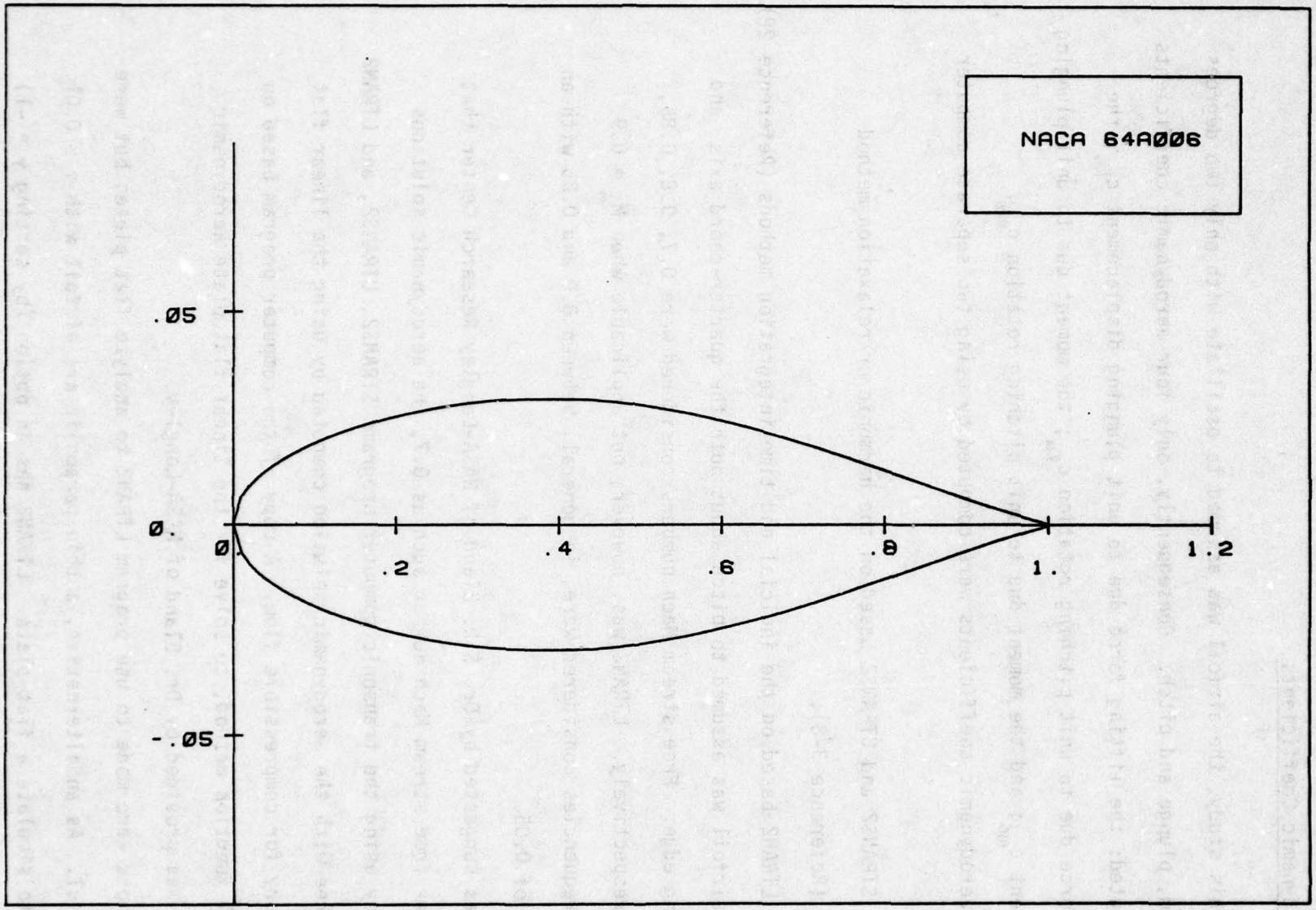

Figure 3. NACA 64A006 Airfoil Configuration

(b) Aerodynamic Coefficients

In this study, the airfoil was assumed to oscillate with only two degrees of freedom, plunge and pitch. Consequently, only four aerodynamic coefficients were computed: the lifting force due to unit plunging displacement $c_{\ell\delta}$; the lifting force due to unit pitching rotation $c_{\ell\alpha}$; the moment due to unit plunging displacement $c_{m\delta}$; and the moment due to unit pitching rotation $c_{m\alpha}$.

The aerodynamic coefficients were computed by using two separate computer programs:

(1) STRANS2 and UTRANS2 based on the harmonic or relaxation method (Reference 3-8);

(2) LTRAN2 based on the indicial and time-integration methods (Reference 28).

The airfoil was assumed to pitch about both the quarter-chord axis and the leading edge. Free stream Mach numbers considered were 0.7, 0.8, 0.85, and 0.9, respectively. LTRAN2 was, however, not applicable when $M_\infty = 0.9$. Reduced frequencies considered were, in general, between 0.0 and 0.25 with an increment of 0.05.

It was suggested by Dr. S.R. Bland of NASA-Langley Research Center that for a lower free stream Mach number such as 0.7, the aerodynamic solutions computed by using the transonic computer programs STRANS2, UTRANS2, and LTRAN2 should agree with the aerodynamic solution computed by using the linear flat plate theory for compressible flow. A copy of the computer program based on the Kernel function method, to solve for the linear flat plate aerodynamic equation, was provided by Dr. Bland of NASA-Langley.

Attempts were made to use program LTRAN2 to analyze flat plates but were unsuccessful. As an alternative, a thin parabolic arc airfoil with $\tau = 0.01$ was used to simulate a flat plate. LTRAN2 has an option (by setting $\gamma = -1$)

for the solution of only the linear aerodynamic equation. This option was used. Although STRANS2 and UTRANS2 can accurately treat a flat plate, the same thin parabolic arc airfoil was chosen for the analysis so that the results obtained from both the time-integration program and the relaxation program can be compared directly.

Figure 4 shows the distributions of steady pressure coefficients for the thin parabolic arc airfoil with $\tau = 0.01$ at $M = 0.7$ obtained by using both STRANS2 and LTRAN2. The two curves are in good agreement. It is noted that for the steady solution, both programs STRANS2 and LTRAN2 are based on the same relaxation method.

Table 1 shows the aerodynamic coefficients for the thin parabolic arc airfoil with $\tau = 0.01$ pitching about the quarter chord axis at $M = 0.7$ obtained by using both the relaxation method (UTRANS2) and the indicial method (LTRAN2). A linear flat plate solution obtained by using the Kernel function method is also shown for comparison. In general, the results of the relaxation method agree with the linear flat plate solution better than the results of the indicial method. This can be attributed to two reasons. First, a relatively coarse mesh (35 x 38) was used in the indicial method. Second, the low frequency approximation (by omitting the ϕ_{tt} term in the aerodynamic equation) used in LTRAN2 is less accurate when the free stream Mach number deviates farther from $M_\infty = 1.0$. The term ϕ_{tt} is, however, retained in the relaxation program UTRANS2.

Figures 5 and 6 show, respectively, the real and imaginary parts of the distributions of the difference in unsteady pressure coefficients across the airfoil. It is seen that all the three solutions obtained from relaxation method, time-integration method, and Kernel function method, respectively,

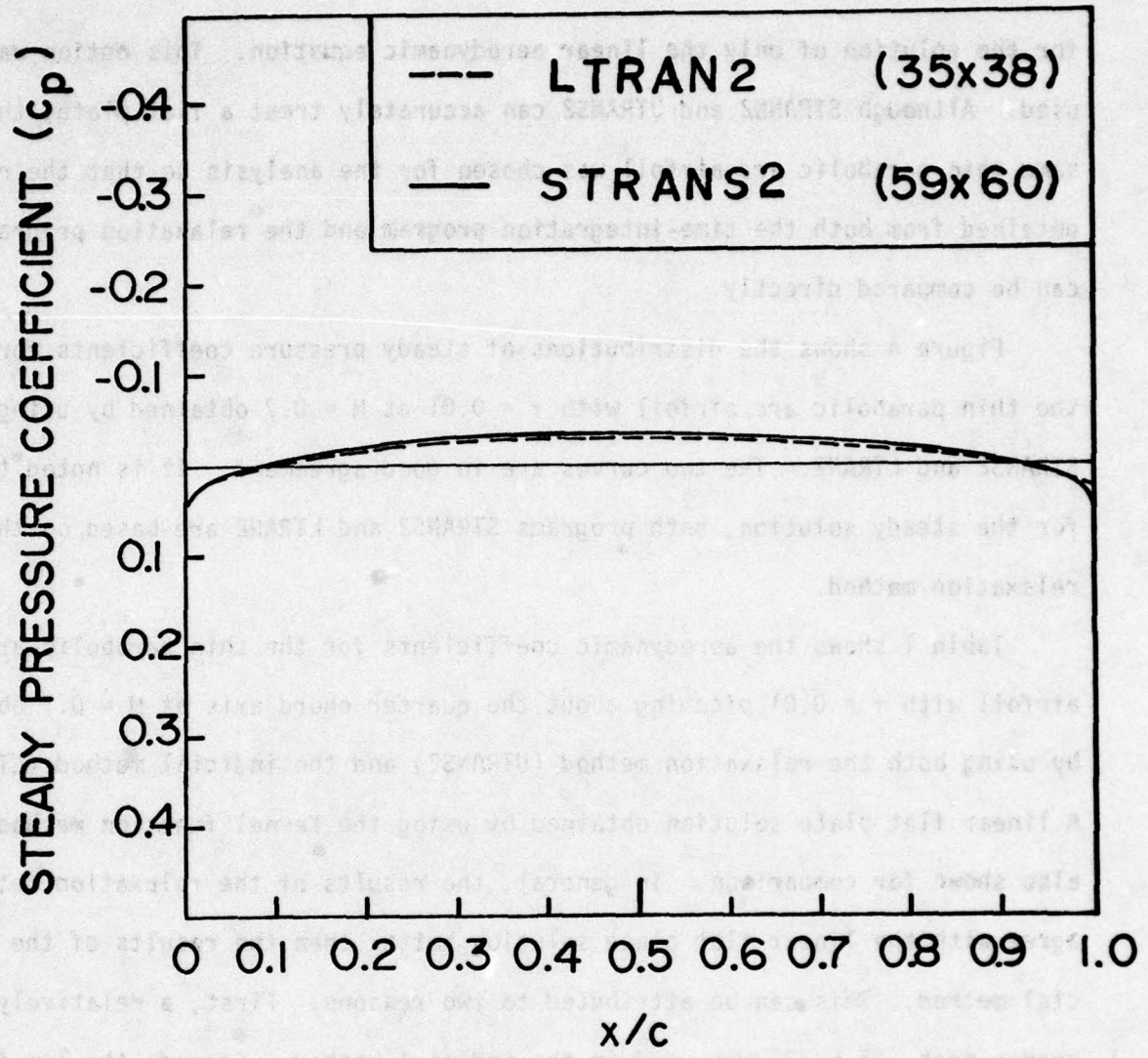

Figure 4. Distribution of Steady Pressure Coefficients for Thin Parabolic Airfoil (τ = 0.01) at M = 0.7

TABLE 1

Aerodynamic Coefficients for flat plates pitching at the quarter chord at M = 0.7

	Method	Reduced Frequency											
		k_c=0.0		k_c=0.05		k_c=0.10		k_c=0.15		k_c=0.20		k_c=0.25	
		Real	Imag	Real	Imag.	Real	Imag.	Real	Imag.	Real	Imag.	Real	Imag.
C_{ℓ_δ}	1	0.0	0.0	0.059	0.462	0.188	0.868	0.330	1.220	0.532	1.540	0.693	1.780
	2	0.0	0.0	0.055	0.385	0.153	0.712	0.271	0.999	0.425	1.210	0.422	1.510
	3	0.0	0.0	0.062	0.397	0.167	0.719	0.272	0.988	0.365	1.222	0.442	1.434
C_{ℓ_α}	1	9.720	0.0	9.230	-1.170	8.680	-1.880	8.140	-2.200	7.680	-2.660	7.120	-2.770
	2	8.284	0.0	8.078	-0.382	7.212	-1.204	6.715	-1.445	6.294	-1.603	5.778	-1.634
	3	8.789	0.0	7.980	-1.033	7.282	-1.308	6.739	-1.323	6.323	-1.222	6.004	-1.066
C_{m_δ}	1	0.0	0.0	-0.002	-0.021	-0.004	-0.039	-0.006	-0.057	-0.010	-0.075	-0.012	-0.090
	2	0.0	0.0	0.002	-0.009	0.006	-0.021	0.013	-0.032	0.021	-0.045	0.042	-0.056
	3	0.0	0.0	0.002	0.000	0.008	-0.002	0.019	-0.004	0.032	-0.008	0.048	-0.013
C_{m_α}	1	-0.427	0.0	-0.409	.029	-0.394	0.042	-0.379	0.041	-0.373	0.049	-0.358	0.047
	2	-0.210	0.0	-0.207	-0.070	-0.204	-0.114	-0.211	-0.168	-0.223	-0.219	-0.231	-0.261
	3	0.0	0.0	-0.005	-0.067	-0.014	-0.140	-0.023	-0.208	-0.031	-0.273	-0.038	-0.337

Method 1: Parabolic arc, τ = 0.01, Indicial method (35 x 38)

Method 2: Parabolic arc, τ = 0.01, Relaxation method (59 x 60)

Method 3: Linear flat plate theory, Kernel function method.

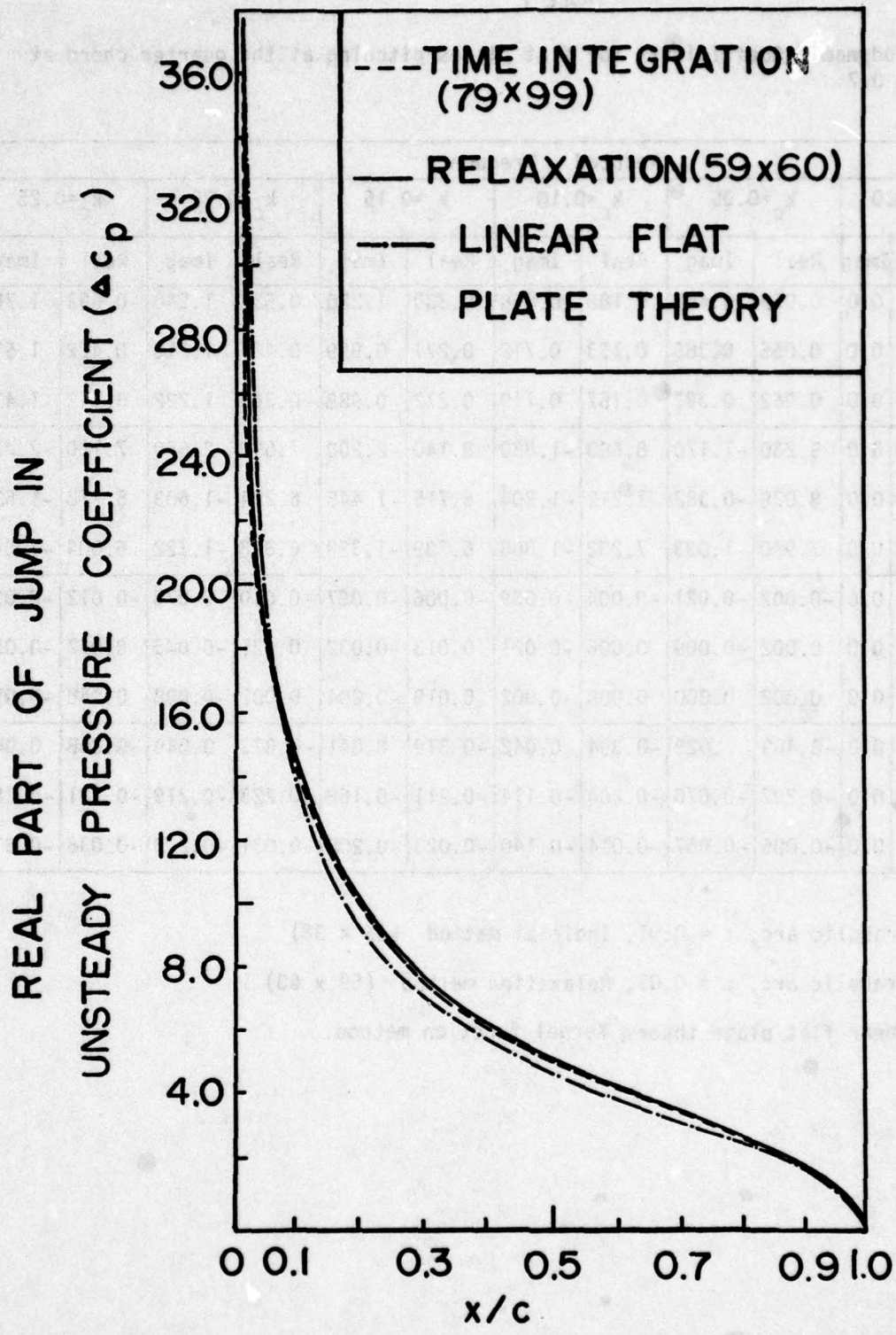

Figure 5. Distribution of Unsteady Pressure Coefficients (Real Part) for Plates Pitching about the Quarter Chord with $k_b = 0.05$ and $M = 0.7$.

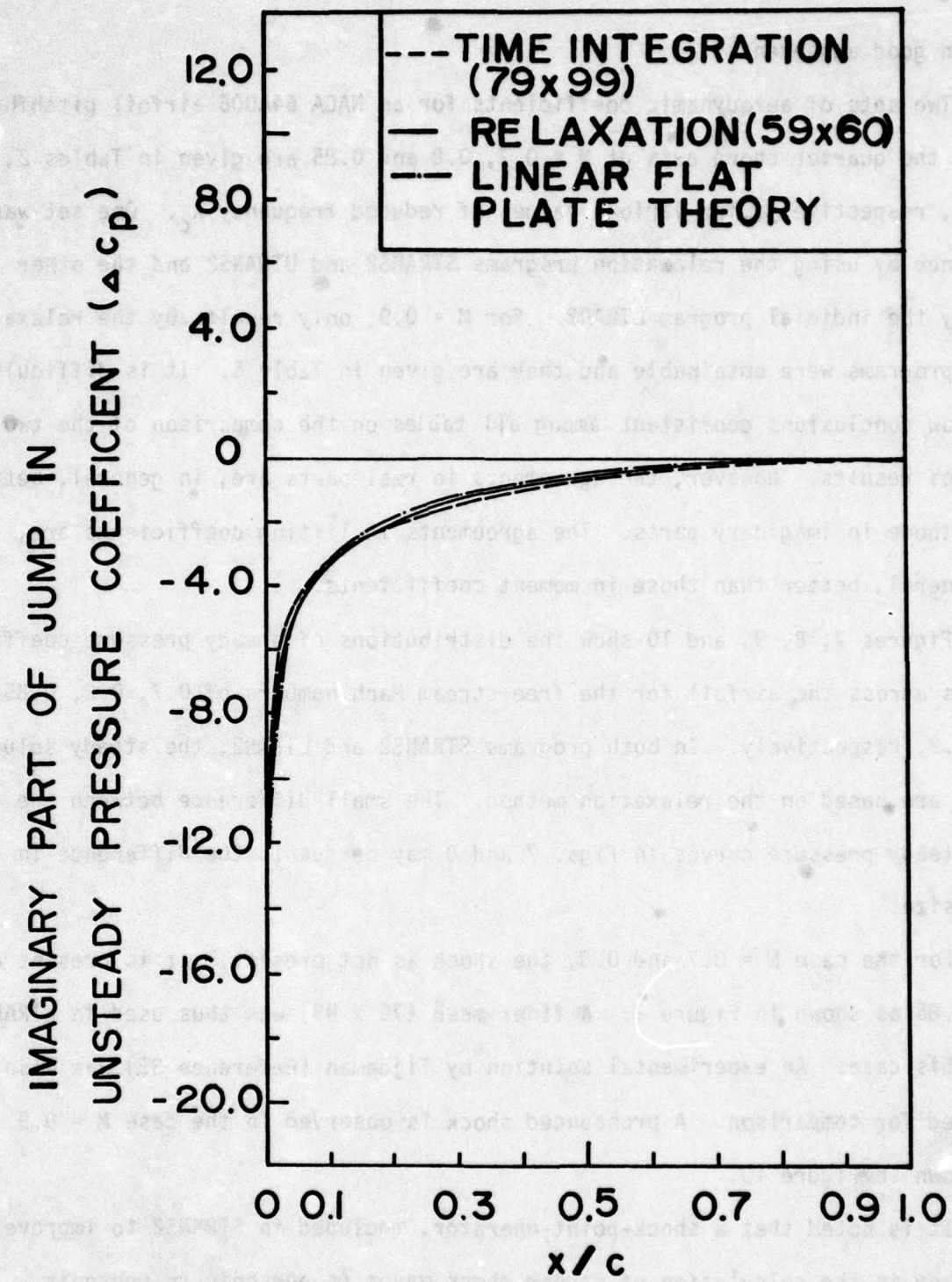

Figure 6. Distribution of Unsteady Pressure Coefficients (Imaginary Part) for Plates Pitching about the Quarter Chord with k_b = 0.05 and M = 0.7

are in good agreement.

Two sets of aerodynamic coefficients for an NACA 64A006 airfoil pitching about the quarter chord axis at M = 0.7, 0.8 and 0.85 are given in Tables 2, 3, and 4, respectively, for various values of reduced frequency k_c. One set was obtained by using the relaxation programs STRANS2 and UTRANS2 and the other set by the indicial program LTRAN2. For M = 0.9, only results by the relaxation programs were obtainable and they are given in Table 5. It is difficult to draw conclusions consistent among all tables on the comparison of the two sets of results. However, the agreements in real parts are, in general, better than those in imaginary parts. The agreements in lifting coefficients are, in general, better than those in moment coefficients.

Figures 7, 8, 9, and 10 show the distributions of steady pressure coefficients across the airfoil for the free stream Mach numbers of 0.7, 0.8, 0.85, and 0.9, respectively. In both programs STRANS2 and LTRAN2, the steady solutions are based on the relaxation method. The small difference between the two steady pressure curves in Figs. 7 and 8 may be due to the difference in mesh size.

For the case M = 0.7 and 0.8, the shock is not present. It is present at M = 0.85 as shown in Figure 9. A finer mesh (79 x 99) was thus used in LTRAN2 for this case. An experimental solution by Tijdeman (Reference 32) was also plotted for comparison. A pronounced shock is observed in the case M = 0.9 as shown in Figure 10.

It is noted that a shock-point-operator, included in STRANS2 to improve accuracy in the calculation of strong shock waves (supersonic to subsonic transition) for supersonic free stream flow was taken out in the present computation of the steady pressure distributions. As pointed out by Holman

TABLE 2

Aerodynamic Coefficients for NACA 64A006 pitching at the quarter chord at M = 0.7

	Method	Reduced Frequency											
		$k_c = 0.0$		$k_c = 0.05$		$k_c = 0.10$		$k_c = 0.15$		$k_c = 0.20$		$k_c = 0.25$	
		Real	Imag.	Real	Imag.	Real	Imag.	Real	Imag.	Real	Imag.	Real	Imag.
C_{ℓ_δ}	1	0.0	0.0	0.061	0.474	0.196	0.884	0.351	1.260	0.552	1.540	0.693	1.820
	2	0.0	0.0	0.043	0.438	0.165	0.759	0.288	1.056	0.468	1.283	0.628	1.466
C_{ℓ_α}	1	10.000	0.0	9.470	-1.220	8.840	-1.960	8.390	-2.340	7.710	-2.760	7.270	-2.770
	2	8.845	0.0	8.693	-0.547	7.769	-1.403	7.073	-1.665	6.545	-1.845	5.983	-1.873
C_{m_δ}	1	0.0	0.0	-0.001	-0.021	-0.004	-0.040	-0.005	-0.059	-0.008	-0.076	-0.008	-0.093
	2	0.0	0.0	0.002	-0.011	0.006	-0.021	0.014	-0.033	0.028	-0.050	0.032	-0.063
C_{m_α}	1	-0.435	0.0	-0.417	0.026	-0.401	0.036	-0.394	0.033	-0.382	0.040	-0.372	0.033
	2	-0.217	0.0	-0.217	-0.071	-0.217	-0.120	-0.219	-0.175	-0.231	-0.226	-0.241	-0.270

Method 1: Indicial Method (35 x 38)

Method 2: Relaxation Method (59 x 60)

Table 3

Aerodynamic Coefficients for NACA 64A006 pitching at the quarter chord at M = 0.8

	Method	Reduced Frequency											
		k_c = 0.0		k_c = 0.05		k_c = 0.10		k_c = 0.15		k_c = 0.20		k_c = 0.22	
		Real	Imag.	Real	Imag.	Real	Imag.	Real	Imag.	Real	Imag.	Real	Imag.
C_{ℓ_δ}	1	0.0	0.0	0.126	0.562	0.347	0.998	0.572	1.290	0.826	1.608	0.951	1.678
	2	0.0	0.0	0.115	0.540	0.253	0.893	0.518	1.154	0.749	1.326	0.797	1.235
C_{ℓ_α}	1	12.580	0.0	11.230	-2.520	9.980	-3.470	8.600	-3.810	8.040	-4.130	7.627	-4.321
	2	11.291	0.0	10.029	-2.028	8.651	-2.853	7.319	-3.063	6.247	-2.830	5.844	-2.683
C_{m_δ}	1	0.0	0.0	-0.002	-0.027	-0.004	-0.052	-0.005	-0.074	-0.004	-0.103	-0.006	-0.114
	2	0.0	0.0	0.002	-0.016	0.011	-0.028	0.019	-0.049	0.026	-0.072	0.020	-0.075
C_{m_α}	1	-0.574	0.0	-0.536	0.044	-0.519	0.039	-0.495	0.035	-0.514	0.020	-0.520	0.029
	2	-0.283	0.0	-0.279	-0.076	-0.292	-0.148	-0.306	-0.204	-0.316	-0.251	-0.319	-0.262

Method 1: Indicial Method (35 x 38)

Method 2: Relaxation Method (59 x 60)

TABLE 4

Aerodynamic Coefficients for NACA 64A006 pitching at the quarter chord at M = 0.85

	Method	Reduced Frequency											
		k_c=0.0		k_c=0.05		k_c=0.10		k_c=0.15		k_c=0.18		k_c=0.25	
		Real	Imag	Real	Imag.	Real	Imag.	Real	Imag.	Real	Imag.	Real	Imag.
C_{ℓ_δ}	1	0.0	0.0	0.136	0.666	0.492	1.180	0.938	1.470	1.187	1.525	1.570	1.480
	2	0.0	0.0	0.163	0.626	0.480	0.962	0.783	1.148	0.832	1.039	——	——
C_{ℓ_α}	1	13.860	0.0	13.310	-2.720	11.820	-4.920	9.770	-6.250	8.474	-6.596	5.900	-6.280
	2	14.653	0.0	11.803	-3.701	9.160	-4.491	7.223	-4.076	5.804	-3.689	——	——
C_{m_δ}	1	0.0	0.0	-0.001	-0.034	-0.005	-0.068	-0.012	-0.102	-0.018	-0.122	-0.037	-0.168
	2	0.0	0.0	0.004	-0.026	0.009	-0.054	0.013	-0.089	0.002	-0.096	——	——
C_{m_α}	1	-0.676	0.0	-0.676	0.021	-0.677	0.053	-0.677	0.082	-0.677	0.101	-0.673	0.148
	2	-0.530	0.0	-0.501	-0.071	-0.510	-0.147	-0.514	-0.210	-0.498	-0.180	——	——

Method 1: Indicial Method (79 x 99)

Method 2: Relaxation Method (59 x 60)

TABLE 5

Aerodynamic Coefficients for NACA 64A006 pitching at the quarter chord at M = 0.90

	Reduced Frequency									
	k_c=0.0		k_c=0.05		k_c=0.07		k_c=0.10		k_c=0.12	
	Real	Imag	Real	Imag.	Real	Imag.	Real	Imag.	Real	Imag.
C_{ℓ_δ}	0.0	0.0	0.095	0.371	0.153	0.481	0.247	0.617	0.309	0.681
C_{ℓ_α}	8.852	0.0	7.444	-1.757	6.898	-1.990	6.098	-2.117	5.527	-2.047
C_{m_δ}	0.0	0.0	-0.016	-0.061	-0.027	-0.080	-0.047	-0.104	-0.062	-0.116
C_{m_α}	-1.437	0.0	-1.228	0.260	-1.150	0.299	-1.031	0.334	-0.940	0.349

Relaxation Method (59 x 60)

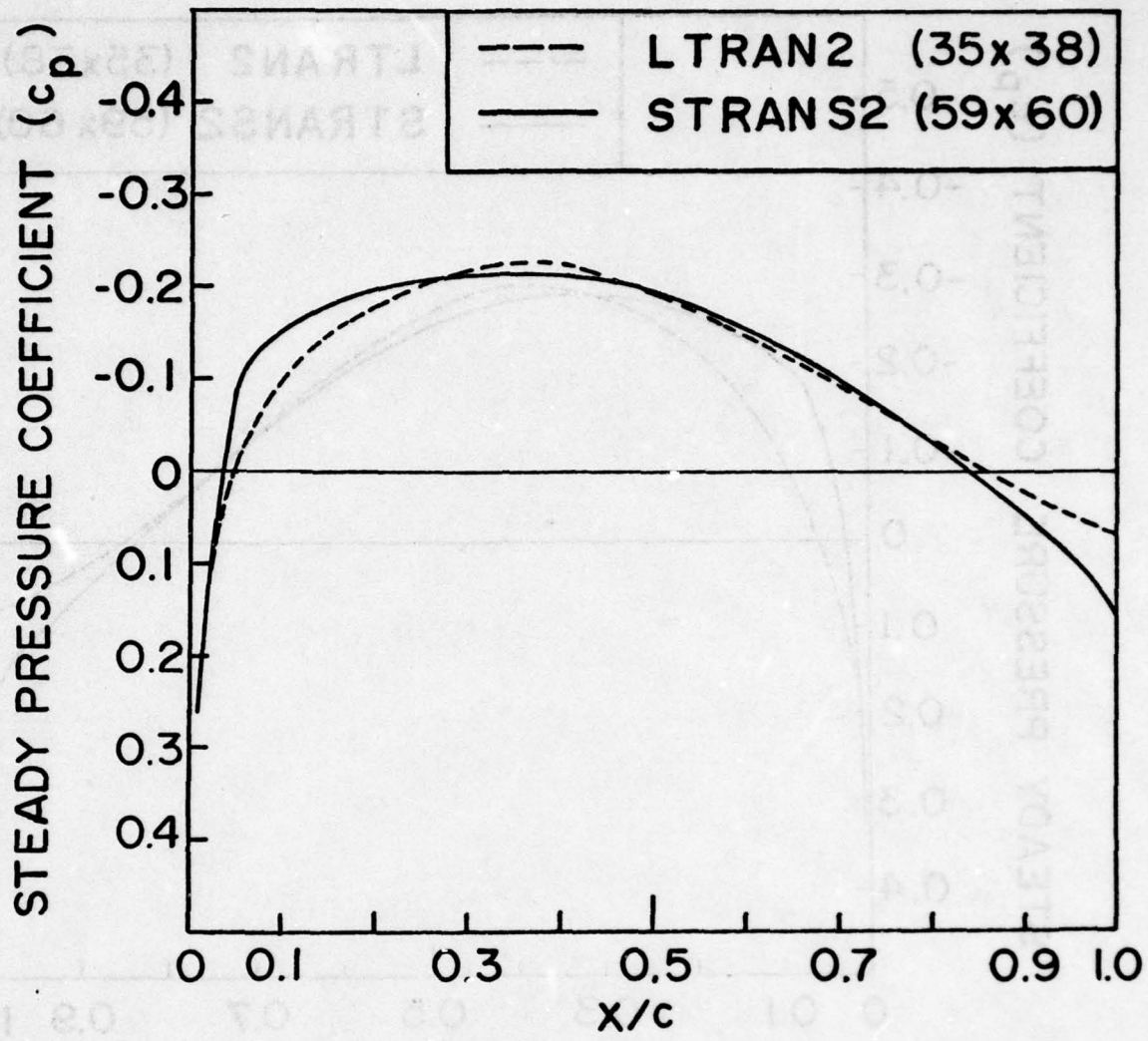

Figure 7. Distribution of Steady Pressure Coefficients for NACA 64A006 Airfoil at M = 0.7

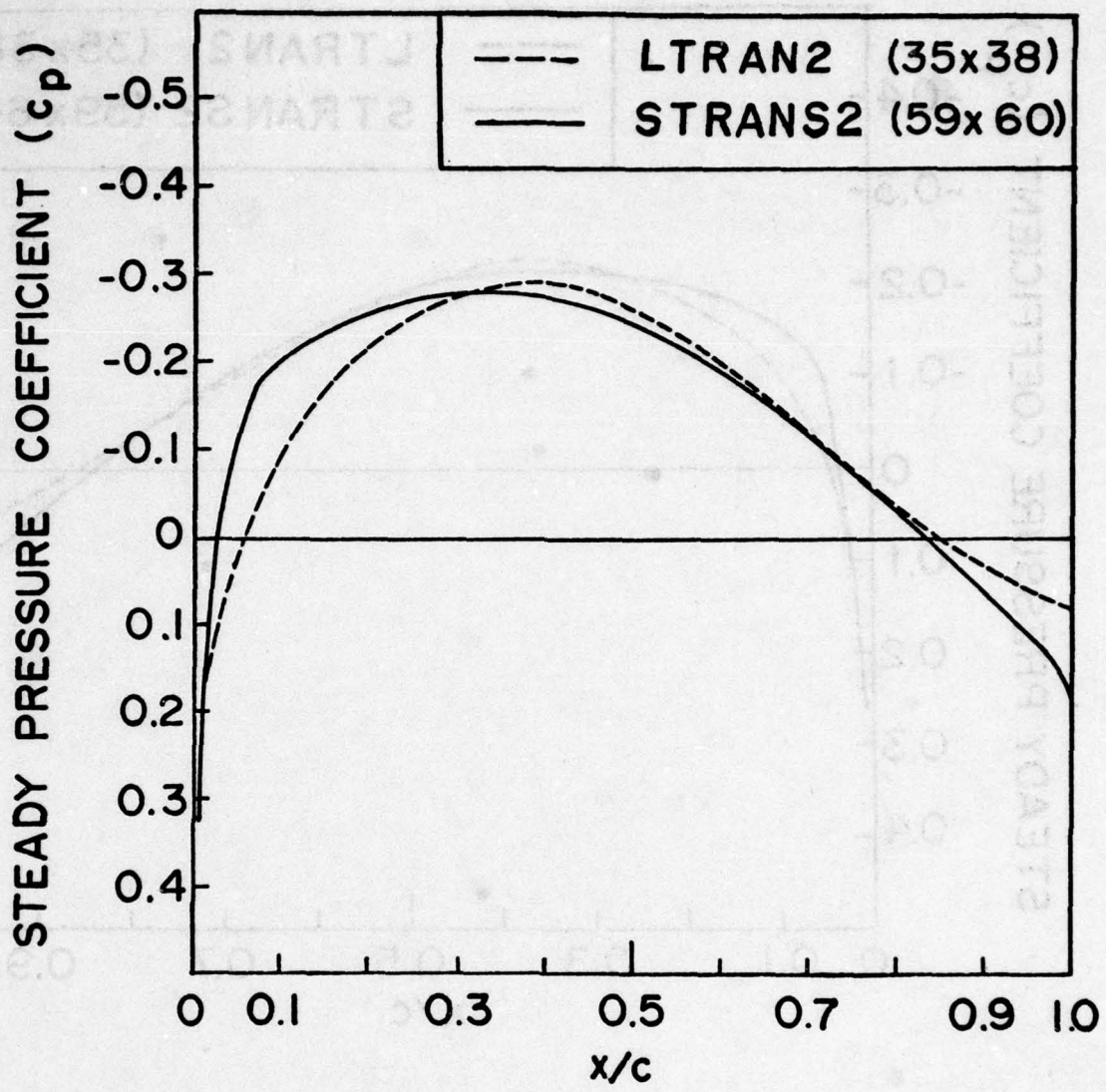

Figure 8. Distribution of Steady Pressure Coefficients for NACA 64A006 Airfoil at M = 0.8

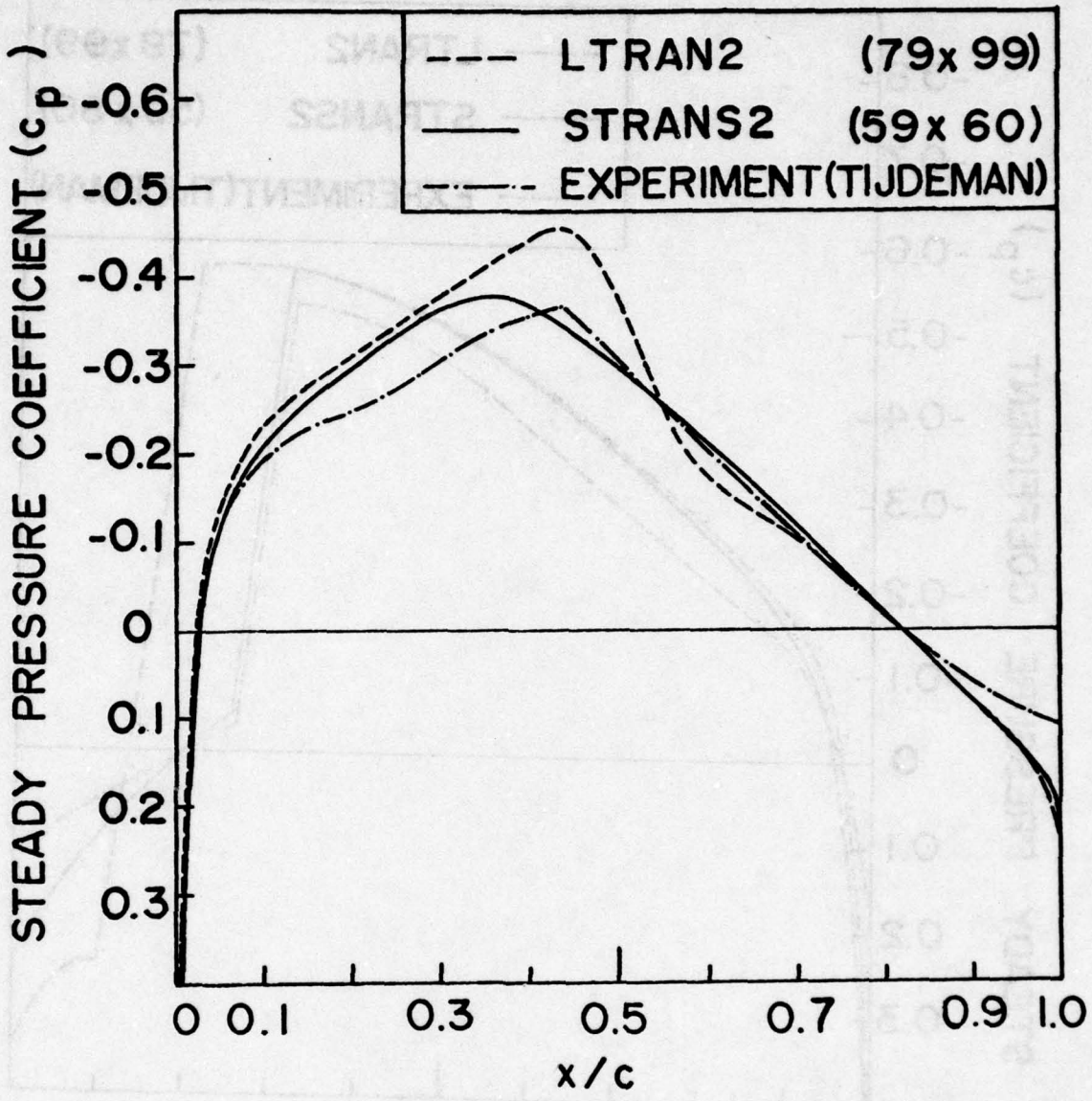

Figure 9. Distribution of Steady Pressure Coefficients for NACA 64A006 Airfoil at M = 0.85

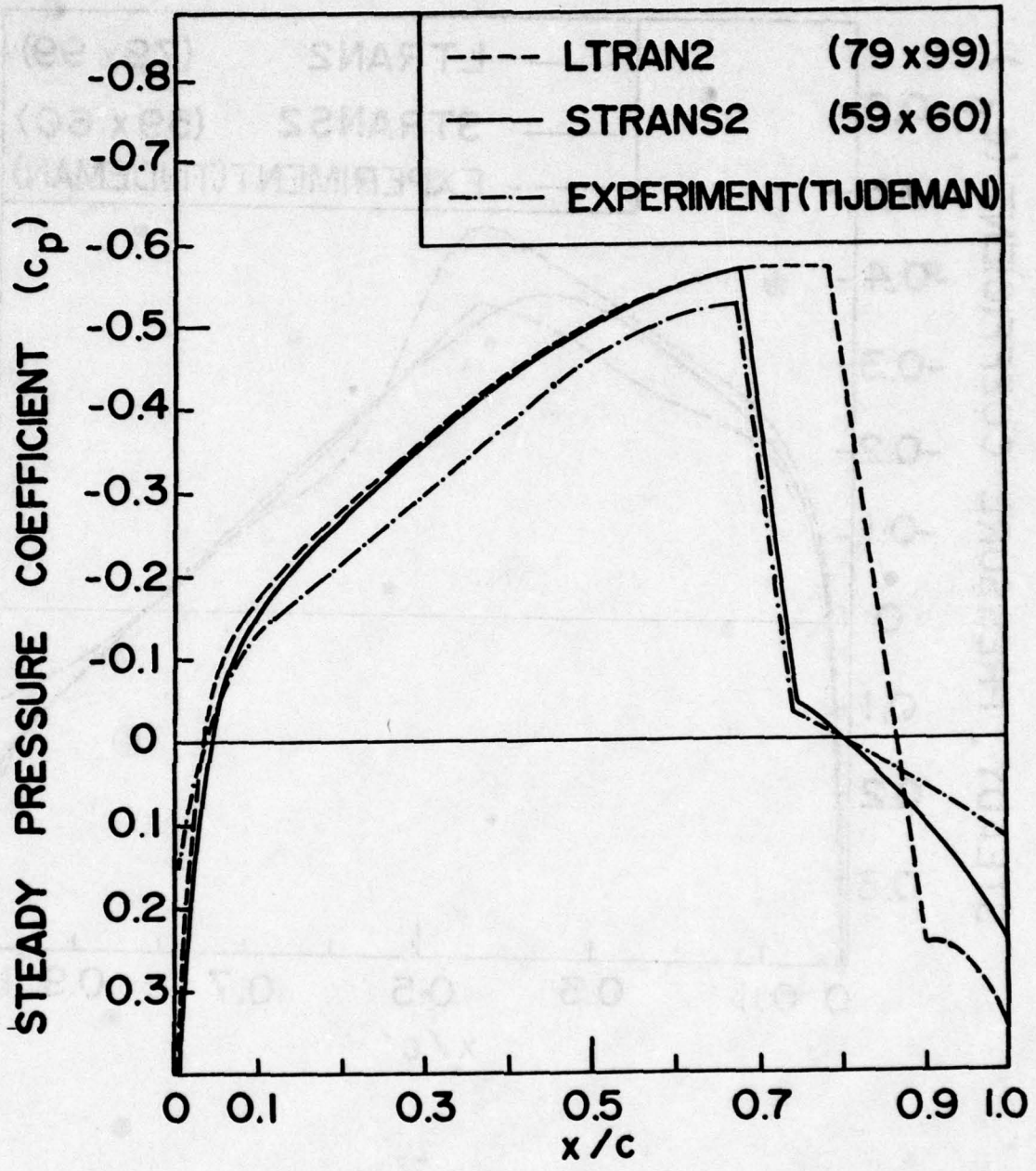

Figure 10. . Distribution of Steady Pressure Coefficients for NACA 64A006 Airfoil at M = 0.9

(Reference 8), the shock-point-operator is essential only for low supersonic flow. It leads to a strong over expansion of the shock waves for high subsonic flows.

In Reference 5, Traci et al. provided the aerodynamic coefficients for an NACA 64A006 airfoil pitching about the leading edge. Their results and the present results for M_∞ = 0.8, 0.85, 0.9, and 0.95 are presented in Tables 6, 7, 8, and 9, respectively, for comparison.

Table 6 shows the results at M_∞ = 0.8 obtained by using the indicial method, the time-integration method with two meshes, the relaxation method, and those provided in Reference 5. The results obtained by using the time-integration method with the finer mesh (79 x 99) should be the most accurate ones.

In Table 7, the results obtained for M_∞ = 0.85 by using the indicial, time-integration, and the relaxation methods compare fairly well with those provided in Reference 5. In Tables 8 and 9, the results obtained for M_∞ = 0.9 and 0.95, respectively, by using STRANS2 and UTRANS2 agree well with those obtained in Reference 5.

It is noted that the aerodynamic coefficients obtained by using the relaxation method drop off in high k_c-values. This may be due to the fact that the convergence becomes more difficult in higher k_c values.

(c) Flutter Results

In this study, the flutter speed is predicted by using the standard U-g method as described in Section V. A typical U-g plot is given in Figure 11 for the case of an NACA 64A006 airfoil pitching about the 1/4-chord axis.

In this flutter analysis, the effects of four parameters were considered: airfoil-air mass ratio μ; position of the mass center x_α; position of the

TABLE 6

Aerodynamic coefficients for NACA 64A006 pitching at the leading edge at M = 0.8

	Method	Reduced Frequency (k_c)									
		0.0		0.05		0.10		0.15		0.20	
		Real	Imag.	Real	Imag.	Real	Imag.	Real	Imag.	Real	Imag.
C_{ℓ_δ}	1	0.0	0.0	.126	.562	.347	.998	.572	1.29	.826	1.61
	2			.091	.574	.328	1.02	.574	1.29	.820	1.61
	3					.309	.951				
	4	0.0	0.0	.147	.551	.259	.837			.674	1.28
	5	0.0	0.0	.175	.47	.259	.817	.471	1.15	.708	1.34
C_{ℓ_α}	1	12.6	0.0	11.2	-2.52	9.98	-3.47	8.60	-3.82	8.00	-4.13
	2			11.5	-1.82	10.3	-2.75	9.04	-2.94	8.74	-2.84
	3					9.66	-2.59				
	4	10.5	0.0	9.5	-1.82	8.35	-2.89			6.58	-3.42
	5	11.5	0.0	10.0	-2.08	8.84	-2.99	7.76	-3.43	6.94	-3.55
C_{m_δ}	1	0.0	0.0	-.027	-.141	-.072	-.256	-.117	-.339	-.165	-.437
	2			-.047	-.137	-.069	-.257	-.111	-.341	-.167	-.435
	3					-.066	-.246				
	4	0.0	0.0	-.036	-.159	-.057	-.245			-.146	-.401
	5	0.0	0.0	-.043	-.130	-.055	-.229	-.096	-.332	-.147	-.401
C_{m_α}	1	-3.13	0.0	-2.82	.540	-2.55	.72	-2.26	.78	-2.18	.83
	2			-2.86	.453	-2.62	.37	-2.37	.38	-2.32	.37
	3					-2.51	.40				
	4	-3.00	0.0	-2.72	.391	-2.43	.72			-2.00	.83
	5	-3.12	0.0	-2.75	.500	-2.46	.70	-2.21	.79	-2.02	.81

Method 1 - LTRAN2 Indicial Method (35 x 38 Grid)

Method 2 - LTRAN2 Time-Integration (35x38 Grid)

Method 3 - LTRAN2 Time-Integration (79 x 99 Grid)

Method 4 - STRANS2 and UTRANS2 (54 x 55 Grid)

Method 5 - STRANS2 and UTRANS2 (Reference 5)

TABLE 7

Aerodynamic coefficients for NACA 64A006 pitching at the leading edge at M = 0.85

	Method	Reduced Frequency (k_c)									
		0.0		0.05		0.10		0.15		0.20	
		Real	Imag.	Real	Imag.	Real	Imag.	Real	Imag.	Real	Imag.
C_{ℓ_δ}	1	0.0	0.0	.238	.689	.598	1.09	.899	1.41	1.22	1.45
	2			.260	.678	.618	1.07	.910	1.40	1.20	1.48
	3	0.0	0.0	.184	.629	.422	.969	.715	1.05	.934	1.07
	4	0.0	0.0	.246	.575	.512	1.04	.816	1.15	.941	1.32
C_{ℓ_α}	1	17.2	0.0	13.8	-4.75	10.9	-5.98	9.37	-5.99	7.26	-6.08
	2			13.8	-4.50	11.4	-5.05	10.1	-4.56	8.44	-4.88
	3	14.2	0.0	11.4	-3.50	9.10	-3.98	7.53	-3.81	6.29	-3.38
	4	17.1	0.0	13.1	-4.36	10.5	-5.30	8.74	-5.38	7.52	-5.34
C_{m_δ}	1	0.0	0.0	-.057	-.199	-.141	-.332	-.207	-.455	-.304	-.516
	2			-.053	-.199	-.146	-.328	-.203	-.457	-.301	-.522
	3	0.0	0.0	-.044	-.189	-.095	-.304	-.174	-.355	-.242	-.394
	4	0.0	0.0	-.060	-.160	-.112	-.303	-.186	-.356	-.206	-.428
C_{m_α}	1	-4.84	0.0	-3.97	1.13	-3.32	1.41	-3.03	1.38	-2.58	1.52
	2			-3.97	1.06	-3.41	1.11	-3.24	.867	-2.89	.94
	3	-4.18	0.0	-3.44	.823	-2.86	.85	-2.49	.73	-2.21	.58
	4	-4.59	0.0	-3.62	1.04	-3.03	1.23	-2.63	1.23	-2.39	1.21

Method 1 - LTRAN2 Indicial Method (35 x 38 Grid)

Method 2 - LTRAN2 Time Integration (35 x 38 Grid)

Method 3 - STRANS2 and UTRANS2 (54 x 55 Grid)

Method 4 - STRANS2 and UTRANS2 (Reference 5)

TABLE 8

Aerodynamic coefficients for NACA 64A006

pitching at the leading edge at M = 0.9

	Reduced Frequency							
	Method	$k_c = 0.0$		$k_c = 0.05$		$k_c = 0.10$		$k_c = 0.15$	
		Real	Imag.	Real	Imag.	Real	Imag.	Real	Imag.
C_{ℓ_δ}	1	0.0	0.0	.147	.442	.327	.691	.479	.795
	2	0.0	0.0	.125	.388	.259	.651	.350	1.07
C_{ℓ_α}	1	10.34	0.0	8.29	-2.21	6.73	-2.50	5.23	-2.32
	2	9.36	0.0	7.10	-2.01	6.34	-2.47	5.29	-2.30
C_{m_δ}	1	0.0	0.0	-.068	-.202	-.159	-.316	-.250	-.361
	2	0.0	0.0	-.056	-.167	-.118	-.283	-.186	-.356
C_{m_α}	1	-4.67	0.0	-3.77	.985	-3.09	1.15	-2.41	1.18
	2	-3.95	0.0	-3.05	.940	-2.75	1.08	-2.43	1.17

Method 1: STRANS2 and UTRANS2 (54 x 55 Grid)

Method 2: STRANS2 and UTRANS2 (Reference 5)

TABLE 9

Aerodynamic Coefficients for NACA 64A006 pitching at the leading edge at M = 0.95

		Reduced Frequency (k_c)							
		0.0		0.05		0.10		0.15	
	Method	Real	Imag	Real	Imag	Real	Imag	Real	Imag
C_{ℓ_δ}	1	0.0	0.0	0.032	0.284	0.043	0.584		
	2	0.0	0.0	0.057	0.315				
C_{ℓ_α}	1	6.652	0.0	5.710	-0.450	6.076	-0.180		
	2	7.095	0.0	6.100	-1.500				
C_{m_δ}	1	0.0	0.0	-0.014	-0.125	-0.018	-0.255		
	2	0.0	0.0	-0.026	-0.137				
C_{m_α}	1	-2.932	0.0	-2.510	0.170	-2.675	-0.004		
	2	-3.050	0.0	-2.700	0.640				

Method 1: STRANS2 and UTRANS2 (54 x 55 Grid)

Method 2: STRANS2 and UTRANS2 (Reference 5)

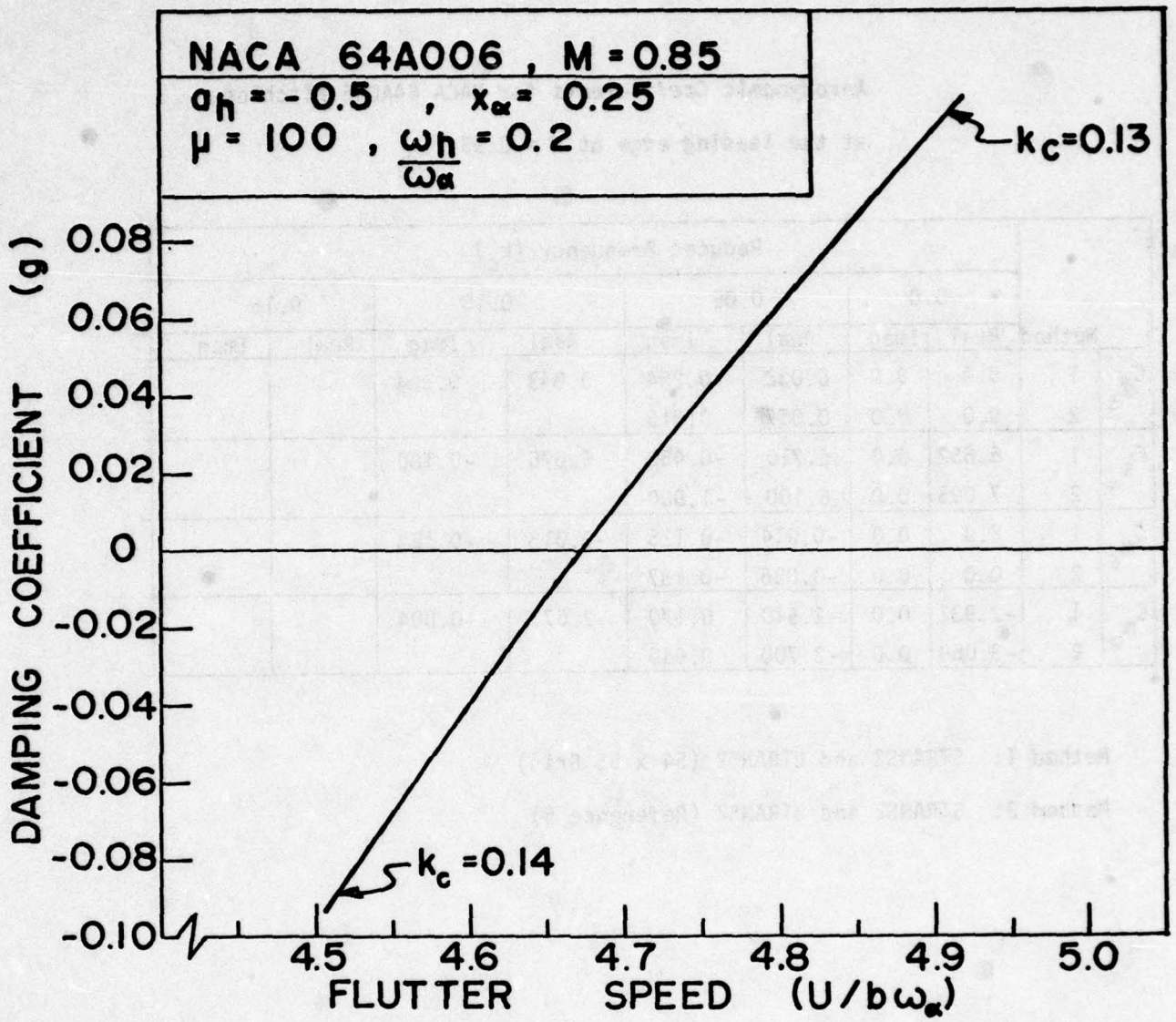

Figure 11. A Typical U-g Plot for NACA 64A006 Airfoil

elastic axis a_h; and the plunge-pitch frequency ratio (ω_h/ω_α). In all the following cases, the values for the radius of gyration r_α and the reference frequency ω_r were assumed as 0.5 and 1.0, respectively.

1. Flutter Speeds for Flat Plate Pitching about 1/4-Chord Axis at $M_\infty = 0.7$

The aerodynamic coefficients obtained in Table 1 were used to perform a flutter analysis of the special case of flat plates pitching about the 1/4-chord axis at $M_\infty = 0.7$. The results for flutter speed and the corresponding reduced frequency versus the airfoil-air mass ratio μ were obtained and shown in Figure 12. The mass center was at 1/8-chord aft the elastic (pitch) axis and the plunge-pitch frequency ratio (ω_h/ω_α) was 0.2.

Figure 12 shows that the curves of flutter speed resulted from both the indicial and relaxation methods are in good agreement. The two curves are higher than that resulted from the Kernel function method by less than 10%. The agreement among the three curves is better in the lower μ range. The predicted flutter speeds are, however, less reliable in the lower μ range because the reduced frequencies k_c become higher than 0.2.

It is noted that the LTRAN2 results become less accurate when $k_c > 0.2$. Since the low frequency approximation was not used in UTRANS2, the valid k_c range can be extended somewhat higher than 0.2.

2. Flutter Speeds for NACA 64A006 Airfoil Pitching about 1/4-Chord Axis with Varying μ at $M_\infty = 0.7$, 0.8, and 0.85

In this analysis, the effect of the airfoil-air mass ratio μ on flutter speed was first studied. The range of the μ value was estimated by considering two extreme cases.

For an aluminum parabolic arc airfoil ($\tau = 0.06$) with skin thickness of 0.1% of the chord length and without stringers at sea level, the μ value was

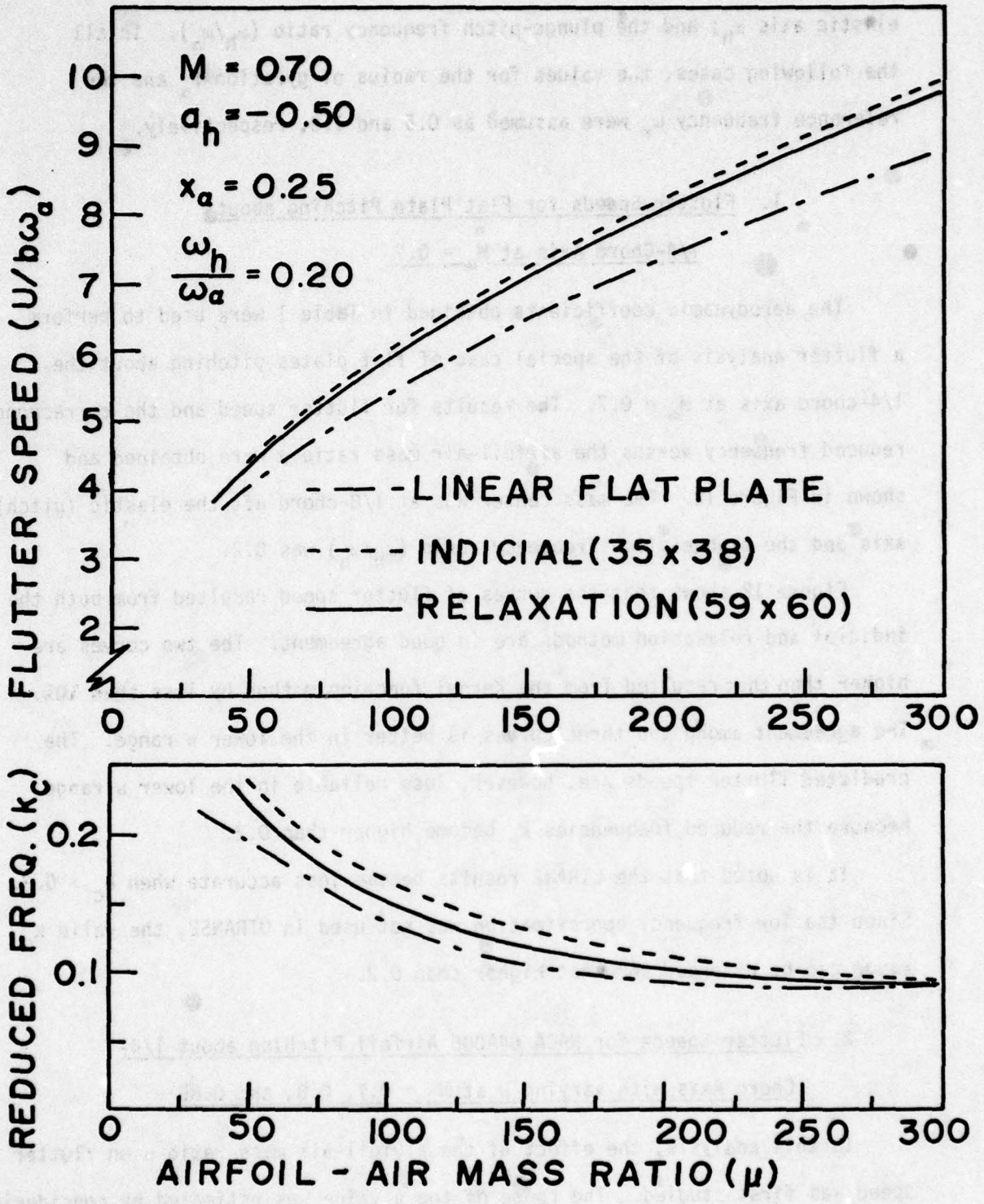

Figure 12. Comparison of Flutter Results between Linear Flat Plate Theory and Present Parabolic Arc Approximations (τ = 0.01) by LTRAN2 and UTRANS2 at M = 0.7

estimated as 6. For the same airfoil filled with solid aluminum at 50,000 feet above sea level, the μ value was estimated as 760.

Figure 13 shows the curves for the flutter speed and the corresponding reduced frequency versus the airfoil-air mass ratio μ for an NACA 64A006 airfoil pitching at the 1/4-chord axis at $M_\infty = 0.7$. The curves were obtained for two different values of the plunge-pitch frequency ratios (ω_h/ω_α): 0.1 and 0.3. The mass center was assumed to be at 1/8-chord length aft the elastic (pitch) axis. The μ values considered ranged from 25 to 300.

Figure 13 shows that the flutter speed increases sharply with increasing μ for $(\omega_h/\omega_\alpha) = 0.1$. Such increasing trend slows down rapidly as (ω_h/ω_α) increases. The curves for flutter speed are lower for higher values of (ω_h/ω_α).

It is important to mention that the reduced frequency k_c increases as μ decreases and k_c increases as (ω_h/ω_α) increases. Thus it becomes difficult to obtain flutter results in the lower μ region and higher (ω_h/ω_α) values since k_c goes out of the valid range of the present methods.

Two flutter speed curves obtained by using the linear flat plate theory for $(\omega_h/\omega_\alpha) = 0.1$ and 0.3, respectively, are also shown in Figure 13. Each curve is seen to be lower but in good agreement with the two corresponding curves for the NACA 64A006 airfoil.

Using the same conditions assumed in obtaining Figure 13, similar flutter results were obtained for $M_\infty = 0.8$ and 0.85 and are shown in Figures 14 and 15, respectively. The same general trends are observed. The curves for flutter speed drop as the free stream Mach number increases. The relaxation results and the indicial results are in good agreement in both figures.

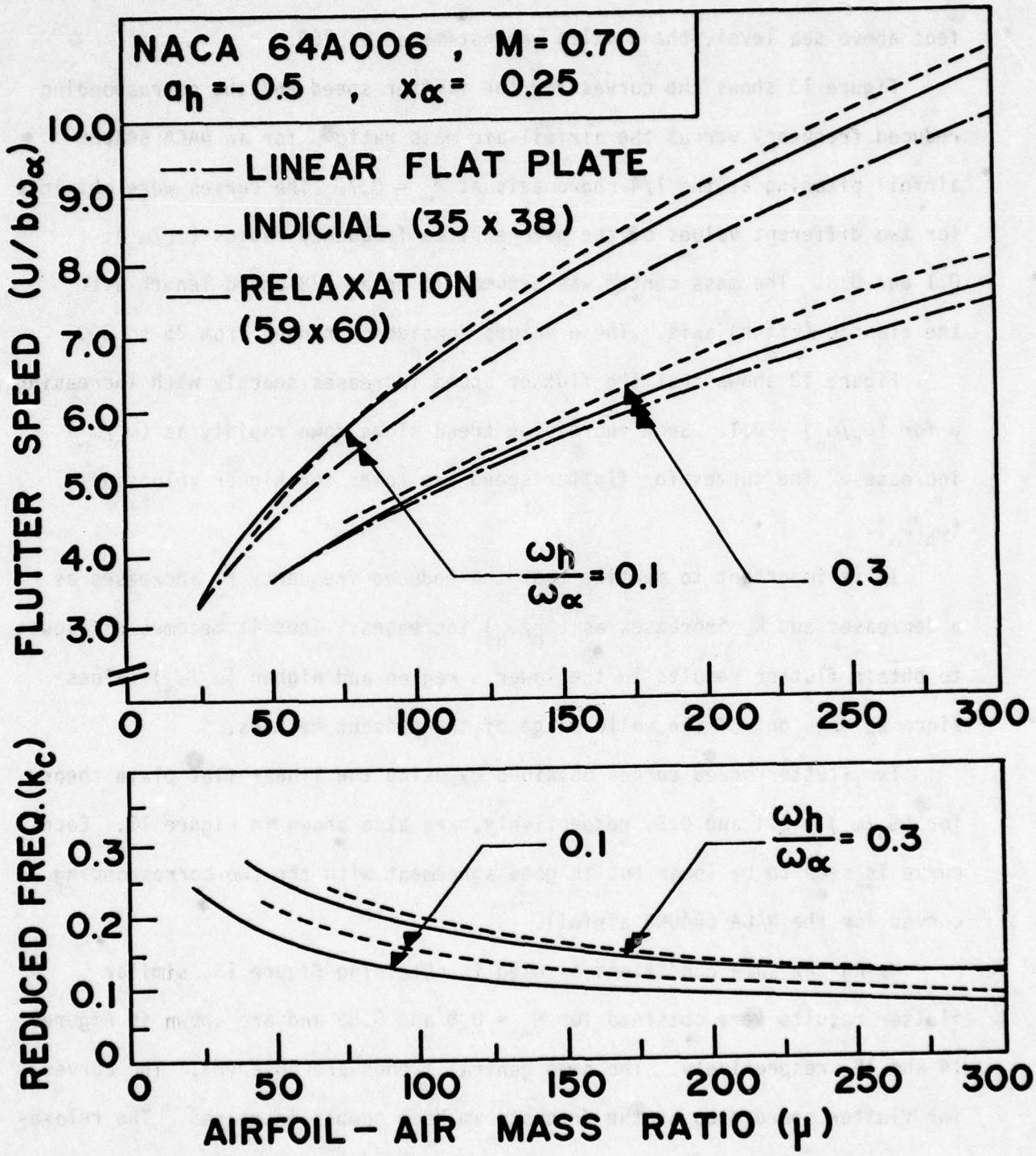

Figure 13. Effect of Mass Ratio on Flutter Speed for NACA 64A006 Airfoil for Various Frequency Ratios at M = 0.7

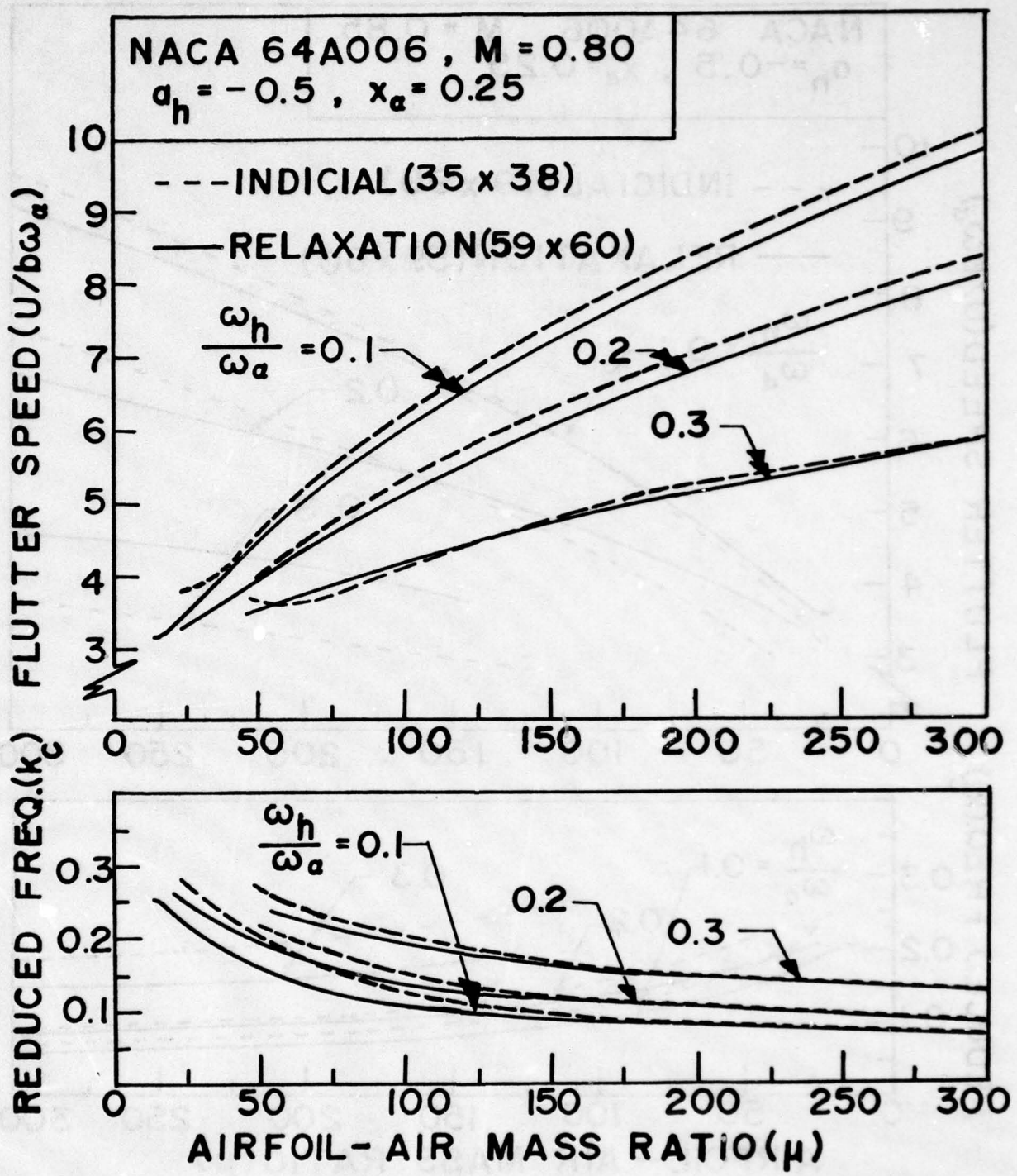

Figure 14. Effect of Mass Ratio on Flutter Speed for NACA 64A006 Airfoil for Various Frequency Ratios at M = 0.8

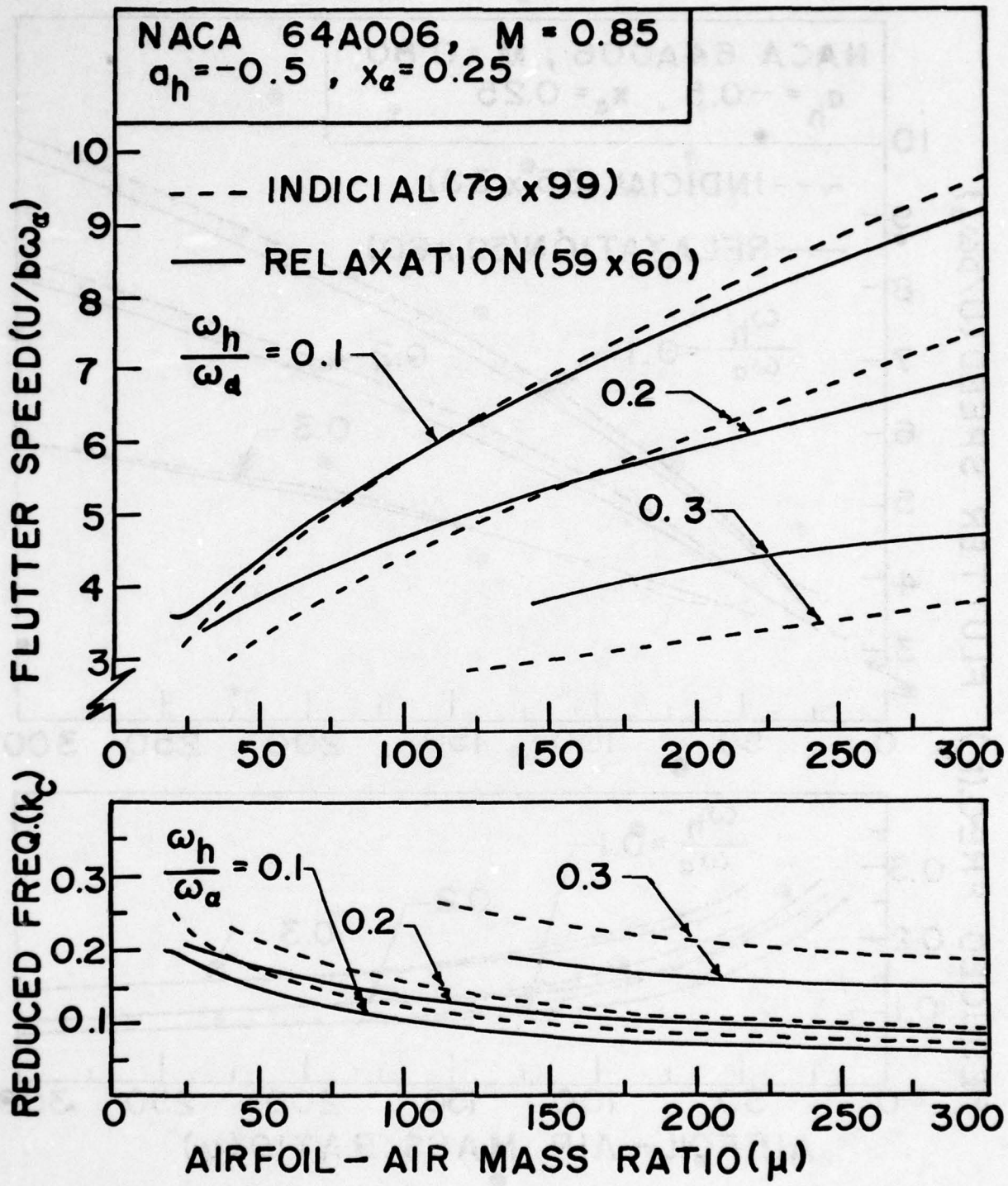

Figure 15. Effect of Mass Ratio on Flutter Speed for NACA 64A006 Airfoil for Various Frequency Ratios at M = 0.85

3. Flutter Speeds for NACA 64A006 Airfoil Pitching about 1/4-Chord Axis with Varying x_α at M_∞ = 0.7, 0.8, and 0.85

In this analysis, the effect of the position of the mass center x_α on flutter speed was studied. The NACA 64A006 airfoil was assumed to pitch about the 1/4-chord axis and the airfoil-air mass ratio μ was assumed as 100.

Curves for flutter speed and the corresponding reduced frequency versus the location of the mass center x_α were obtained for three different values of (ω_h/ω_α). The mass center location was moved from the 1/4-chord to 1/2-chord. These curves are shown in Figures 16, 17, and 18 for M_∞ = 0.7, 0.8, and 0.85, respectively.

All three figures illustrate the same general trend. The flutter speed decreases as the mass center is moved from the elastic (pitch) axis (1/4-chord) toward the 1/2-chord. The flutter speed decreases as (ω_h/ω_α) increases. The curves for the reduced frequency demonstrate a behavior opposite to that of the flutter curves. Again, the curves for flutter speed drop slightly as the free stream Mach number increases.

It is important to point out that the agreements in flutter speed between the indicial and the relaxation methods are good in all three figures. However, such agreements are better when the mass center is farther away from the elastic (pitch) axis. The flutter speed increases sharply as the mass center approaches the pitching axis which is at ¼-chord.

4. Flutter Speeds for NACA 64A006 Airfoil Pitching about ¼-Chord Axis with Varying a_h at M_∞ = 0.7, 0.8, and 0.85

In this analysis, the effect of the location of the elastic (pitch) axis of the NACA 64A006 airfoil on flutter speed was studied. The airfoil-air

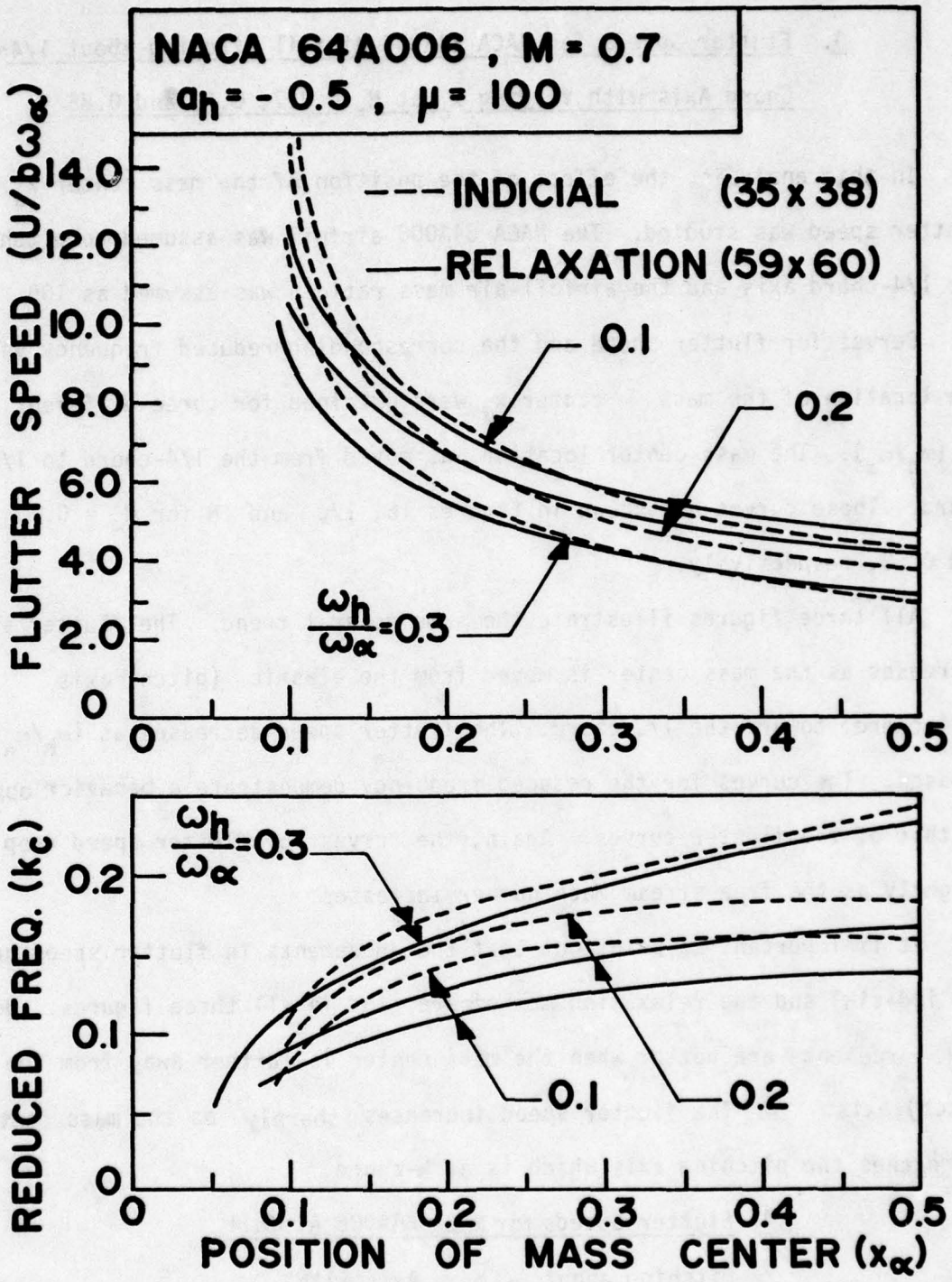

Figure 16. Effect of Position of Mass Center on Flutter Speed for NACA 64A006 Airfoil for Various Frequency Ratios at M = 0.7

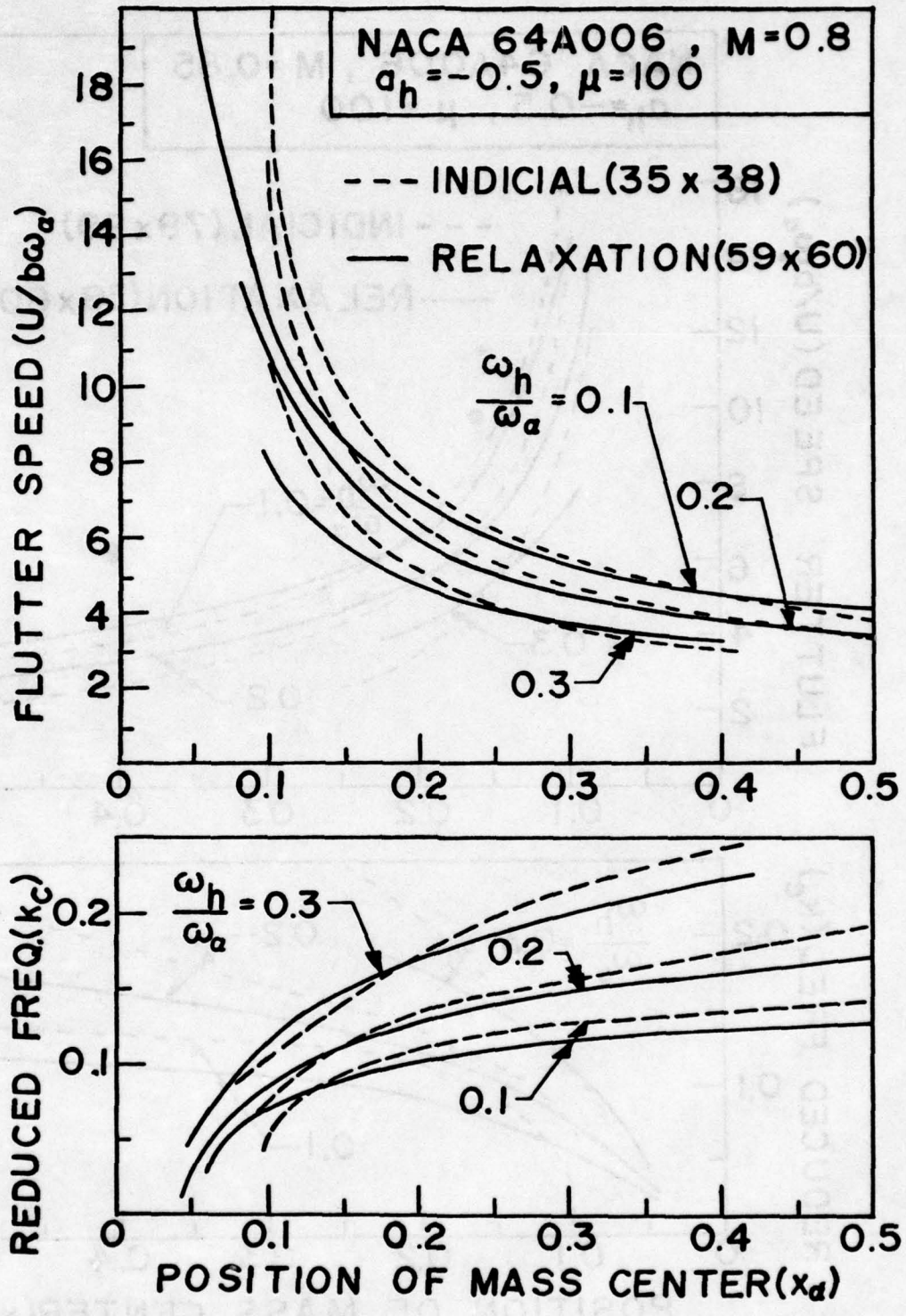

Figure 17. Effect of Position of Mass Center on Flutter Speed for NACA 64A006 Airfoil for Various Frequency Ratios at M = 0.8

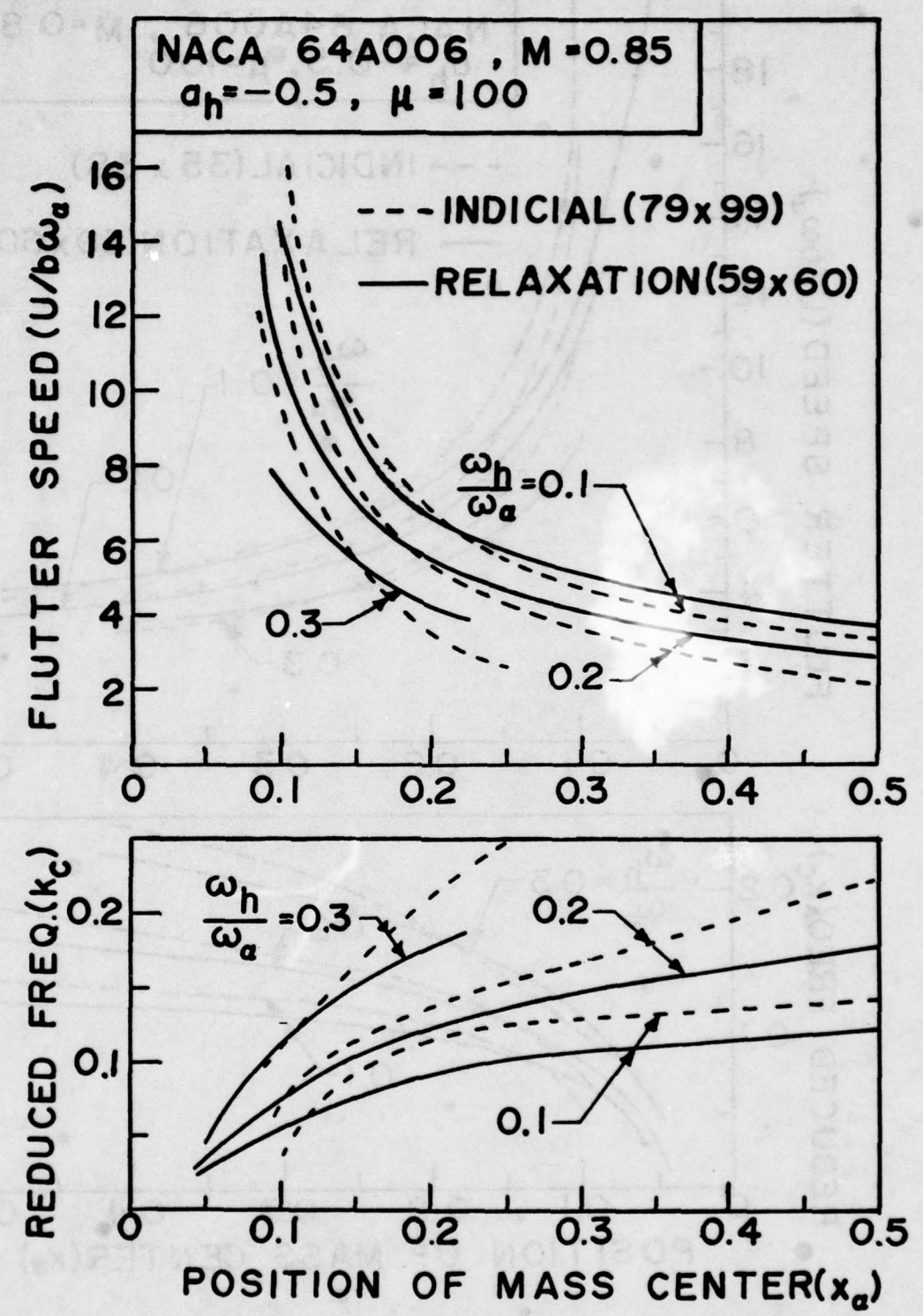

Figure 18. Effect of Position of Mass Center on Flutter Speed for NACA 64A006 Airfoil for Various Frequency Ratios at M = 0.85

mass ratio μ was assumed as 100. The mass center was assumed to be constantly at 1/8-chord aft the elastic axis.

Curves for flutter speed and the corresponding reduced frequency versus the location of the elastic (pitch) axis a_h were obtained for three different values of (ω_h/ω_α). The elastic axis was moved from the 20%-chord to 45%-chord. These curves are shown in Figures 19, 20, and 21 for M_α = 0.7, 0.8, and 0.85, respectively.

All three figures illustrate the same general trend. The flutter speed decreases as both the elastic axis and the mass center move toward the trailing edge. The flutter speed decreases as (ω_h/ω_α) increases. The curves for flutter speed drop very slightly as the free stream Mach number increases. The curves for the reduced frequency demonstrate a behavior opposite to that of the curves for flutter speed. For M_∞ = 0.85 and (ω_h/ω_α) = 0.3, difficulties were encountered in obtaining flutter speed because flutter occurred in the high reduced frequency region.

The agreements in flutter speed between the indicial and relaxation solutions are good. However, the flutter speed increases sharply when the elastic axis approaches the leading edge. Thus the discrepancies in flutter speed between the two methods also become higher when the elastic axis approaches the leading edge.

5. Effect of Transformation of Aerodynamic Coefficients on the Flutter Results of NACA 64A006 Airfoil at M_∞ = 0.8 and 0.85

The aerodynamic coefficients for an NACA 64A006 airfoil pitching about the leading edge were obtained and presented in Tables 6 and 7 for M_∞ = 0.8 and 0.85, respectively. It is of interest to transform these aerodynamic coefficients at the leading edge to those at the elastic axis (1/4-chord)

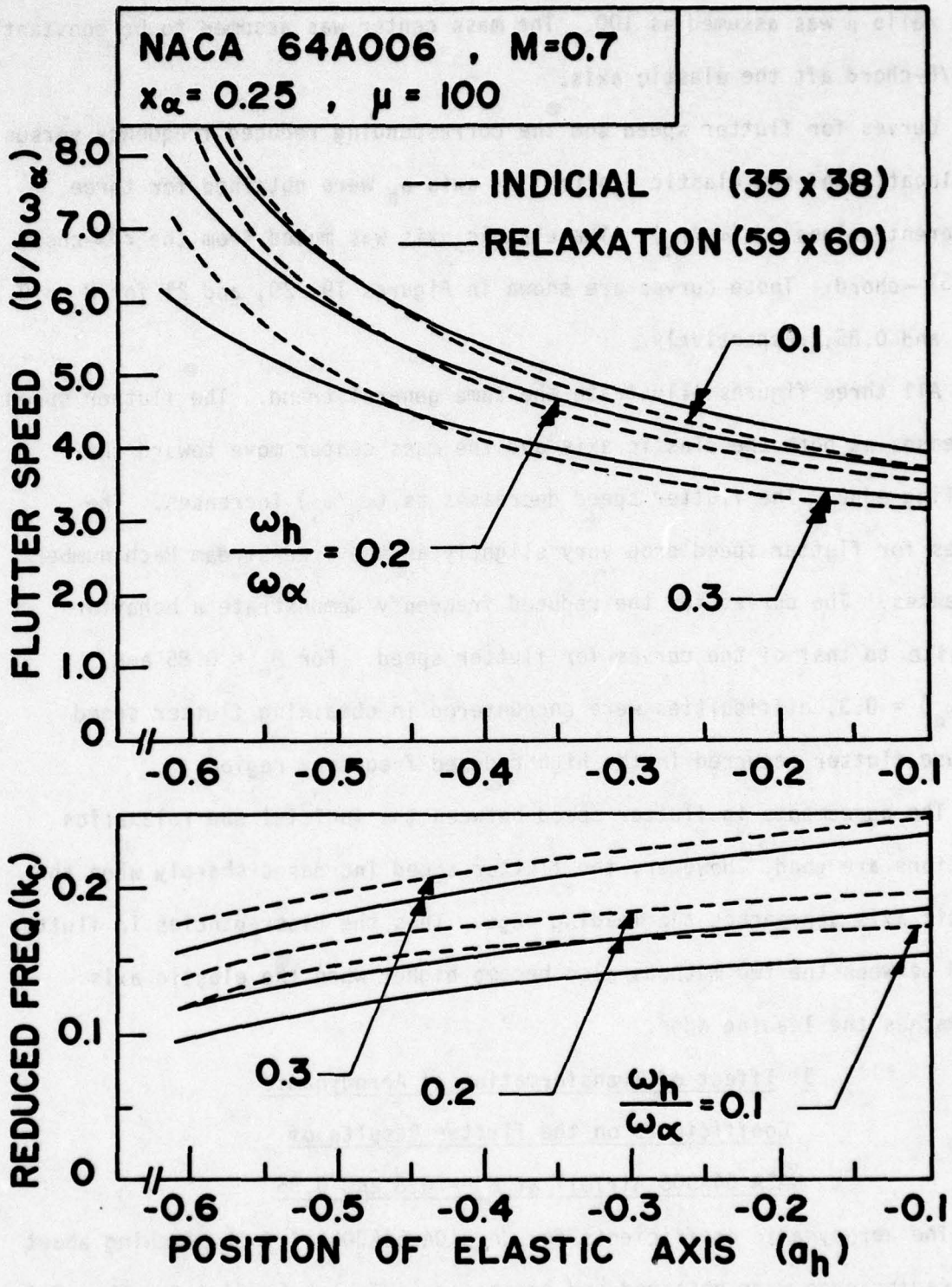

Figure 19. Effect of Position of Elastic Axis on Flutter Speed for NACA 64A006 Airfoil for Various Frequency Ratios at M = 0.7

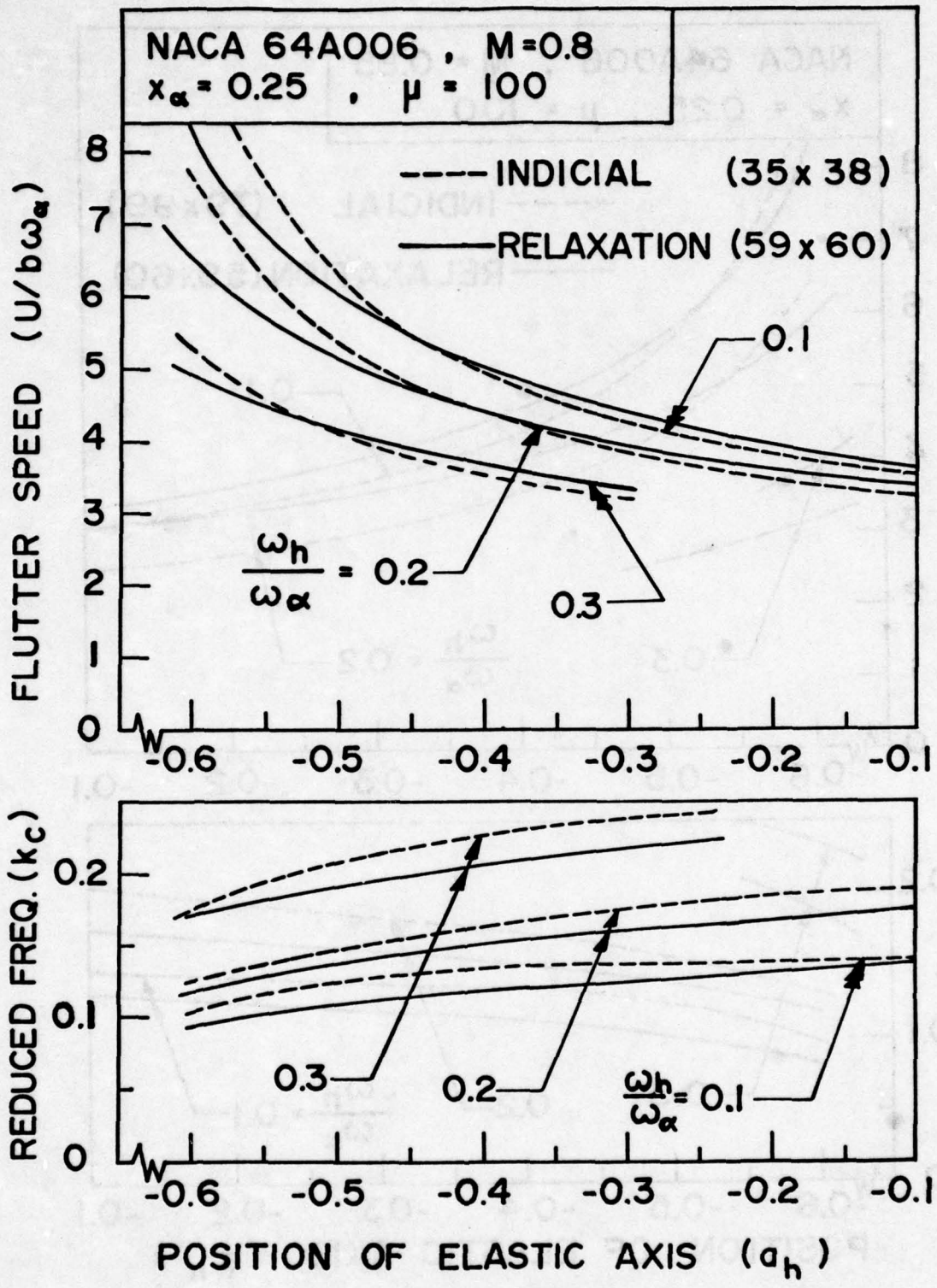

Figure 20. Effect of Position of Elastic Axis on Flutter Speed for NACA 64A006 Airfoil for Various Frequency Ratios at M = 0.8

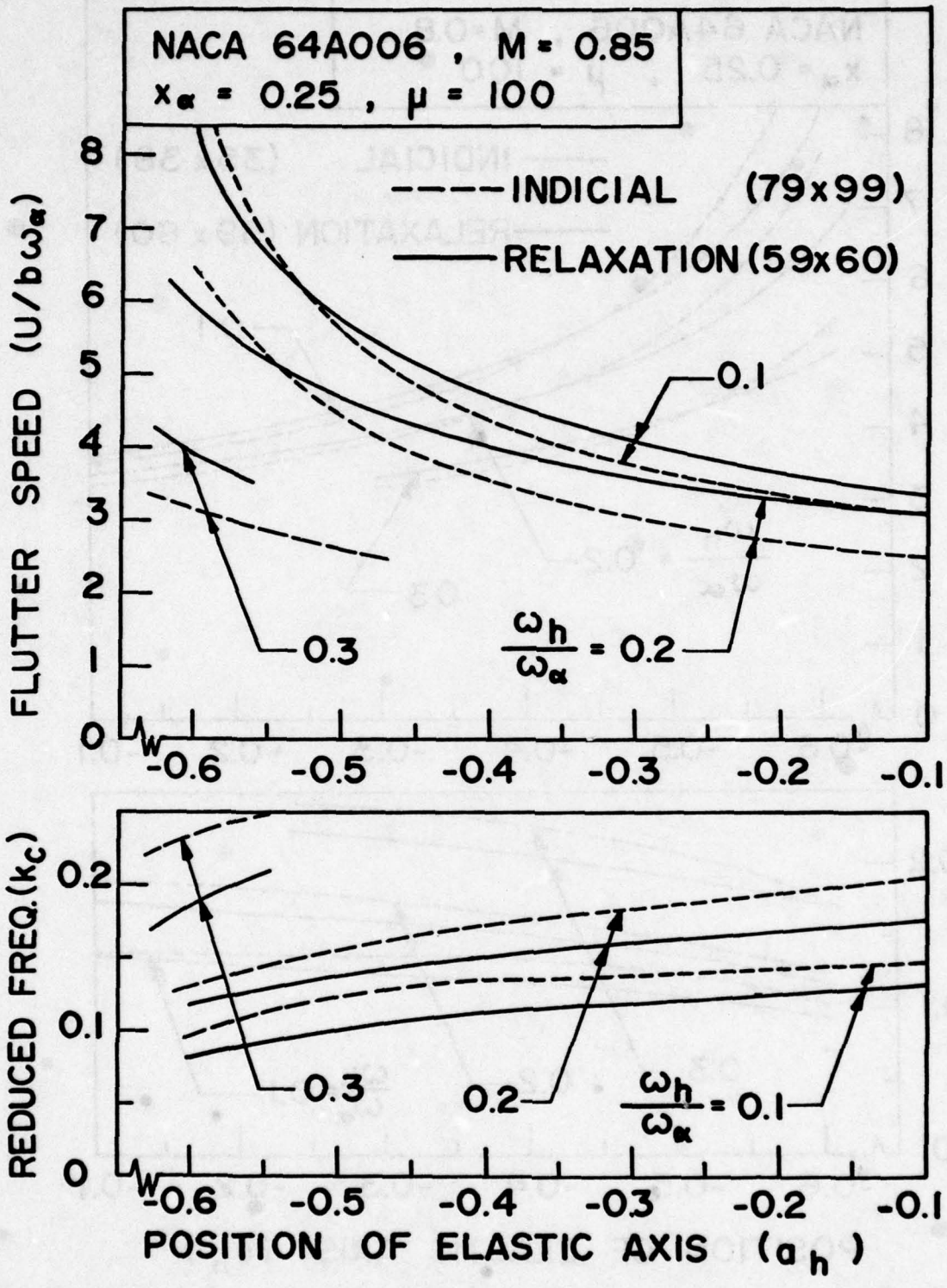

Figure 21. Effect of Position of Elastic Axis on Flutter Speed for NACA 64A006 Airfoil for Various Frequency Ratios at M = 0.85

to perform a flutter analysis. It is also of interest to compare such flutter results with those obtained directly without such transformation.

Curves for flutter speed and the corresponding reduced frequency versus the airfoil-air mass ratio were obtained for three different values of (ω_h/ω_α). The mass center was assumed to be at a distance of 1/8-chord aft the elastic (pitch) axis which is at 1/4-chord.

The results obtained on the basis of the relaxation method are shown in Figures 22 and 23 for M_∞ = 0.8 and 0.85, respectively. In both figures, the two sets of results, one obtained with and one without transformation of aerodynamic coefficients, are in fairly good agreement.

The results obtained based on the indicial method are shown in Figures 24 and 25 for M_∞ = 0.8 and 0.85, respectively. In these two figures, the discrepancies between the two sets of results, one obtained with and one without transformation of aerodynamic coefficients, are more pronounced than those found in Figures 22 and 23.

Such discrepancy may be attributed to different numerical errors introduced in the two sets of aerodynamic coefficients, one computed for pitching axis at the leading edge and one at 1/4-chord. It may also be attributed to the effect of local angle of attack which depends on the point of pitching for the nonlinear case. Such effect could not be considered during the transformation process.

6. Effect of Mach Number on Flutter Speed for NACA 64A006 Airfoil

Thus far, flutter results have been presented only for given Mach numbers. It is of interest to study the effect of Mach number on flutter speed of an NACA 64A006 airfoil pitching about the 1/4-chord axis. The mass center was assumed to be at 1/8-chord aft the elastic (pitch) axis.

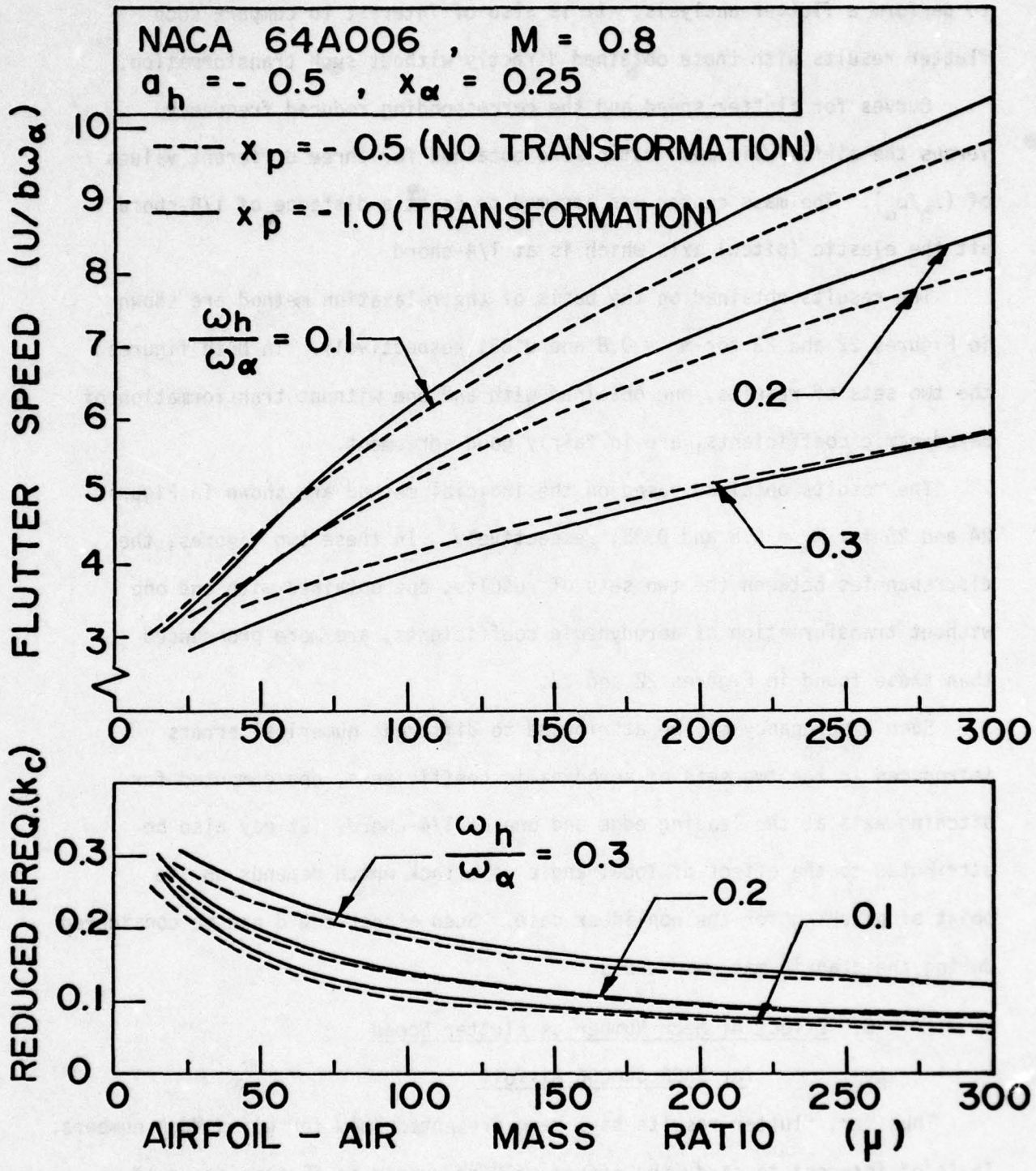

Figure 22. Effect of Transformation of Aerodynamic Coefficients (by Relaxation Method) on Flutter Speed for NACA 64A006 Airfoil at M = 0.8

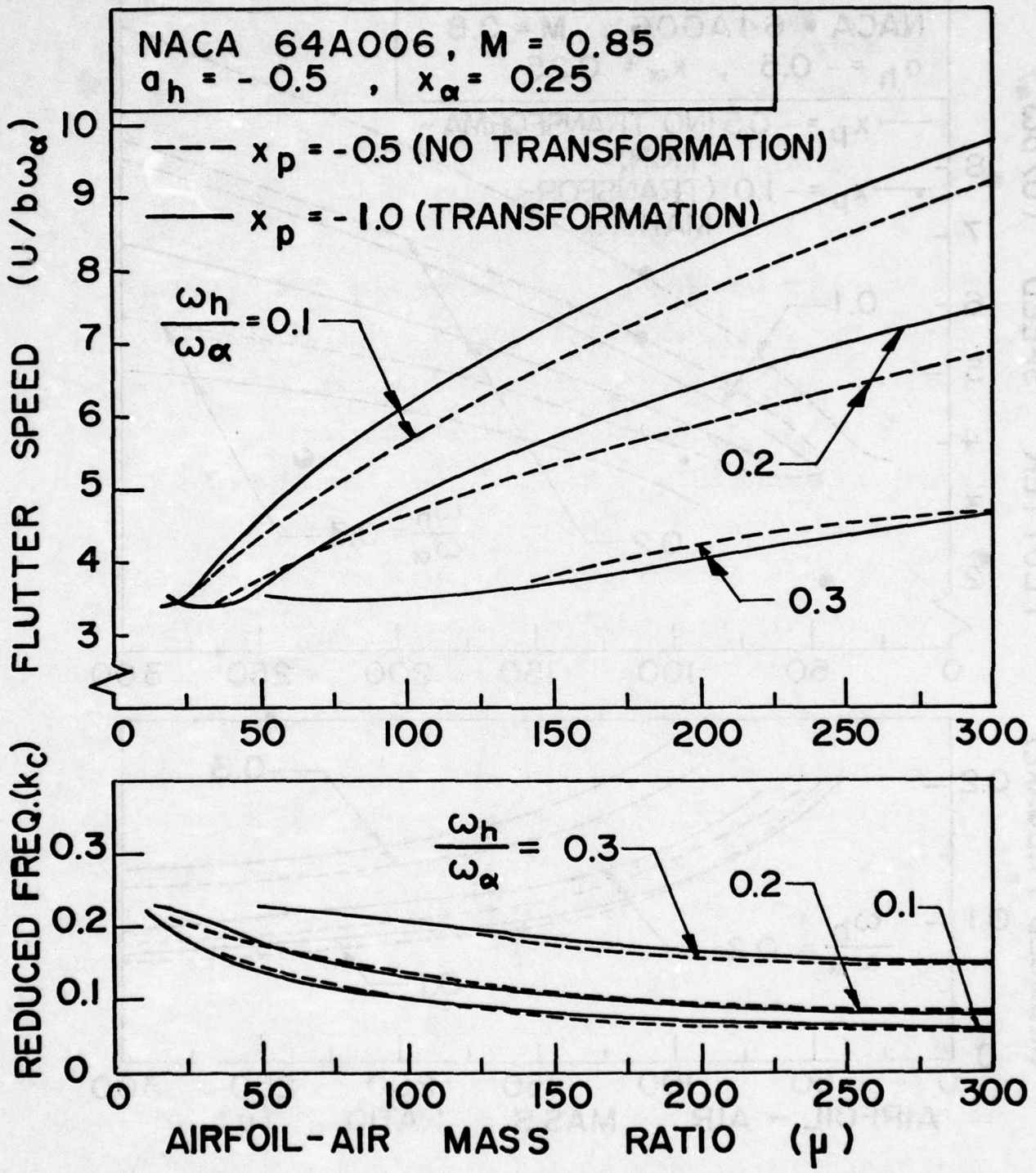

Figure 23. Effect of Transformation of Aerodynamic Coefficients (by Relaxation Method) on Flutter Speed for NACA 64A006 Airfoil at M = 0.85

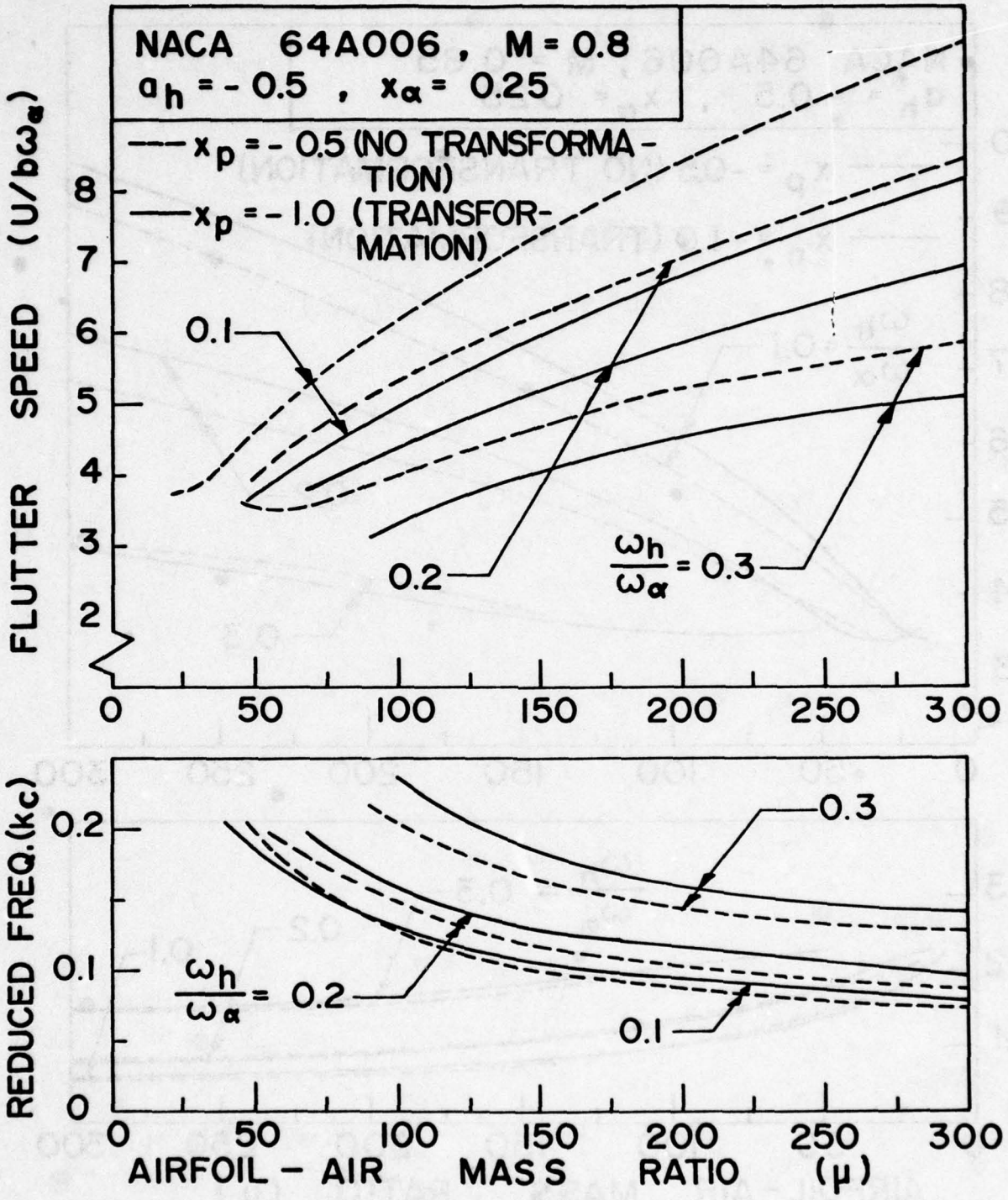

Figure 24. Effect of Transformation of Aerodynamic Coefficients (by Indicial Method) on Flutter Speed for NACA 64A006 Airfoil at M = 0.8

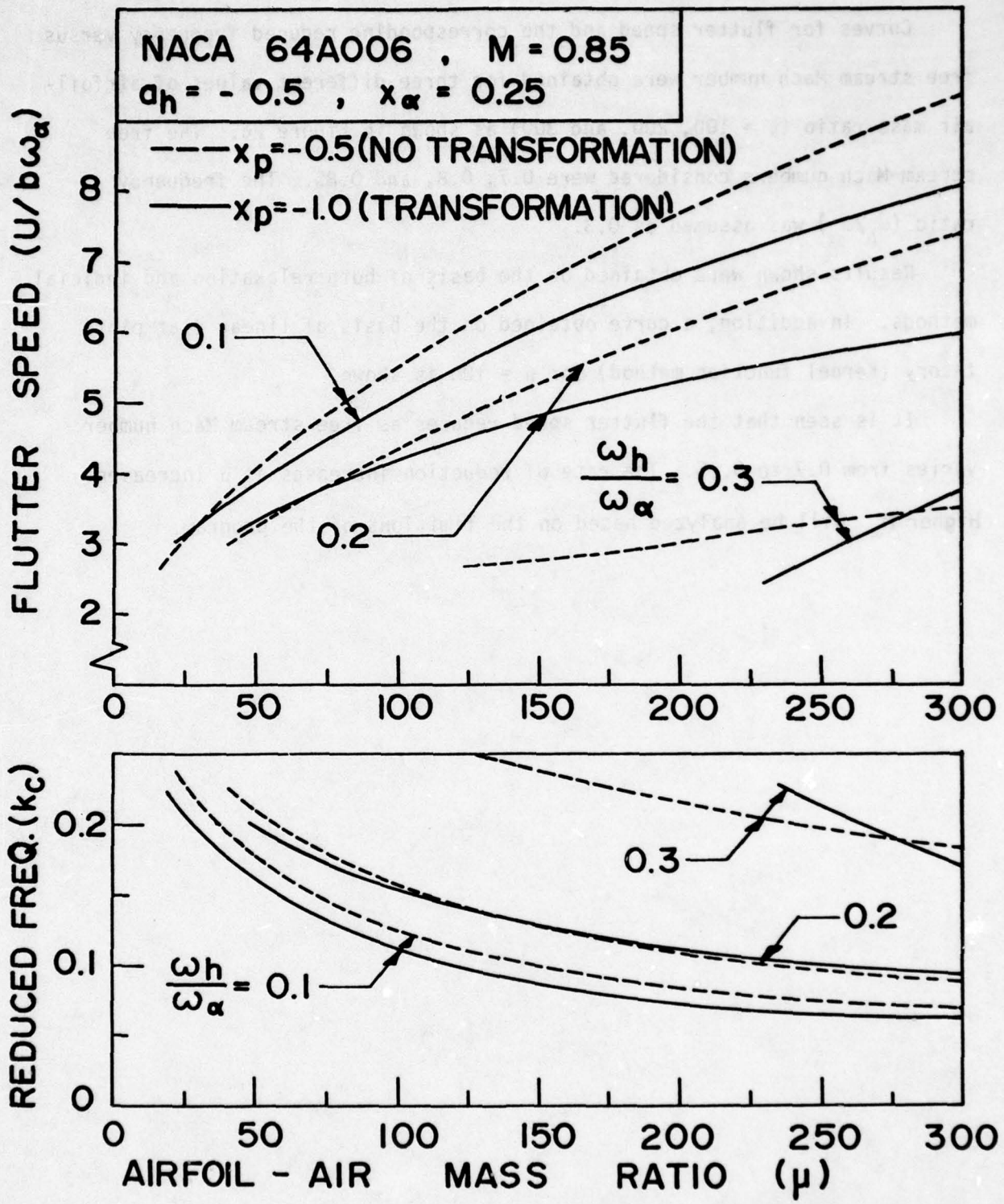

Figure 25. Effect of Transformation of Aerodynamic Coefficients (by Indicial Method) on Flutter Speed for NACA 64A006 Airfoil at M = 0.85

Curves for flutter speed and the corresponding reduced frequency versus free stream Mach number were obtained for three different values of airfoil-air mass ratio (μ = 100, 200, and 300) as shown in Figure 26. The free stream Mach numbers considered were 0.7, 0.8, and 0.85. The frequency ratio (ω_h/ω_α) was assumed as 0.3.

Results shown were obtained on the basis of both relaxation and indicial methods. In addition, a curve obtained on the basis of linear flat plate theory (Kernel function method) for μ = 100 is shown.

It is seen that the flutter speed reduces as free stream Mach number varies from 0.7 to 0.85. The rate of reduction increases as μ increases. Higher M_∞ will be analyzed based on the limitions of the program.

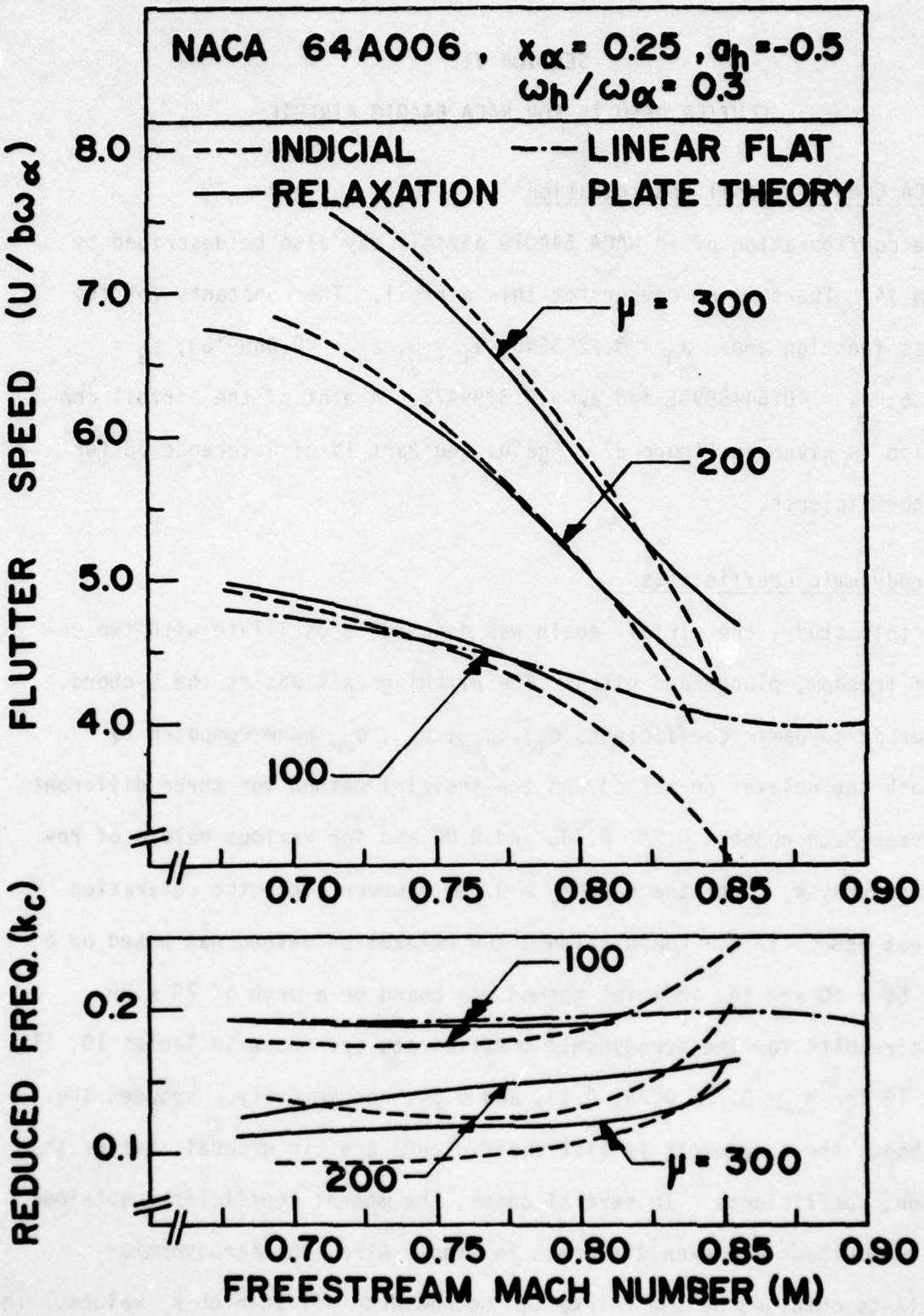

Fig. 26. Effect of Mach number on Flutter Speed of NACA 64A006 Airfoil for Various Frequency Ratios.

SECTION VII

FLUTTER RESULTS FOR NACA 64A010 AIRFOIL

(a) NACA 64A010 Airfoil Configuration

The configuration of an NACA 64A010 airfoil may also be described by Equation 44. There is no camber for this airfoil. The constants for the thickness function are: $a_0 = 0.2255645$; $a_1 = 0$; $a_2 = -0.0699163$; $a_3 = 0.0664236$; $a_4 = -0.5415990$; and $a_5 = 0.3199472$. A plot of the airfoil configuration is given in Figure 27. Again, see Part IV of Reference 38 for better coefficients.

(b) Aerodynamic Coefficients

In this study, the airfoil again was assumed to oscillate with two degrees of freedom, plunge and pitch. The pitching axis was at the ¼-chord. Thus four aerodynamic coefficients $c_{\ell\delta}$, $c_{\ell\alpha}$, $c_{m\delta}$, $c_{m\alpha}$ were computed by using both the relaxation method and the indicial method for three different free stream Mach numbers 0.72, 0.76, and 0.80 and for various values of reduced frequency k_c. For the case $M_\infty = 0.84$, however, only the relaxation method was used. In all computations, the relaxation method was based on a mesh of 59 x 60 and the indicial method was based on a mesh of 79 x 99.

The results for the aerodynamic coefficients are shown in Tables 10, 11, 12, and 13 for $M_\infty = 0.72$, 0.76, 0.80, and 0.84, respectively. Between the two methods, the agreements in lift coefficients are, in general, better than the moment coefficients. In several cases, the moment coefficients obtained by the two methods are even different in sign. Also, the aerodynamic coefficients obtained by the relaxation method drop off in high k_c values. This may be attributed to the fact that the relaxation program UTRANS2 has convergence difficulty in higher k_c values.

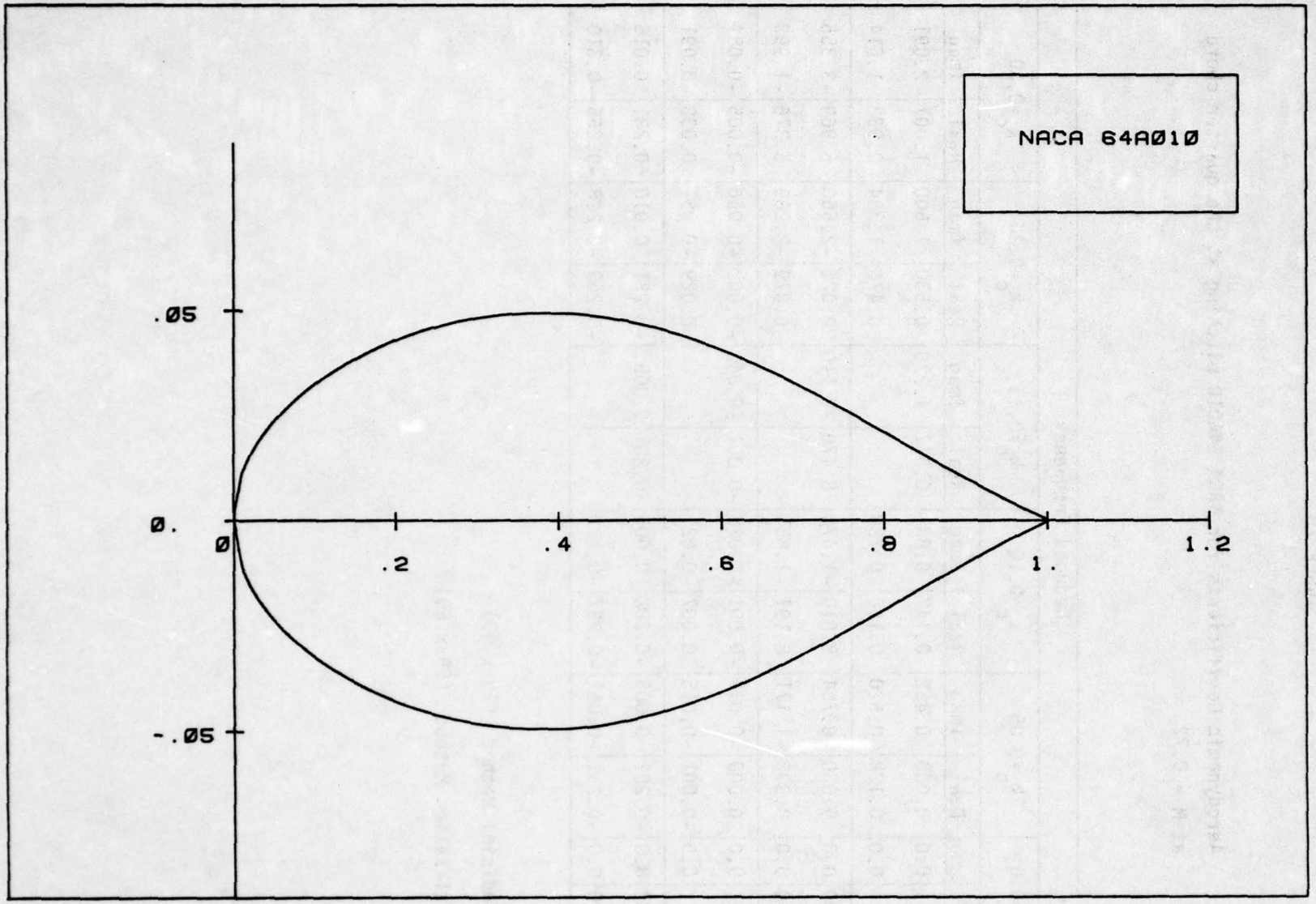

Figure 27. NACA 64A010 Airfoil Configuration

TABLE 10

Aerodynamic Coefficients for NACA 64A010 pitching at the quarter chord at M = 0.72

	Method	Reduced Frequency											
		k_c=0.0		k_c=0.05		k_c=0.10		k_c=0.15		k_c=0.20		k_c=0.30	
		Real	Imag	Real	Imag	Real	Imag	Real	Imag	Real	Imag	Real	Imag
C_{ℓ_δ}	1	0.0	0.0	0.038	0.452	0.147	0.881	0.317	1.270	0.530	1.600	1.007	2.091
	2	0.0	0.0	0.128	0.520	0.168	0.780			0.476	1.384	0.933	1.614
C_{ℓ_α}	1	9.100	0.0	9.030	-0.754	8.810	-1.470	8.470	-2.110	8.020	-2.650	6.969	-3.355
	2	9.710	0.0	8.933	-1.171	8.197	-1.851			6.679	-2.289	5.376	-1.993
C_{m_δ}	1	0.0	0.0	0.000	-0.014	-0.001	-0.028	-0.001	-0.042	-0.002	-0.056	-0.005	-0.084
	2	0.0	0.0	-0.001	-0.015	0.007	-0.021			0.029	-0.051	0.038	-0.091
C_{m_α}	1	-0.282	0.0	-0.282	0.003	-0.282	0.005	-0.281	0.008	-0.281	0.010	-0.281	0.015
	2	-0.240	0.0	-0.231	-0.062	-0.237	-0.122			-0.253	-0.228	-0.265	-0.310

Method 1: Indicial Method (79 x 99)

Method 2: Relaxation Method (59 x 60)

TABLE 11

Aerodynamic Coefficients for NACA 64A010 pitching at the quarter chord at M = 0.76

	Method	Reduced Frequency											
		k_c=0.0		k_c=0.05		k_c=0.10		k_c=0.15		k_c=0.20		k_c=0.25	
		Real	Imag	Real	Imag	Real	Imag	Real	Imag	Real	Imag	Real	Imag
C_{ℓ_δ}	1	0.0	0.0	0.068	0.519	0.252	0.976	0.503	1.330	0.762	1.590	0.985	1.770
	2	0.0	0.0	0.106	0.495	0.273	0.860	0.501	1.100	0.668	1.258	0.850	1.370
C_{ℓ_α}	1	10.610	0.0	10.380	-1.360	9.760	-2.520	8.890	-3.350	7.930	-3.810	7.070	-3.940
	2	10.672	0.0	9.766	-1.682	8.650	-2.485	7.620	-2.769	6.724	-2.711	5.925	-2.553
C_{m_δ}	1	0.0	0.0	0.000	-0.019	-0.001	-0.037	-0.003	-0.056	-0.005	-0.075	-0.008	-0.093
	2	0.0	0.0	0.001	-0.014	0.007	-0.027	0.013	-0.043	0.020	-0.058	0.025	-0.079
C_{m_α}	1	-0.374	0.0	-0.374	0.006	-0.374	0.013	-0.373	0.019	-0.373	0.025	-0.372	0.032
	2	-0.267	0.0	-0.264	-0.068	-0.271	-0.134	-0.283	-0.194	-0.293	-0.249	-0.305	-0.290

Method 1: Indicial Method (79 x 99)

Method 2: Relaxation Method (59 x 60)

TABLE 12

Aerodynamic Coefficients for NACA 64A010 pitching at the quarter chord at M = 0.80

	Method	Reduced Frequency											
		k_c=0.0		k_c=0.05		k_c=0.10		k_c=0.15		k_c=0.20		k_c=0.25	
		Real	Imag	Real	Imag	Real	Imag	Real	Imag	Real	Imag	Real	Imag
C_{ℓ_δ}	1	0.0	0.0	0.112	0.638	0.408	1.160	0.797	1.500	1.160	1.670	1.440	1.720
	2	0.0	0.0	0.143	0.557	0.394	0.918	0.639	1.117	0.860	1.235	—	—
C_{ℓ_α}	1	13.160	0.0	12.750	-2.230	11.610	-4.080	10.030	-5.310	8.350	-5.820	6.890	-5.750
	2	12.640	0.0	11.109	-2.673	9.211	-3.621	7.702	-3.647	6.510	-3.352	—	—
C_{m_δ}	1	0.0	0.0	0.000	-0.028	-0.001	-0.057	-0.002	-0.086	-0.003	-0.116	-0.006	-0.149
	2	0.0	0.0	0.001	-0.021	0.005	-0.041	0.009	-0.063	0.012	-0.088	—	—
C_{m_α}	1	-0.564	0.0	-0.564	0.005	-0.567	0.009	-0.572	0.013	-0.582	0.017	-0.597	0.023
	2	-0.416	0.0	-0.409	-0.060	-0.407	-0.126	-0.411	-0.192	-0.417	-0.244	—	—

Method 1: Indicial Method (79 x 99)

Method 2: Relaxation Method (59 x 60)

TABLE 13

Aerodynamic Coefficients for NACA 64A010 pitching at the quarter chord at M = 0.84

	Reduced Frequency									
	k_c=0.0		k_c=0.05		k_c=0.10		k_c=0.15		k_c=0.20	
	Real	Imag	Real	Imag	Real	Imag	Real	Imag	Real	Imag
C_{ℓ_δ}	0.0	0.0	0.126	0.469	0.324	0.791	0.530	0.945	0.695	1.017
C_{ℓ_α}	10.914	0.0	9.256	-2.177	7.746	-2.893	6.466	-2.993	5.267	-2.771
C_{m_δ}	0.0	0.0	-0.019	-0.075	-0.049	-0.130	-0.087	-0.159	-0.126	-0.176
C_{m_α}	-1.719	0.0	-1.474	0.283	-1.266	0.364	-1.094	0.370	-0.932	0.363

Relaxation Method (59 x 60)

The distributions of the steady pressure coefficient along the airfoil obtained by using both STRANS2 and LTRAN2 for the NACA 64A010 airfoil at M_∞ = 0.72, 0.76, 0.80, and 0.84 are shown in Figures 28, 29, 30, and 31, respectively. It should be noted that steady solutions in both STRANS2 and LTRAN2 are based on the relaxation method. The discrepancies between the two solutions may lie in the difference in mesh and the difference in the procedure of treating the shock.

(c) Flutter Results

In the flutter analysis of the NACA 64A010 airfoil, the standard U-g method was used. The effects of four parameters were considered: airfoil-air mass ratio μ; position of the mass center x_α; position of the elastic axis a_h; and the plunge - pitch frequency ratio (ω_h/ω_α). In all the following cases the values for the radius of gyration r_α and the reference frequency ω_r were assumed as 0.5 and 1.0, respectively.

1. Flutter Speeds for NACA 64A010 Airfoil Pitching about ¼-Chord Axis with Varying μ at M_∞ = 0.72, 0.76, and 0.8

The effect of airfoil - air mass ratio was first studied. The NACA 64A010 airfoil was assumed to pitch about the elastic axis located at ¼-chord (a_h =-0.5). The mass center was assumed to be at 1/8-chord aft the elastic axis (x_α = ¼) or at 37.5%-chord from the leading edge. The range of μ considered was between 25 to 300. The frequency ratios (ω_h/ω_α) considered were 0.1, 0.2, 0.3, and 0.4

Figure 32 shows a plot of the nondimensional flutter speed ($U/b\omega_\alpha$) and the corresponding reduced frequency (k_c) versus airfoil-air mass ratio at M_∞ = 0.72 and ω_h/ω_α = 0.1, 0.2, 0.3, and 0.4, respectively. It is seen that at ω_h/ω_α = 0.1, the flutter speed increases as μ increases. Such increasing rate reduces as the frequency ratio ω_h/ω_α increases. The curves

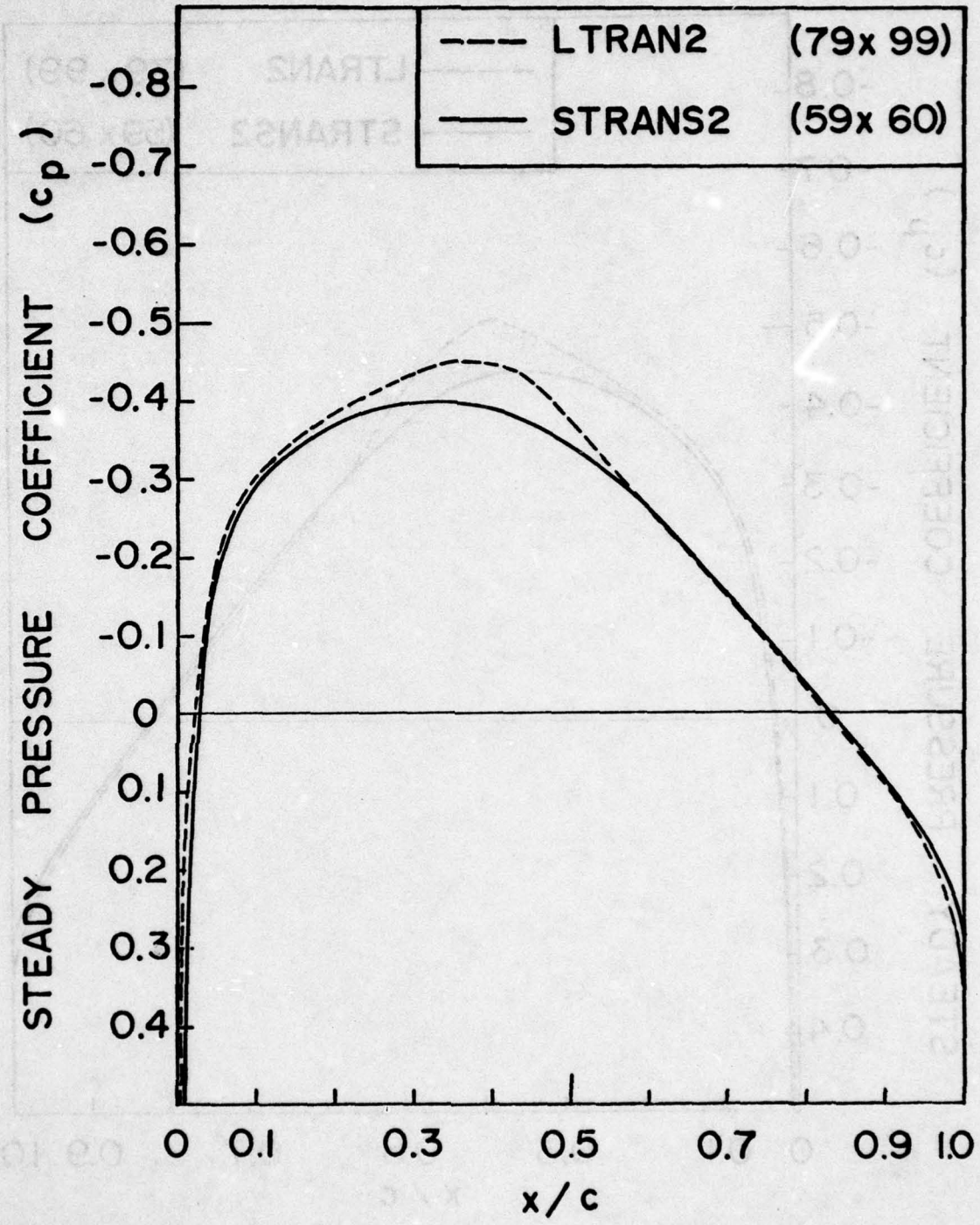

Figure 28. Distribution of Steady Pressure Coefficients for NACA 64A010 Airfoil at M = 0.72

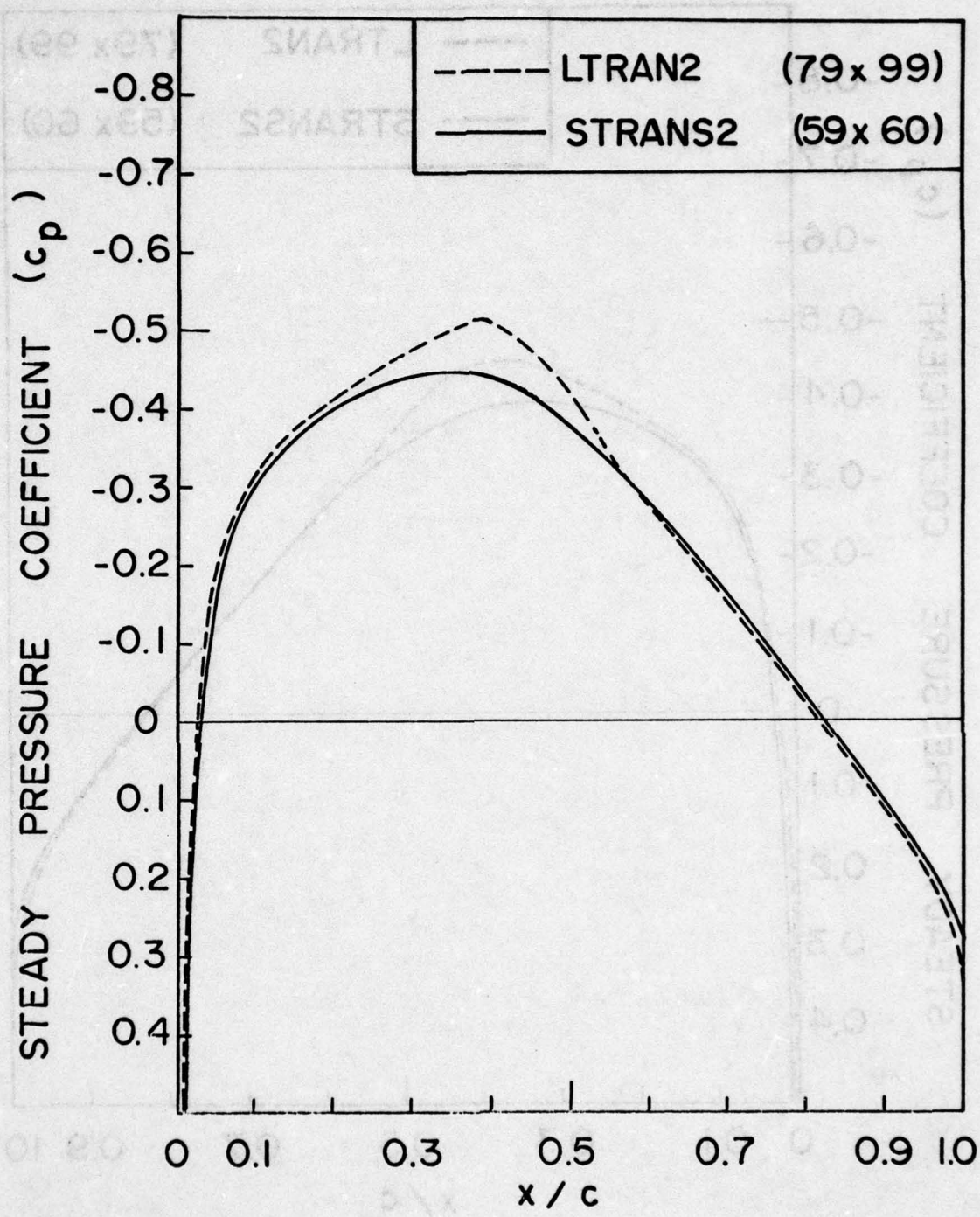

Figure 29. Distribution of Steady Pressure Coefficients for NACA 64A010 Airfoil at M = 0.76

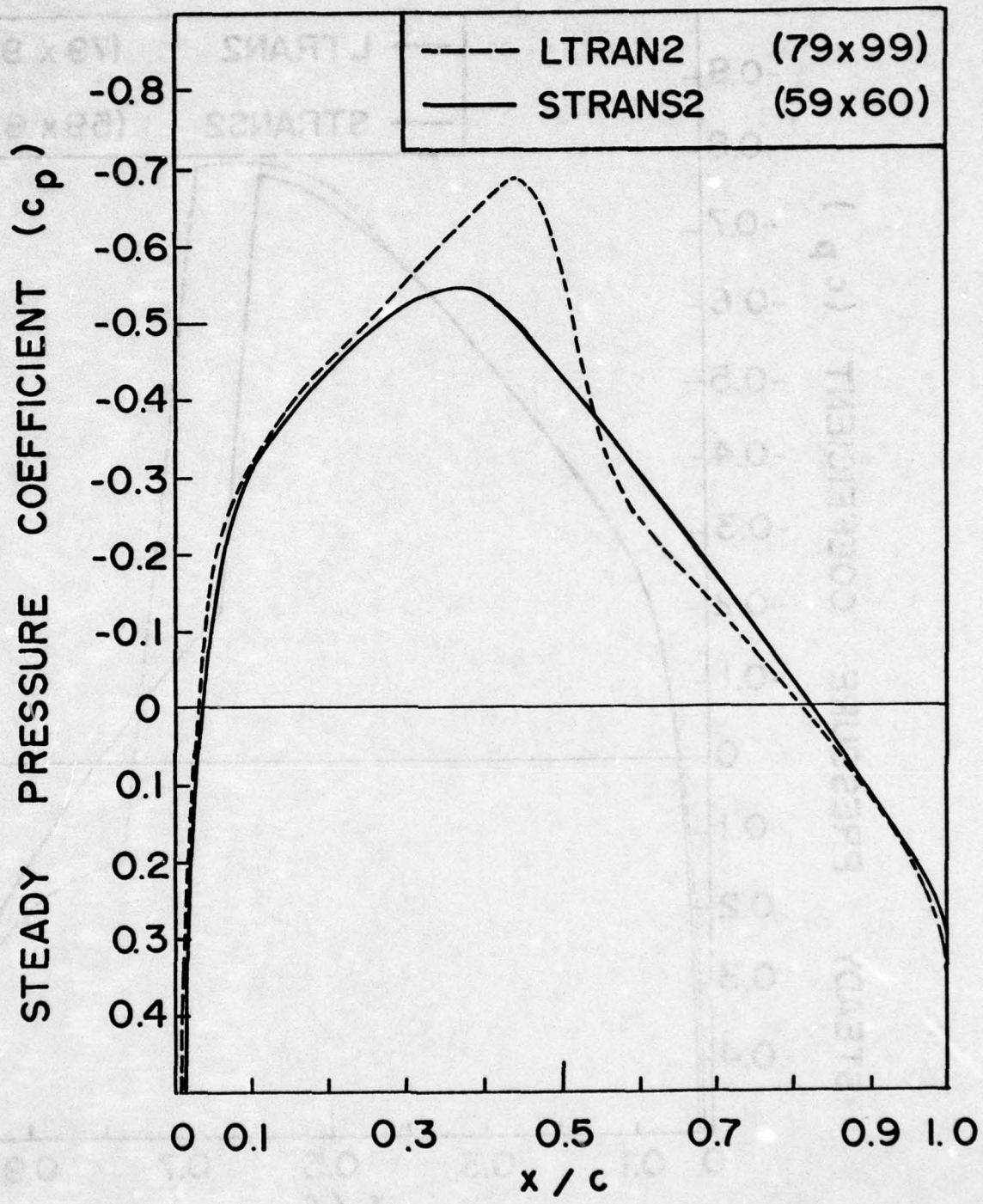

Figure 30. Distribution of Steady Pressure Coefficients for NACA 64A010 Airfoil at M = 0.8

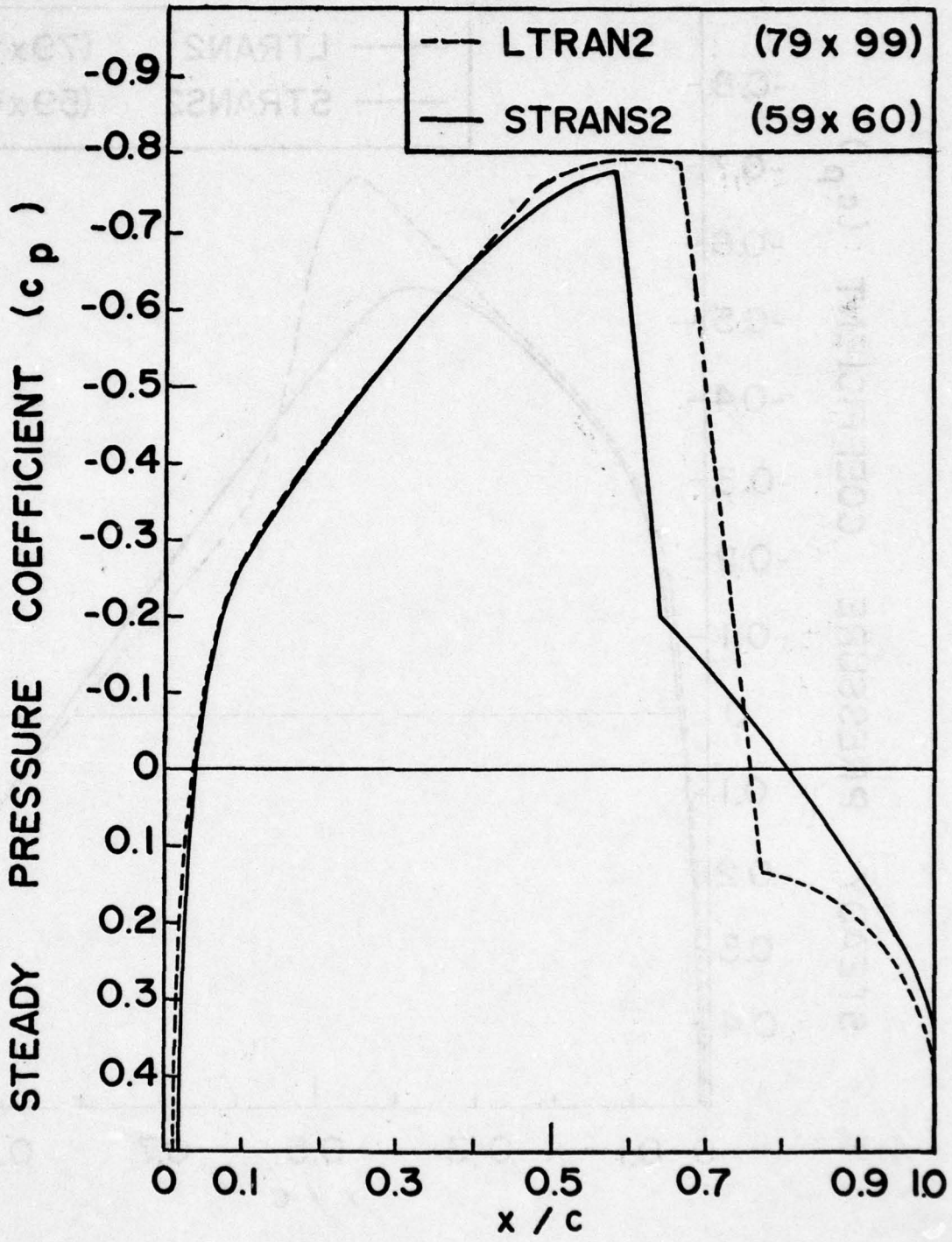

Figure 31. Distribution of Steady Pressure Coefficients for NACA 64A010 Airfoil at M = 0.84

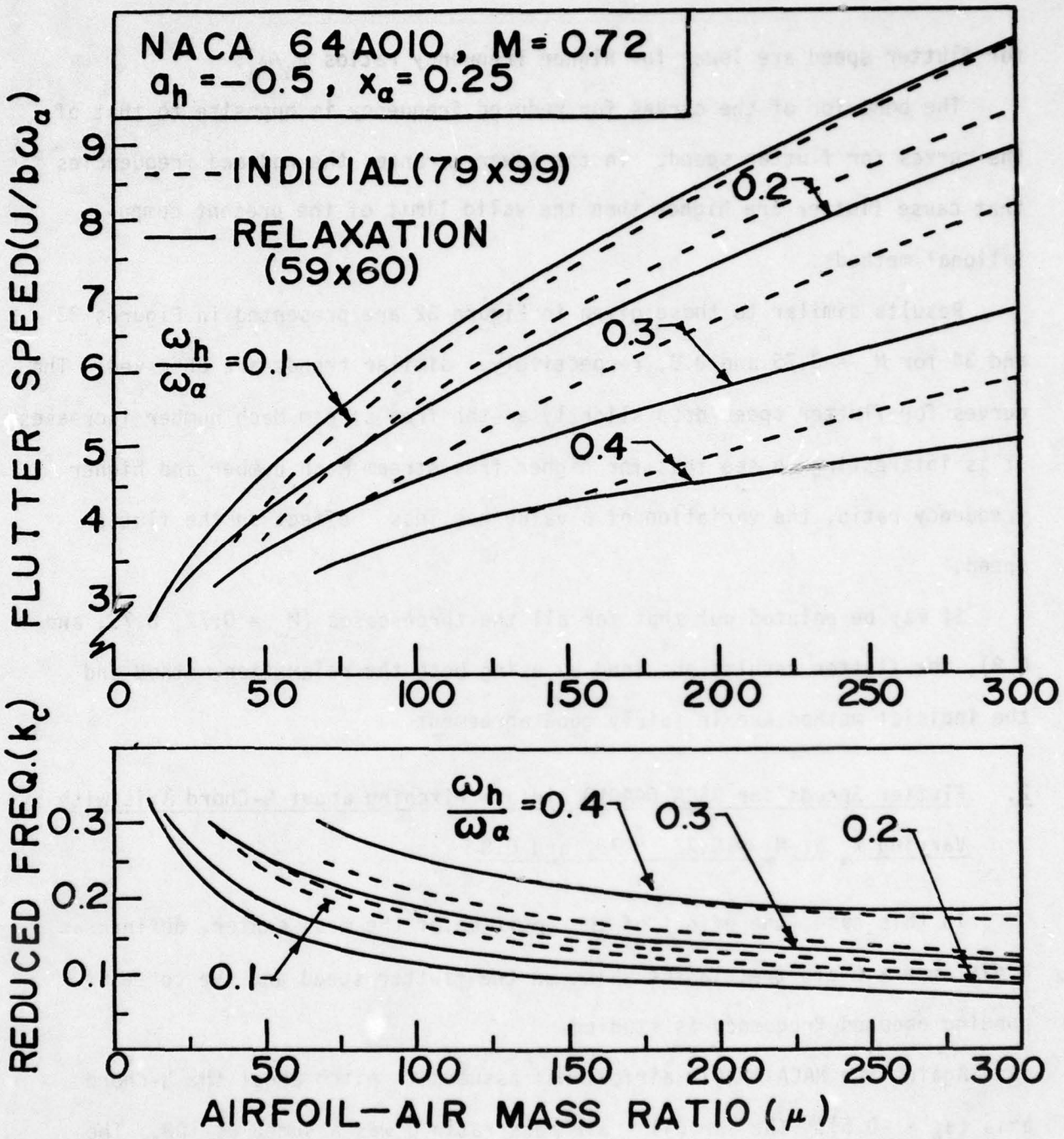

Figure 32. Effect of Mass Ratio on Flutter Speed for NACA 64A010 Airfoil for Various Frequency Ratios at M = 0.72

AD-A069 223 PURDUE UNIV LAFAYETTE IND SCHOOL OF AERONAUTICS AND --ETC F/G 20/4
FLUTTER ANALYSIS OF TWO-DIMENSIONAL AND TWO-DEGREE-OF-FREEDOM A--ETC(U)
DEC 78 T Y YANG, A G STRIZ, P GURUSWAMY AFOSR-78-3523

UNCLASSIFIED AFFDL-TR-78-202 NL

2 OF 2
AD
A069223

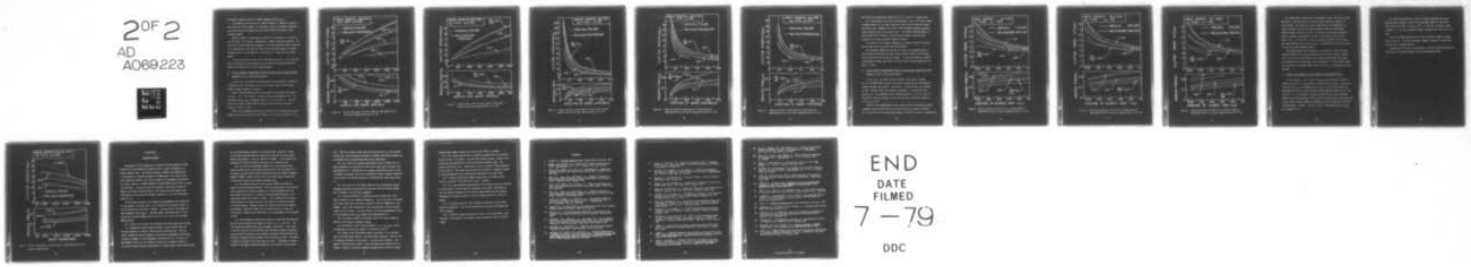

END
DATE
FILMED
7-79
DDC

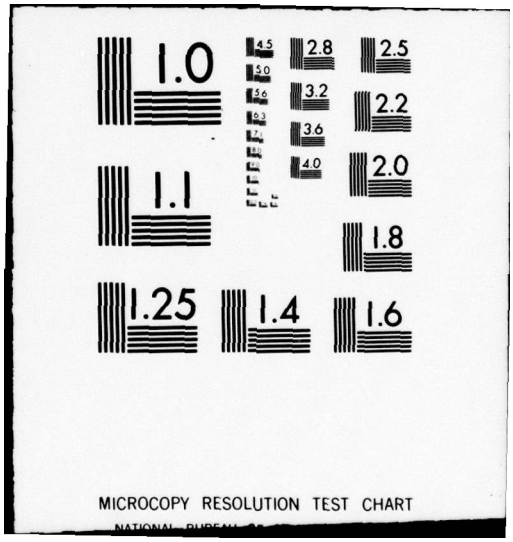
1.0
1.1
1.25
1.4
1.6
1.8
2.0
2.2
2.5
2.8
3.2
3.6
4.0
4.5
5.0
5.6
6.3
MICROCOPY RESOLUTION TEST CHART

for flutter speed are lower for higher frequency ratios ω_h/ω_α.

The behavior of the curves for reduced frequency is opposite to that of the curves for flutter speed. In the lower μ range, the reduced frequencies that cause flutter are higher than the valid limit of the present computational methods.

Results similar to those given in Figure 32 are presented in Figures 33 and 34 for M_∞ = 0.76 and 0.8, respectively. Similar trends are observed. The curves for flutter speed drop slightly as the free stream Mach number increases. It is interesting to see that for higher free stream Mach number and higher frequency ratio, the variation of μ value has less effect on the flutter speed.

It may be pointed out that for all the three cases (M_∞ = 0.72, 0.76, and 0.8), the flutter results obtained by using both the relaxation method and the indicial method are in fairly good agreement.

2. Flutter Speeds for NACA 64A010 Airfoil Pitching about ¼-Chord Axis with Varying x_α at M_∞ = 0.72, 0.76, and 0.8

In this case, the effect of the position of the mass center, defined as a distance $x_\alpha b$ aft the elastic axis, on the flutter speed and the corresponding reduced frequency is studied.

Again, the NACA 64A010 airfoil was assumed to pitch about the ¼-chord axis (a_h = -0.5). The airfoil - air mass ratio μ was assumed as 100. The frequency ratios (ω_h/ω_α) considered were 0.1, 0.2, 0.3, and 0.4. The mass center was assumed to move from the elastic axis at ¼-chord to ½-chord (from x_α = 0 to x_α = 0.5).

Plots of the nondimensional flutter speed and the corresponding reduced frequency versus the position of mass center x_α are shown in Figures 35, 36,

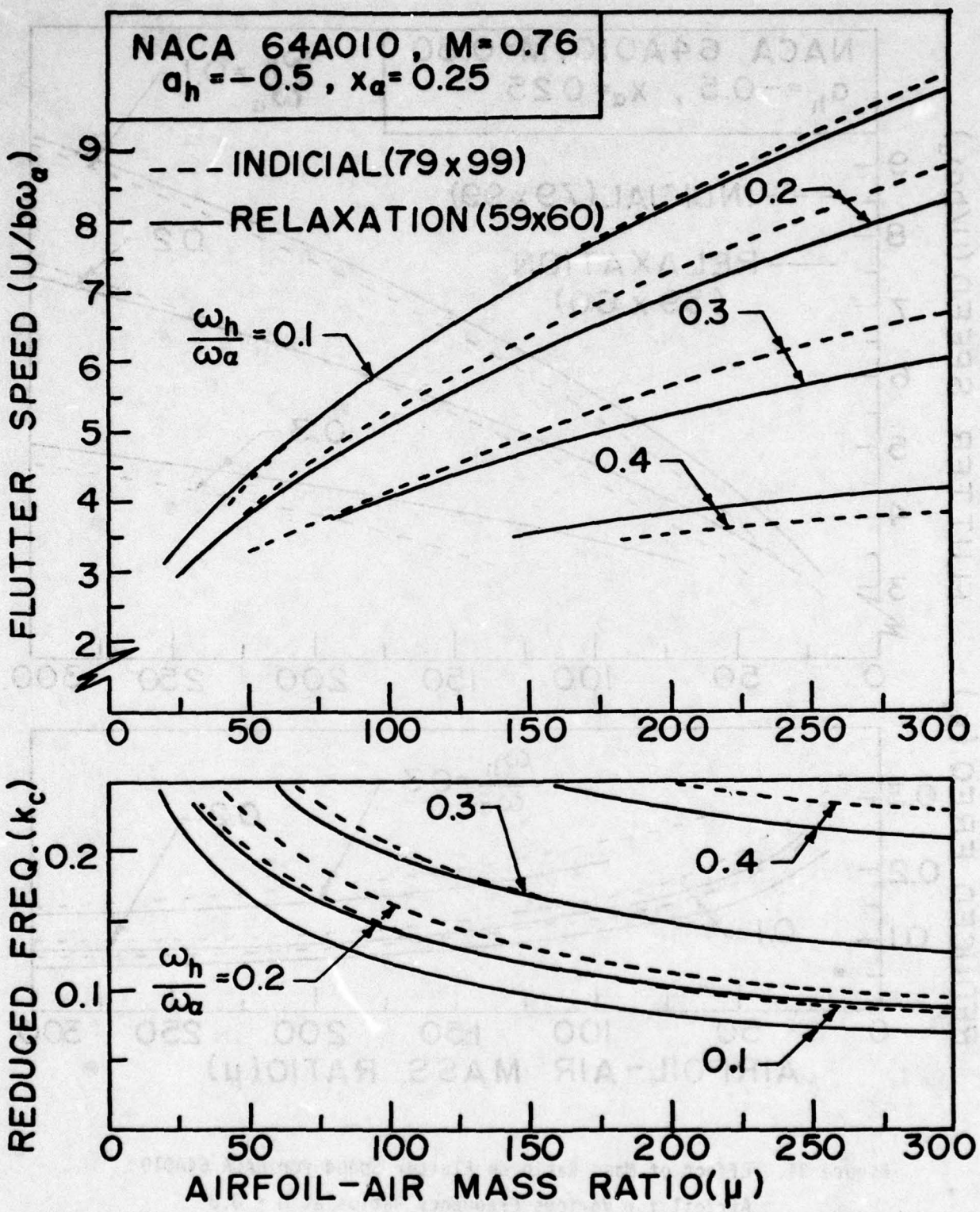

Figure 33. Effect of Mass Ratio on Flutter Speed for NACA 64A010 Airfoil for Various Frequency Ratios at M = 0.76

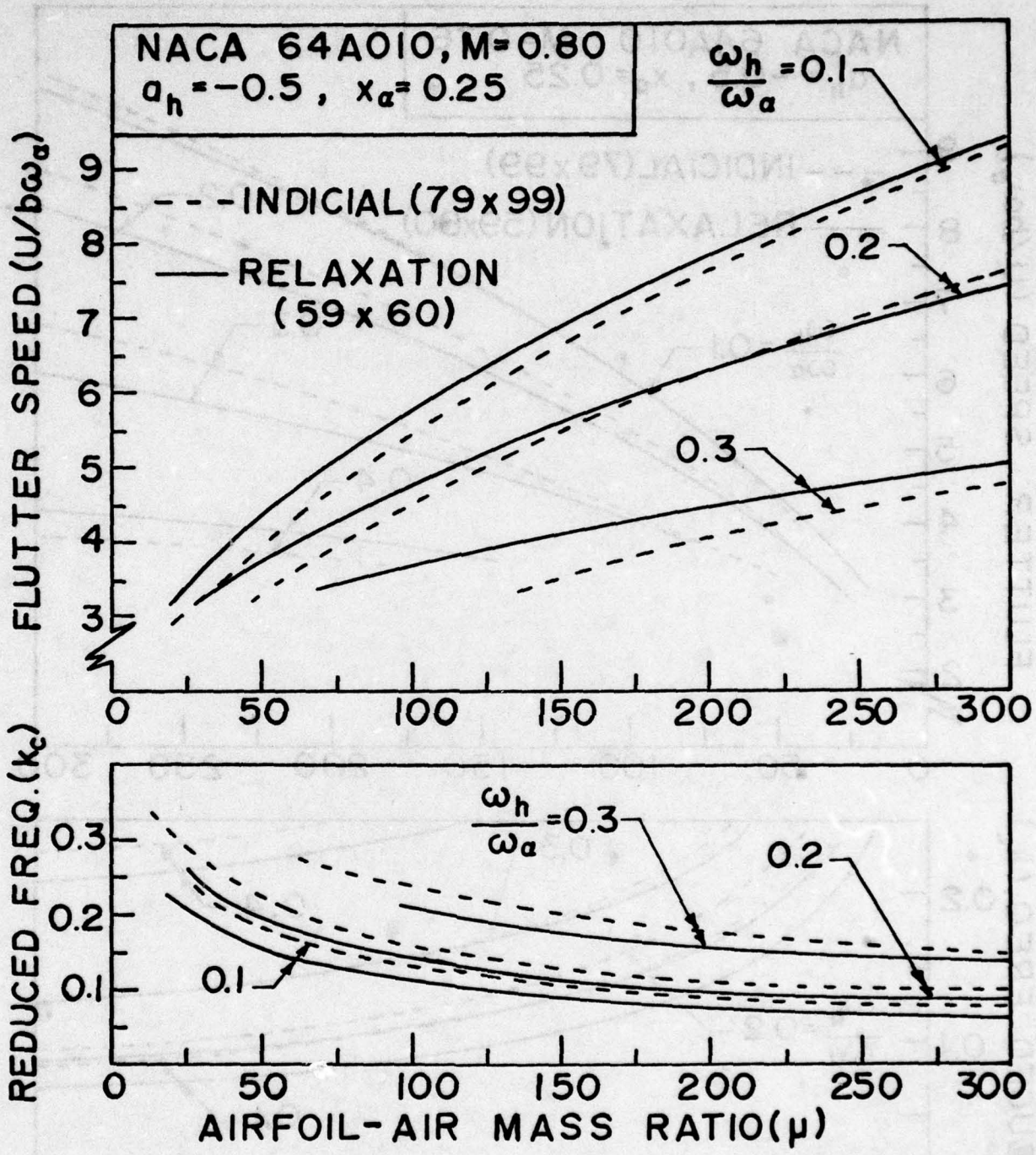

Figure 34. Effect of Mass Ratio on Flutter Speed for NACA 64A010 Airfoil for Various Frequency Ratios at M = 0.8

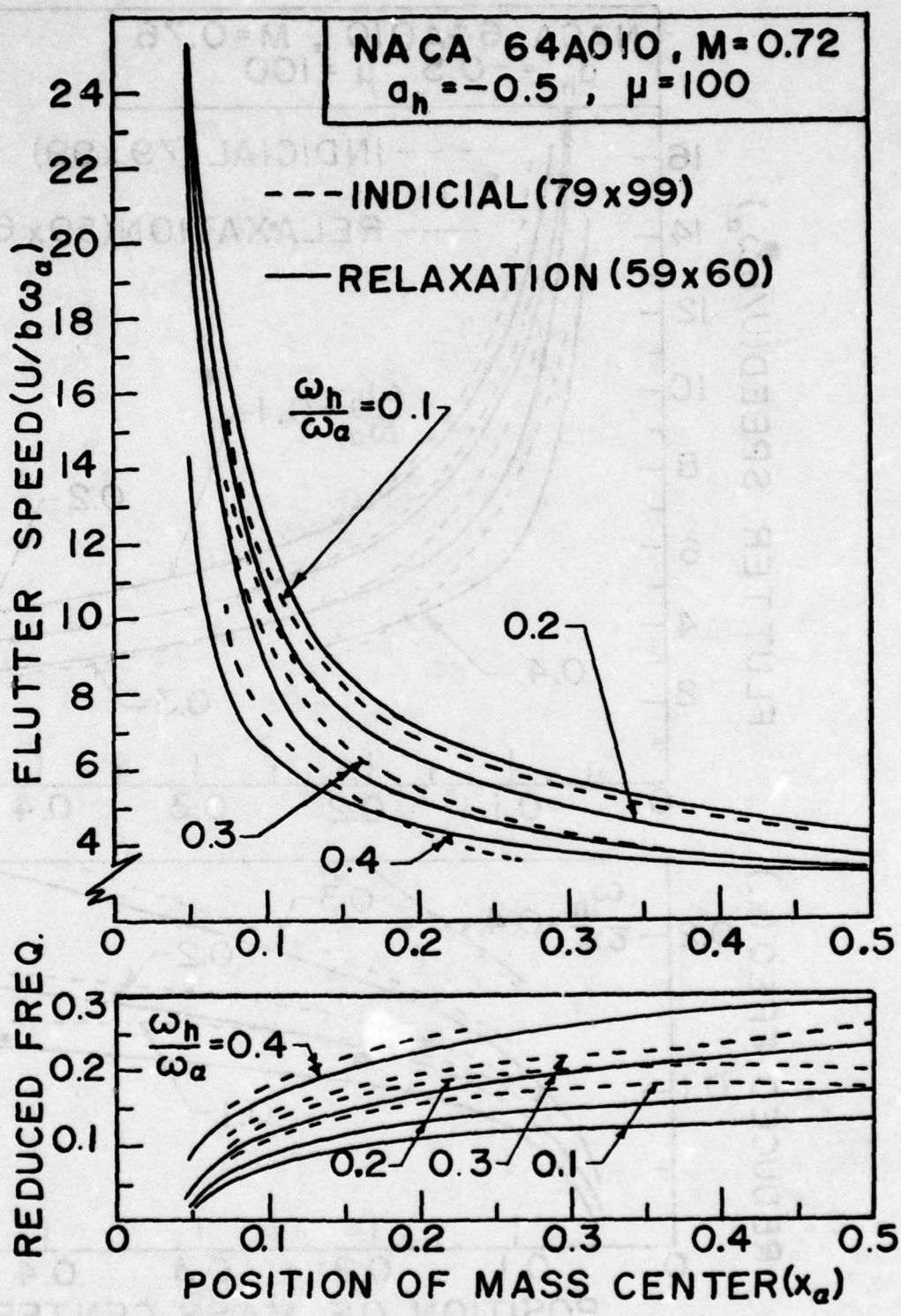

Figure 35. Effect of Position of Mass Center on Flutter Speed for NACA 64A010 Airfoil for Various Frequency Ratios at M = 0.72

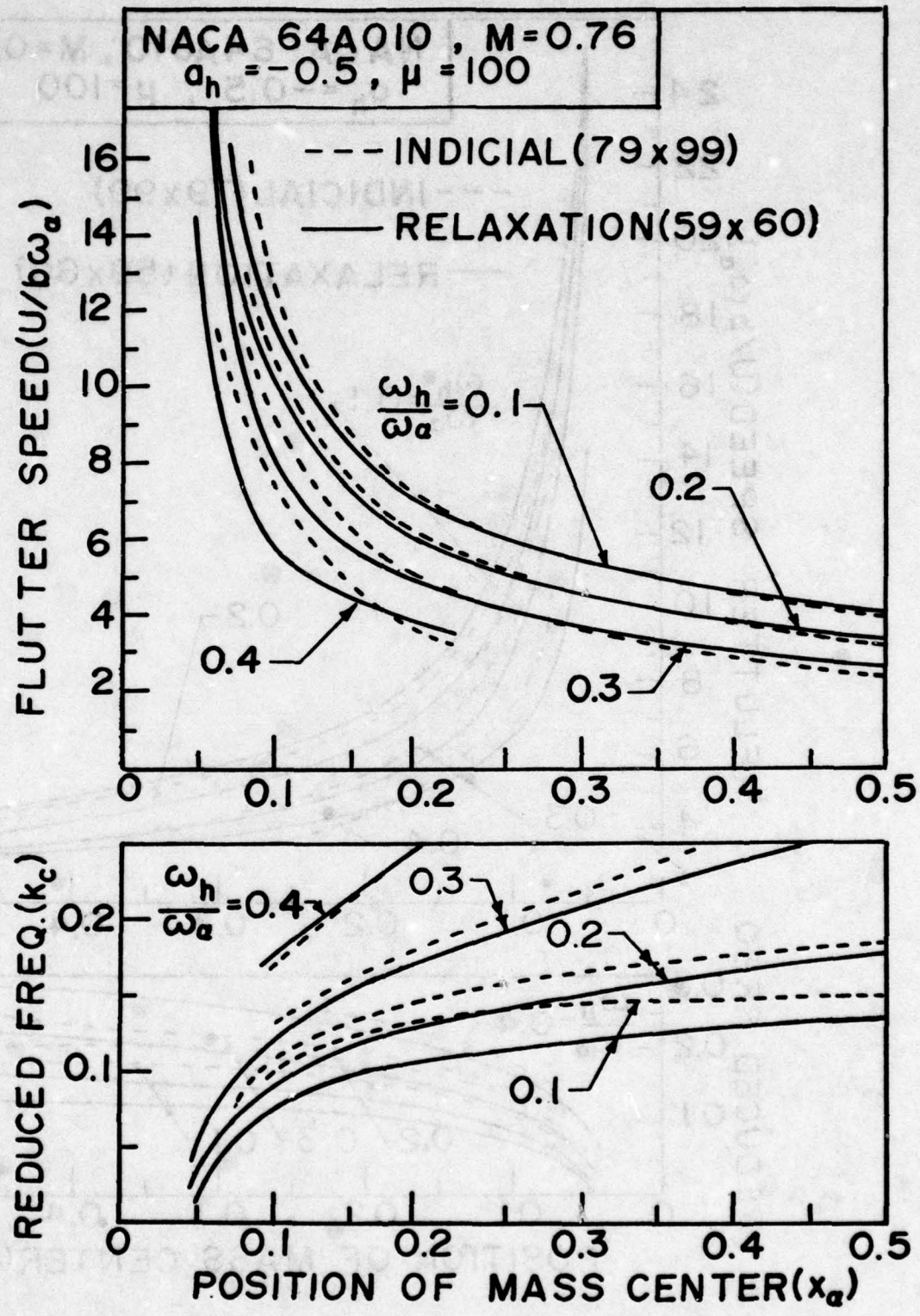

Figure 36. Effect of Position of Mass Center on Flutter Speed for NACA 64A010 Airfoil for Various Frequency Ratios at M = 0.76

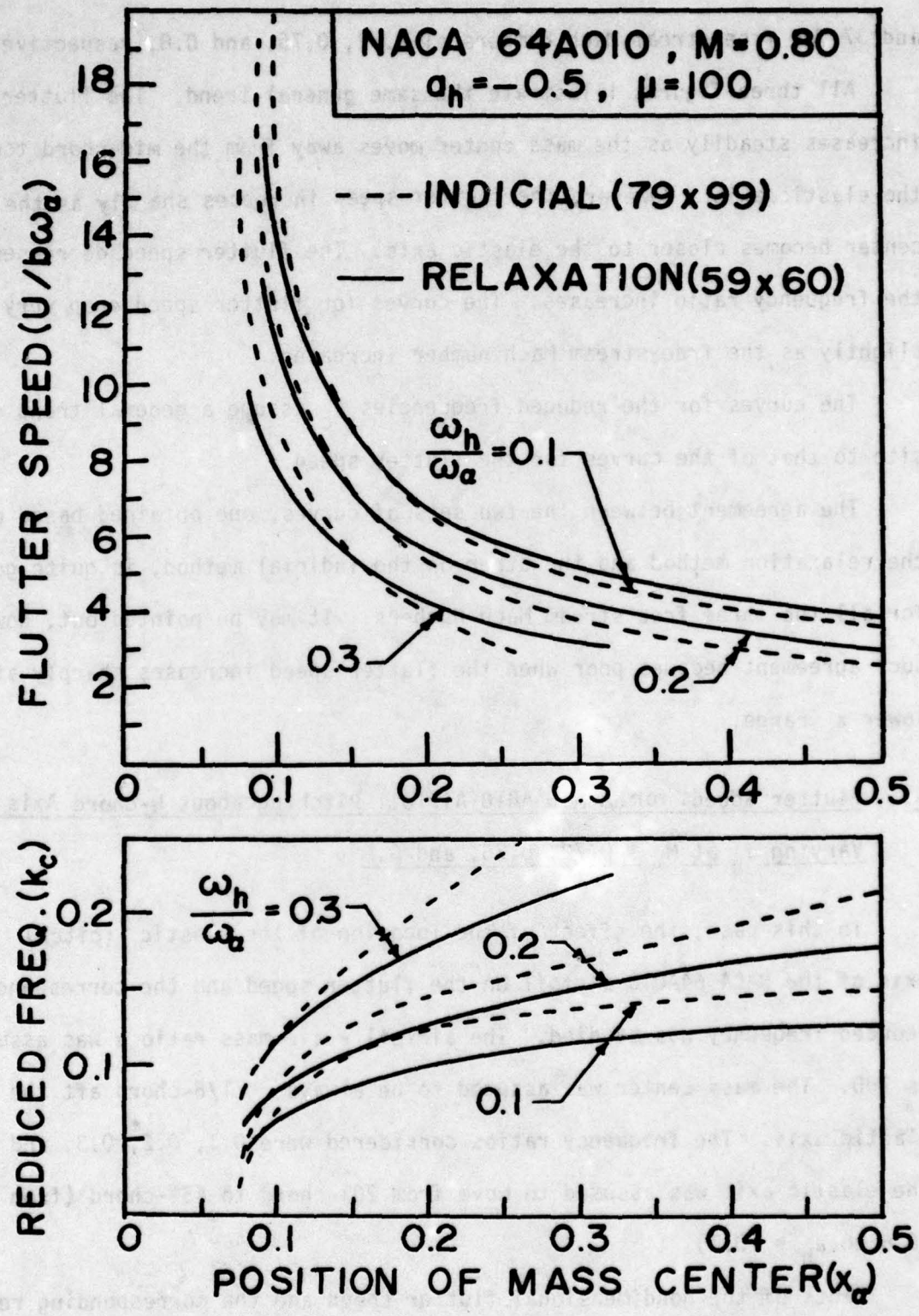

Figure 37. Effect of Position of Mass Center on Flutter Speed for NACA 64A010 Airfoil for Various Frequency Ratios at M = 0.8

and 37 for free stream Mach numbers of 0.72, 0.76, and 0.8, respectively.

All three figures illustrate the same general trend. The flutter speed increases steadily as the mass center moves away from the mid-chord toward the elastic axis. However, the flutter speed increases sharply as the mass center becomes closer to the elastic axis. The flutter speed decreases as the frequency ratio increases. The curves for flutter speed drop very slightly as the free stream Mach number increases.

The curves for the reduced frequencies k_c assume a general trend opposite to that of the curves for the flutter speed.

The agreement between the two sets of curves, one obtained based on the relaxation method and the other on the indicial method, is quite good for all the three free stream Mach numbers. It may be pointed out, however, such agreement becomes poor when the flutter speed increases sharply at the lower x_α range.

3. Flutter Speeds for NACA 64A010 Airfoil Pitching about ¼-Chord Axis with Varying a_h at M_∞ = 0.72, 0.76, and 0.8

In this case, the effect of the location of the elastic (pitch) axis of the NACA 64A010 airfoil on the flutter speed and the corresponding reduced frequency was studied. The airfoil - air mass ratio μ was assumed as 100. The mass center was assumed to be always 1/8-chord aft the elastic axis. The frequency ratios considered were 0.1, 0.2, 0.3, and 0.4. The elastic axis was assumed to move from 20%-chord to 45%-chord (from a_h = -0.6 to a_h = -0.1).

Plots of the nondimensional flutter speed and the corresponding reduced frequency versus the position of the elastic axis a_h are shown in Figures 38, 39, and 40 for free stream Mach numbers of 0.72, 0.76, and 0.8, respectively.

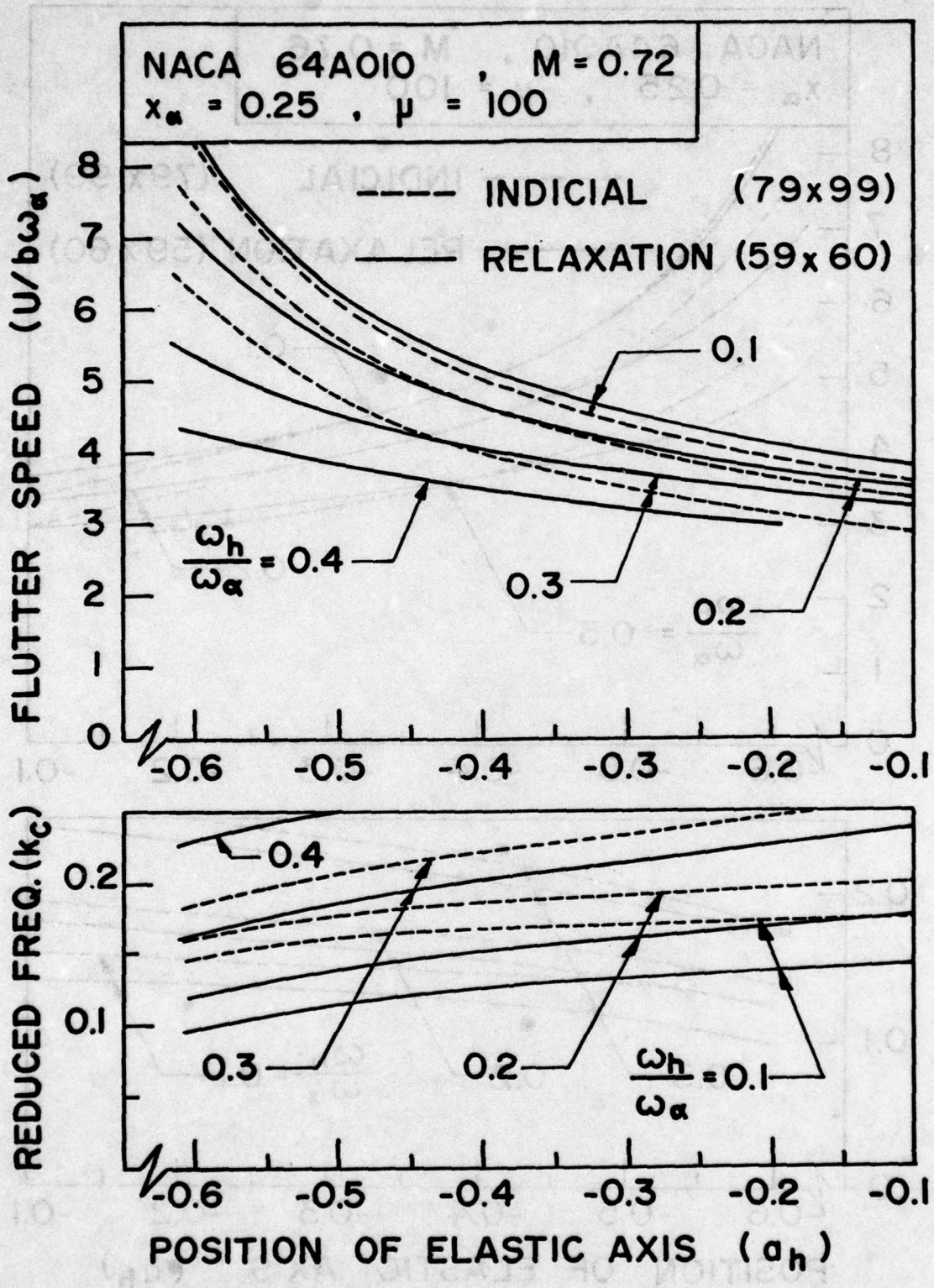

Figure 38. Effect of Position of Elastic Axis on Flutter Speed for NACA 64A010 Airfoil for Various Frequency Ratios at M = 0.72

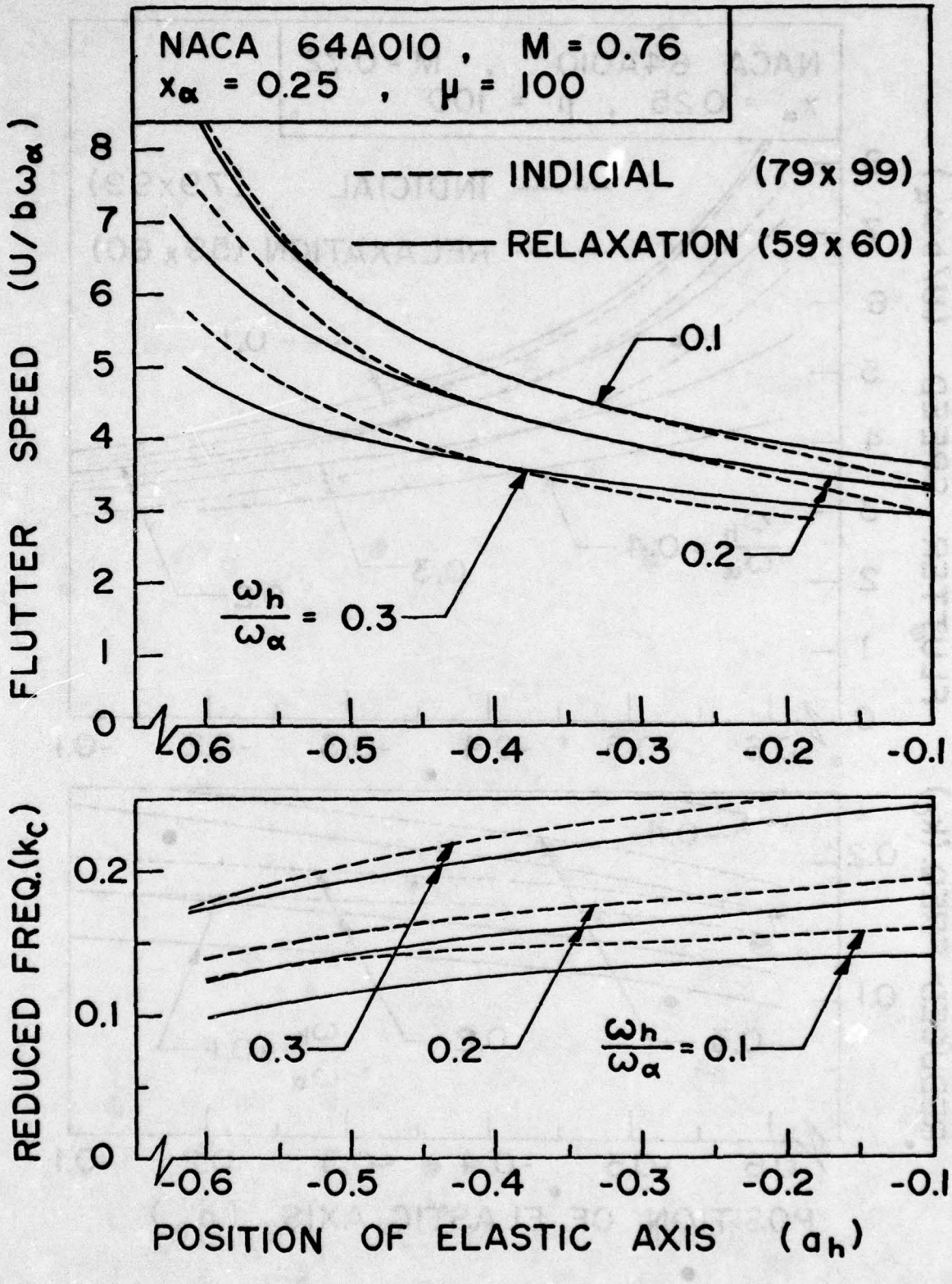

Figure 39. Effect of Position of Elastic Axis on Flutter Speed for NACA 64A010 Airfoil for Various Frequency Ratios at M = 0.76

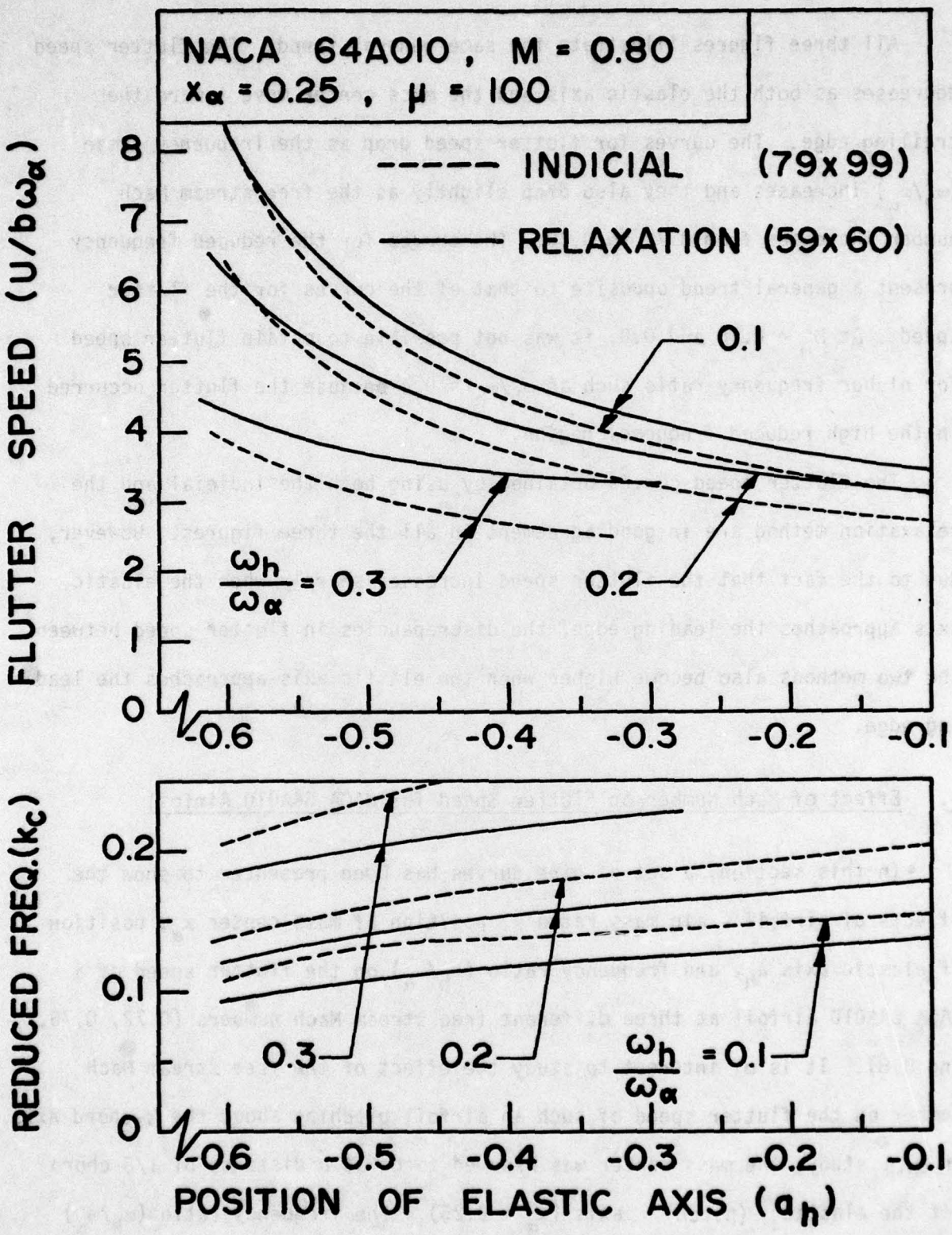

Figure 40. Effect of Position of Elastic Axis on Flutter Speed for NACA 64A010 Airfoil for Various Frequency Ratios at M = 0.8

All three figures illustrate the same general trend. The flutter speed decreases as both the elastic axis and the mass center move toward the trailing edge. The curves for flutter speed drop as the frequency ratio (ω_h/ω_α) increases and they also drop slightly as the free stream Mach number increases from 0.72 to 0.80. The curves for the reduced frequency present a general trend opposite to that of the curves for the flutter speed. At M_∞ = 0.76 and 0.8, it was not possible to obtain flutter speed for higher frequency ratio such as ω_h/ω_α = 0.4 because the flutter occurred in the high reduced frequency region.

The flutter speed curves obtained by using both the indicial and the relaxation method are in good agreement in all the three figures. However, due to the fact that the flutter speed increases sharply when the elastic axis approaches the leading edge, the discrepancies in flutter speed between the two methods also become higher when the elastic axis approaches the leading edge.

4. Effect of Mach Number on Flutter Speed for NACA 64A010 Airfoil

In this section, a set of nine curves has been presented to show the effects of airfoil - air mass ratio μ, position of mass center x_α, position of elastic axis a_h, and frequency ratio (ω_h/ω_α) on the flutter speed of a NACA 64A010 airfoil at three different free stream Mach numbers (0.72, 0.76, and 0.8). It is of interest to study the effect of the free stream Mach number on the flutter speed of such an airfoil pitching about the ¼-chord axis. In this study, the mass center was assumed to be at a distance of 1/8-chord aft the elastic (pitch) axis (x_α = 0.25). The frequency ratio (ω_h/ω_α) was assumed as 0.3.

The results were obtained as plots of flutter speed and the corresponding reduced frequency versus free stream Mach number for three different values of airfoil - air mass ratio (μ = 100, 200, and 300) as shown in Figure 41. The free stream Mach numbers considered were 0.72, 0.76, and 0.80.

The flutter speed decreases as the free stream Mach number increases from 0.72 to 0.8. The rate of decrease, however, decreases as the airfoil - air mass ratio μ becomes smaller.

The two sets of curves, one obtained by using the relaxation method and the other by the indicial method, show the same general trend.

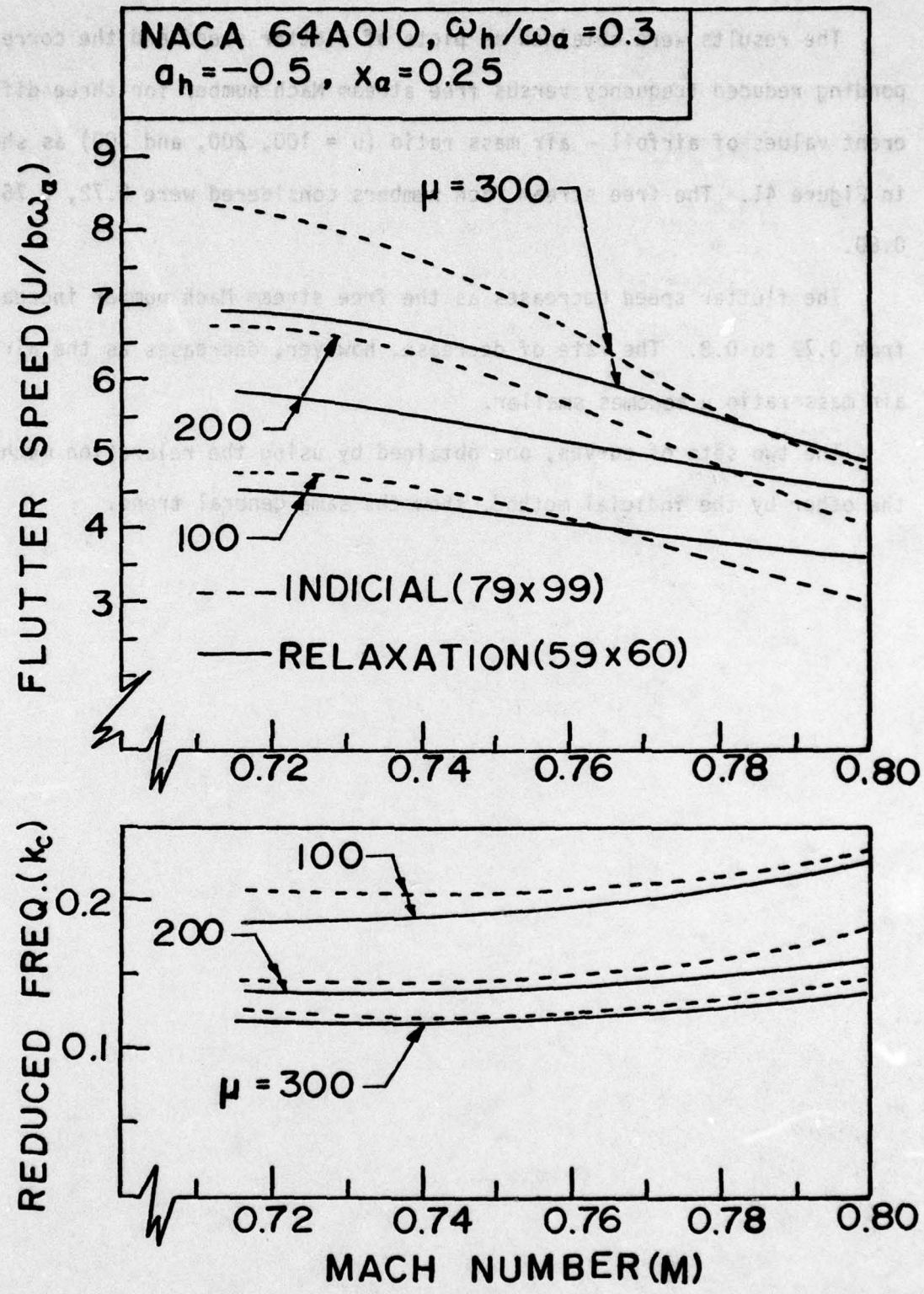

Fig. 41. Effect of Mach Number on Flutter Speed of NACA 64A010 Airfoil for Various Frequency Ratios.

SECTION VIII

CONCLUDING REMARKS

The purpose of this research was to study the flutter behavior of two-dimensional and two degree-of-freedom airfoils in small disturbance, unsteady transonic flow. Two computer programs, STRANS2 and UTRANS2 based on the harmonic or relaxation method and LTRAN2 based on the indicial and time-integration methods, were used to compute the aerodynamic coefficients for flutter analysis. An NACA 64A006 and an NACA 64A010 airfoil were selected for this study. A flat plate was also selected in the study in order to compare the flutter solutions based on the linear flat plate theory with those based on the present two computer programs at a low free stream Mach number of 0.7.

In the flutter analysis, the effects of four parameters were considered: (1) the airfoil - air mass ratio μ; (2) the position of the mass center x_α; (3) the position of the elastic (pitch) axis a_h; and (4) the plunge to pitch frequency ratio (ω_h/ω_α). The Mach numbers considered were 0.7, 0.8, and 0.85 for the NACA 64A006 airfoil and 0.72, 0.76, and 0.8 for the NACA 64A010 airfoil.

As a result of this study, the following concluding remarks may be made:

(1) Although the time-integration method is more accurate than the relaxation method, it requires relatively more computing time. Thus the indicial method was used to compute all the present aerodynamic coefficients. In order to compute all the aerodynamic coefficients at $M_\infty = 0.76$ for the NACA 64A010 airfoil for five different values of k_c as shown in Table 11, the indicial method required approximately 2.1 hours central processing (CP) time

on a CDC 6500 computer whereas the relaxation method required 4.7 hours. If the time-integration method is used for the same mesh as the indicial method, approximately 7 hours CP time will be needed. In the present computations, the finite difference mesh plays a very important role.

(2) At a low free stream Mach number of 0.7, the results for the steady pressure curves, the unsteady pressure curves, the aerodynamic coefficients, and the flutter speeds obtained by using the computer programs STRANS2, UTRANS2, LTRAN2, and the linear flat plate theory program based on the Kernel function method agree reasonably well.

(3) The steady solutions of both programs STRANS2 and LTRAN2 are based on the same relaxation method. Thus the steady pressure distribution curves obtained by using both programs are in good agreement in the low Mach numbers that result in no shocks and present some difference in the higher Mach numbers that result in shocks. This difference may be due to the difference in the mesh size and in the manner the shocks are treated in the two programs. Because in both the relaxation and indicial methods the unsteady computation depends on the steady solution as input, the differences in steady results contribute to the disagreement in the unsteady results.

(4) The aerodynamic coefficients obtained by using both the relaxation and the indicial methods are compared in Tables 1-4, 6-7, and 10-12. The lift coefficients agree better than the moment coefficients. This is due to the fact that the lift coefficients were obtained by merely integrating the area under the pressure curves whereas the moment coefficients were obtained by integrating the area-moment under the pressure curves. The former integration resulted in less error than the latter. Furthermore, the magnitudes of the moment coefficients depend on the location of the pitching

axis. They are relatively small when the pitching axis is at the ¼-chord. In that case, the percentage differences in moment coefficients between the two methods could be magnified and may not be significant.

(5) Due to the low frequency approximation used in LTRAN2, the reduced frequencies k_c considered in most of the cases were not higher than approximately 0.2. Although the low frequency approximation was not used in UTRANS2, convergence could not be obtained at higher reduced frequencies. In this study, the reduced frequencies considered were never higher than 0.3.

(6) The curves for the flutter speed and the corresponding reduced frequency obtained by using both the relaxation and the indicial methods are, in general, in fairly good agreement.

(7) The main difficulty in obtaining flutter results was in the upper limitation of the reduced frequency k_c. In all the cases, the search for flutter points was below the k_c values of 0.25 for LTRAN2 and 0.3 for UTRANS2. Due to such limitations, it was not possible to obtain flutter results for the airfoil - air mass ratios μ less than approximately 25 and for the frequency ratios ω_h/ω_α higher than approximately 0.4.

(8) The general trend of the present curves for flutter speed are similar to the curves in subsonic region.

(9) The effect of each of the parameters μ, x_α, a_h, ω_h/ω_α, and M_∞ is presented and discussed in detail in Sections VI and VII.

(10) Based on the limited Mach numbers considered, it was observed that the flutter speed reduces as the Mach number increases. But the rate of reduction decreases as the airfoil - air mass ratio decreases. More general conclusions may be made if more and higher Mach numbers were considered. However, the present computer programs are not valid for higher

transonic Mach numbers because the inviscid flow theory is assumed.

(11) This analysis may provide a systematic procedure for the transonic flutter analysis of airfoils. The study may further provide a review of the limitations and capabilities of the two existing transonic codes. The present results may give some insight into the transonic flutter behaviors of the airfoils. The present results may also be used as a comparative basis by the experimentalists and other analysts who work in the same field.

(12) In order to make more rigorous conclusions, the study of more airfoils, especially the supercritical ones, is needed.

(13) For a more complete understanding of the transonic flutter behaviors of the airfoils in wider ranges of parameters, the present limitations on very low reduced frequency and low transonic Mach numbers must be removed. Improvement in transonic codes to allow for higher values of k_c and M_∞ is needed.

(14) To be more realistic, the structural flexibility of the airfoil should be considered. This can be accounted for by using curved beam-type finite elements.

(15) In order to study more practical cases of full wing flutter, the extension of the present 2-D transonic code to account for the 3-D case is needed.

REFERENCES

1. Landahl, M., Unsteady Transonic Flow, Pergamon Press, New York, 1961.

2. Murman, E.M. and Cole, J.D., "Calculation of Plane Steady Transonic Flows," AIAA Journal, Vol. 9, No. 1, January 1971, pp. 114-121.

3. Traci, R.M., Albano, E.D., Farr, J.L., and Cheng, H.K., "Small Disturbance Transonic Flows About Oscillating Airfoils," AFFDL-TR-74-37, June 1974.

4. Farr, J.L., Traci, R.M., and Albano, E.D., "Computer Programs for Calculating Small Disturbance Transonic Flows About Oscillating Airfoils," AFFDL-TR-74-135, November 1974.

5. Traci, R.M., Albano, E.D., and Farr, J.L., "Small Disturbance Transonic Flows About Oscillating Airfoils and Planar Wings," AFFDL-TR-75-100, June 1975.

6. Farr, J.L., Traci, R.M., and Albano, E.D., "Computer Programs for Calculating Small Disturbance Transonic Flows About Oscillating Planar Wings," AFFDL-TR-75-103, August 1975.

7. Traci, R.M., Albano, E.D., and Farr, J.L., "Perturbation Method for Transonic Flows About Oscillating Airfoils," AIAA Journal, Vol. 14, No. 9, September 1976, pp. 1258-1265.

8. Holman, W.L., "A User's Guide for the Improved Versions of the Computer Programs STRANS and UTRANS," AFFDL-TM-75-168-FYS.

9. Ehlers, F.E., "A Finite Difference Method for the Solution of the Transonic Flow Around Harmonically Oscillating Wings," NASA CR-2257, 1974.

10. Weatherill, W.H., Sebastian, J.D., and Ehlers, F.E., "On the Computation of the Transonic Perturbation Flow Fields Around Two- and Three-Dimensional Oscillating Wings," AIAA Paper 76-99, January 1976.

11. Ballhaus, W.F. and Bailey, F.R., "Numerical Calculation of Transonic Flow About Swept Wings," AIAA Paper No. 72-677, June 1972.

12. Ballhaus, W.F., Bailey, F.R., and Frick, J., "Improved Computational Treatment of Transonic Flow About Swept Wings," Proceedings of the 13th Annual Meeting of the Society of Engineering Science, Inc. CP-2001, Vol. 4, NASA, November 1976, pp. 1311-1320.

13. Krupp, J.A. and Cole, J.D., "Studies in Transonic Flow IV. Unsteady Transonic Flow," NASA Grant Report, ENG-76104, University of California at Los Angeles, October 1976.

14. Ballhaus, W.F., Jameson, A., and Albert, J., "Implicit Approximate-Factorization Schemes for Steady Transonic Flow Problems," AIAA Journal, Vol. 16, No. 6, June 1968, pp. 573-579.

15. Magnus, R.J. and Yoshihara, H., "Inviscid Transonic Flow Over Airfoils," AIAA Paper 70-47, January 1970.

16. Magnus, R.J. and Yoshihara, H., "Calculations of Transonic Flow Over an Oscillating Airfoil," AIAA Paper 75-98, January 1975.

17. Beam, R.M. and Warming, R.F., "Numerical Calculations of Two-Dimensional, Unsteady Transonic Flows with Circulation," NASA TN D-7605, 1974.

18. Ballhaus, W.F. and Lomax, H., "The Numerical Simulation of Low Frequency Unsteady Transonic Flow Fields," Lecture Notes in Physics, Vol. 35, Springer-Verlag, 1975, pp. 57-63.

19. Beam, R.M. and Warming, R.F., "An Implicit Finite-Difference Algorithm for Hyperbolic Systems in Conservation-Law Form," Journal of Computational Physics, Vol. 22, No. 1, 1976, pp. 87-110.

20. Ballhaus, W.F. and Steger, J.L., "Implicit Approximate-Factorization Schemes for the Low-Frequency Transonic Equations," NASA TM X-73,082 , November, 1975.

21. Ballhaus, W.F. and Goorjian, P.M., "Implicit Finite-Difference Computations of Unsteady Transonic Flows About Airfoils, Including the Treatment of Irregular Shock-Wave Motions," AIAA Paper 77-205, January 1977.

22. Isogai, K., "Calculation of Unsteady Transonic Flow Over Oscillating Airfoils Using the Full Potential Equation," AIAA Paper No. 77-448, April 1977.

23. Jameson, A., "Transonic Potential Flow Calculations Using Conservative Form," Second AIAA Conference on Computational Fluid Dynamics, Hartford, Connecticut, June 1975.

24. Bauer, F. and Korn, D., "Computer Simulation of Transonic Flow Past Airfoils with Boundary Layer Correction," Second AIAA Conference on Computational Fluid Dynamics, Hartford, Connecticut, June 1975.

25. Yu, N.J., Seebass, A.R., and Ballhaus, W.F., "Implicit Shock-Fitting Scheme for Unsteady Transonic Flow Computations," AIAA Journal, Vol. 16, No. 7, July 1978, pp. 673-678.

26. Fung, K.Y., Yu, N.J., and Seebass, R., "Small Unsteady Perturbations in Transonic Flows," AIAA Journal, Vol. 16, No. 8, August 1978, pp. 815-822.

27. Nixon, D., "Perturbation of a Discontinuous Transonic Flow," AIAA Journal, Vol. 16, No. 1, January 1978, pp. 47-52.

28. Ballhaus, W.F. and Goorjian, P.M., "Computation of Unsteady Transonic Flows by the Indicial Method," AIAA Journal, Vol. 16, No. 2, February 1978, pp. 117-124.

29. Tobak, M., "On the Use of Indicial Function Concept in the Analysis of Unsteady Motion of Wings and Wing-Tail Combinations," NACA Report 1188, 1954.

30. "Session 3: Transonic Flow", Proceedings of the 2nd International Symposium on the Finite Element Methods in Flow Problems, Santa Margherita Ligure, Italy, June 1976.

31. Chan, S.T.K., Chen, H.C., and Brashears, M.R., "Finite Element Analysis of Transonic Flows Over Thin Airfoils," AFFDL-TR-76-49, Vol. I, May 1976.

32. Tijdeman, H., "Investigations of the Transonic Flow Around Oscillating Airfoil," National Aerospace Laboratory Report, NLR-TR-77090U, The Netherlands, December 1977.

33. Fung, Y.C., Theory of Aeroelasticity, Dover Publication, New York, 1969.

34. Rizzetta, D.P., "Transonic Flutter Analysis of a Two-Dimensional Airfoil," AFFDL-TM-75-168-FYS, May 1977.

35. Rizzetta, D.P., "A Comparative Study of Two Computational Methods for Calculating Unsteady Transonic Flows About Oscillating Airfoils," AFFDL-TR-77-118, November 1977.

36. Rizzetta, D.P., "The Aeroelastic Analysis of a Two-Dimensional Airfoil in Transonic Flow," AFFDL-TR-77-126, December 1978.

37. McCormick, J.M. and Salvadori, M.G., Numerical Methods in FORTRAN, Prentice-Hall, Inc., Englewood Cliffs, New Jersey, 1964, p. 54.

38. Olsen, J.J., "AGARD Standard Configurations for Aeroelastic Applications of Transonic Unsteady Aerodynamics, Part III, Candidate Airfoil Data," AFFDL-TM-78-6-FBR, Part III, January 1978.

*U.S.Government Printing Office: 1979 — 657-002/545